TÜRKİYE CUMHURİYETİ
ANKARA ÜNİVERSİTESİ
SAĞLIK BİLİMLERİ ENSTİTÜSÜ

GENERATION OF PATIENT SPECIFIC IPSC-DERIVED HEALTHY ORGANOIDS FROM PRIMARY COLORECTAL CANCER PATIENTS WITH/WITHOUT METASTASIS AND TRANSCRIPTOME ANALYSIS

Zeynep Büşra ÖZER

DİSİPLİNLER ARASI KÖK HÜCRE VE YENİLEYİCİ TIP ANABİLİM DALI

DOKTORA TEZİ

DANIŞMAN
Prof. Dr. Kâmil Can AKÇALI

ANKARA
2023

TÜRKİYE CUMHURİYETİ
ANKARA ÜNİVERSİTESİ
SAĞLIK BİLİMLERİ ENSTİTÜSÜ

GENERATION OF PATIENT SPECIFIC IPSC-DERIVED HEALTHY ORGANOIDS FROM PRIMARY COLORECTAL CANCER PATIENTS WITH/WITHOUT METASTASIS AND TRANSCRIPTOME ANALYSIS

Zeynep Büşra ÖZER

DİSİPLİNLER ARASI KÖK HÜCRE VE YENİLEYİCİ TIP ANABİLİM DALI
DOKTORA TEZİ

DANIŞMAN
Prof. Dr. Kâmil Can AKÇALI

Bu araştırma 3210467 numaralı TÜBİTAK-TEYDEB 1501 projesi ile desteklenmiştir.

ANKARA
2023

Ankara Üniversitesi

Sağlık Bilimleri Enstitüsü Müdürlüğü'ne,

Yüksek Lisans olarak hazırlayıp sunduğum "Generation of Patient Specific iPSC-Derived Healthy Organoids from Primary Colorectal Cancer Patients With/Without Metastasis and Transcriptome Analysis" başlıklı tez; bilimsel ahlak ve değerlere uygun olarak tarafımdan yazılmıştır. Tezimin hipotezi tümüyle tez danışmanım ve bana aittir. Tezde yer alan deneysel çalışma tarafımdan yapılmış olup, tüm cümleler, yorumlar bana aittir.

Yukarıda belirtilen hususların doğruluğunu beyan ederim.

Öğrencinin Adı Soyadı:

Tarih:

İmza:

Ankara Üniversitesi Sağlık Bilimleri Enstitüsü
Kök Hücre ve Yenileyici Tıp Anabilim Dalı'nda
Zeynep Büşra Özer tarafından hazırlanan
"Generation Of Patient Specific iPSC-Derived Healthy Organoids from Primary Colorectal Cancer Patients With/Without Metastasis and Transcriptome Analysis"
adlı tez çalışması aşağıdaki jüri tarafından DOKTORA TEZİ olarak
OY BİRLİĞİ ile kabul/ret edilmiştir.

Tez Savunma Tarihi:

Jüri Başkanı
İmza

Raportör	Üye
İmza	İmza
Üye	Üye
İmza	İmza

Tez hakkında alınan jüri kararı, Ankara Üniversitesi Sağlık Bilimleri Enstitüsü Yönetim Kurulu tarafından onaylanmıştır.

İmza

Sağlık Bilimleri Enstitüsü Müdürü

TABLE OF CONTENTS

ACKNOWLEDGMENTS

In this thesis study, blood samples from colorectal cancer patients with and without metastases were used to create patient-specific induced pluripotent stem cells (iPSC). After that, iPSCs were used to generate intestinal organoids. Immunohistochemical studies have established the presence of fundamental cell groups that ought to be present in intestinal tissue in the produced organoids, which are an in vitro model of healthy tissue from cancer patients. After intestinal organoids were confirmed, RNA sequencing was used to assess the organoids' mRNA and non-coding RNA levels. According to the donors' health status, three stages were taken into account while comparing profiles. In order to compare the profiles of colorectal cancer patients with and without metastases, the profiles of control donors' (healthy people) were compared with those of colorectal cancer patients without metastases. The differences in the RNA level of healthy intestinal cells in a microenvironment where cancer has not yet developed are thought to have the potential to be evaluated as an early marker in the development of cancerization and metastasis by comparing the RNA profiles of organoids obtained by a non-invasive method and having the capacity to be an alternative to healthy tissue.

I would like to thank my advisor Prof. Dr. Kamil Can Akçalı for his support and his faith in me. I will always be grateful to you. To my beloved friends Doç. Dr. Verda Bitirim and Kardelen Genç, who were with me during the most difficult and stressful periods of my doctorate studies. I thank my dear friend Recep Uyar for his help in the bioinformatics analysis of my thesis project. I am grateful to my dear mother and father, my little sister Berrin, my grandmother, and my grandfather Hikmet, who helped me choose my profession. My dearest husband, Kemal Özer, who has trusted me more than I have through all my higher education and who is always with me, I thank you once again for your presence and love.

ABBREVIATIONS

Bp	Base pair
cDNA	Complementary DNA
DMEM	Dulbecco's modified eagle medium
DMSO	Dimethyl sulphoxide
DNA	Deoxyribonucleic acid
DNMT	DNA methyl transferase
dNTP	Deoxynucleotide triphosphate
EB	Embryoid body
EEM	Erythroid expansion medium
EPC	Erythroid progenitor cell
ECM	Extracellular matrix
FBS	Fetal bovine serum
g	Gravity
İPSC	İnduced pluripotent stem cell
kDa	Kilo Dalton
µg	Microgram
µL	Microliter
µm	Micromolar
mL	Milliliter
min	Minute
nM	Nanomolar
PBS	Phospho buffer saline
PBMC	Peripheral blood mononuclear cell
RNA	Ribonucleic acid
RPM	Rotation per minute
SeV	Sendai virus

INDEX OF FIGURES

INDEX OF TABLES

1. INTRODUCTION

1.1 Stem Cells

Stem cells are the one of the fundamental aspects of regenerative medicine. They enable the lifelong renewal of numerous tissues, including the nervous system, muscle, bone, blood, gametes, and epithelia. Additional stem cells are latent but may awaken at specific points in the life cycle or after injury. Depending on their potential, they can differentiate into one or more cell types. They can renew and develop into specialized cell types, and they are present in practically every tissue. More than one stage is required for cells to become specialized, and each step results in a loss in their differentiation potential. Adult stem cells can be uni- or multipotent. Comparing differentiation spectra to totipotent and pluripotent cells, adult stem cells are relatively constrained. Hematopoietic stem cells (HSCs) and mesenchymal stem cells (MSCs) are commonly studied two examples of the distinct cell linages that multipotent stem cells can differentiate into. Unipotent stem cells can only differentiate into only one type of cell. Totipotent stem cells were cells with the ability to self-organize into an organism. Both the embryo and the extra-embryonic tissues can be formed by totipotent cells. The only totipotent cell is the zygote that develops after fertilization. The blastocyst develops about the fourth day after fertilization, and embryonic stem cells reside in the inner cell mass. All three germ layer cell types can be differentiated into by pluripotent stem cells; however, they are unable to create extraembryonic tissues. As a result, it is unable to create an organism on its own. Induced pluripotent stem cells, often known as iPSCs, are another type of pluripotent stem cell. Stem cells are restrained within specific tissue microenvironments known as "niches". The largest barrier to understanding stem cell biology is still correctly identifying stem cells in vivo. Rarely can tissues' normal stem cells and adjacent cells be identified using histology techniques (Barker et al., 2007 ; Kiel et al., 2007). The microenvironment of stem cells called as stem cell niches, and researchers are starting to understand the variables that control the preservation of these stem cells. However, there is little conclusive evidence available regarding the neighbor cells that stem cells connect with or the cells that create the essential components that control stem cell maintenance. These researchers found that the intestinal epithelium's expression of the Lgr5 was restricted to columnar epithelial cells at the basement of crypts. Individual Lgr5-positive crypt has the ability of self-renewal *in vivo* and can give rise to all intestinal epithelial cells.

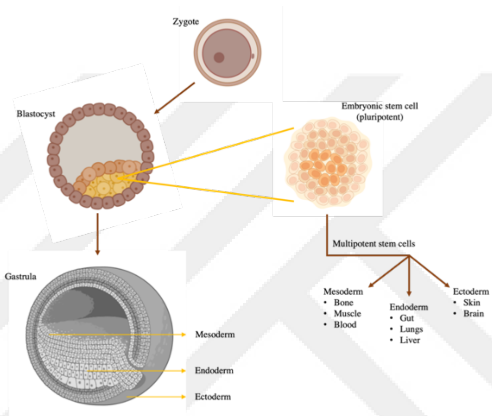

Figure 1.1: Zygote development and stem cell formation (adapted from Zakrzewski, 2019) by using BioRender).

1.2 Induced Pluripotent Stem Cells

Stem cells have limitless proliferative capacity and produce cells with the same characteristics. The pluripotent stem cells can differentiate into specialized cell types derived from the three germ layers (ectoderm, endoderm, and mesoderm) when specific conditions or signals are met. Inner cell masses (ICM) of pre-implantation embryos are the source of ESCs, which can be grown and maintained forever in the pluripotent condition in vitro. Cell reprogramming, a recently developed in vitro technique, can also be used to induce the de-differentiation of somatic cells to produce PSCs. iPS cells can be multiplied endlessly, just like ES cells can, and they can develop into all three derivatives of the three germ layers.

Shinya Yamanaka at Kyoto University carried out the first reprogramming by transfecting transcription factors Oct3/4, Sox2, c-Myc, and Klf4 into skin cells isolated from biopsy biopsies. iPSCs are the name given to the pluripotent cells produced in this manner. Due to ethical issues, the use of ESCs is currently not permitted in clinical settings. Some transcription factor genes (OKSM; Oct4, Sox2, Klf4, and c-Myc), are transmitted during the formation of iPSCs. These transcription factors are transmitted through a variety of techniques (retrovirus, lentivirus, plasmid, fuGene, etc.), and their expression confers pluripotency in somatic cells. The integration of viral vector systems into host genome, which raises the danger of cancer formation, is the most significant drawback of iPSC technique in clinical research. Although easy in theory, the procedures employed for reprogramming are complex and ineffective. To get beyond these restrictions, new techniques are constantly being created. The Sendai vector system is the most effective, non-genome-integrated, and straightforward to use technique currently available. It is also non-pathogenic to humans. The Paramyxoviridae family includes the negative strand RNA virus known as the Sendai virus. They can multiply in the cytoplasm of the host cells they infect, as opposed to other RNA viruses, which must transition into the DNA phase in order to integrate themselves into the host genome.

As embryonic stem cells (ESCs) or iPSCs behave in accordance with their cell-fate decisions throughout differentiation, their capacity for pluripotency gradually decreases. Cell-type-specific transcription factors (TFs) have critical roles in controlling the destiny of individual cells. Throughout the developing process, cells acquire tissue-specific characteristics, which is facilitated by the growing number of epigenetic alterations to DNA and chromatin. In a brief, the epigenetic memory forms and maintains the cellular identity. Through in vitro manipulations such the transduction of Yamanaka factors, the fate of the cell can be changed. The total erasure of the somatic epigenetic memory serves as the foundation for iPSC production. Although Yamanaka factors can be expressed ectopically using current transfection techniques, the efficiency is incredibly poor. The somatic chromatin alterations that already exist are thought to be a significant obstacle during iPSC production. De-differentiation occurs when Yamanaka factors are used to induce somatic cells [26].

The comparability of iPSCs from many donors is necessary for PSCs to be employed therapeutically. For the cell line to be referred to as an iPSC, quality checks and morphological analyses of the created iPSCs must be finished. The main parameters to be checked are the deletion of the vector system used in reprogramming from cells (residual vector testing), display of pluripotency markers in karyotype analysis at both the transcript and protein levels, and demonstration of differentiation potential into three germ layers (teratoma or embryoid body formation). Human iPSCs express hESC-specific surface antigens, SSEA-3 and SSEA-4 stage-specific antigens, the TRA-1-60 and TRA-1-81 tumor-related antigens, pluripotency-related transcription factors (TFs), elevated telomerase activity, and the capacity to differentiate into 3-germ layers through spontaneous teratoma formation (Kim et al., 2009 ; Park et al., 2008 ; Takahashi Yamanaka, 2006 ; YuJ., 2007). The existence of an inactive X chromosome in female iPSCs, however, suggests that human iPSCs are in a primed condition (Cheung et al., 2011 ; Mekhoubad et al., 2012 ; Pomp et al., 2011 ; Tchieu et al., 2010). Human iPSCs can be converted into a naive state, just like hESCs, by being cultured in certain medium.

The majority of OSKM-induced cells ultimately undergo apoptosis and senescence. P53 and p21CIP1 can be induced in murine and human fibroblasts when Yamanaka factors are expressed, according to numerous publications (Banito et al., 2009 ; HongH. et al., 2009 ; Kawamura et al., 2009). The efficiency of iPSC colony formation is increased when p53 is knocked down or reprogramming is induced in p53-null MEFs (HongH. et al., 2009 ; Kawamura et al., 2009 ; Marión et al., 2009), suggesting that the p53/p21 mediated pathways serve as a limitation to reprogramming. Additionally, numerous studies found that DNA damage response (DDR) pathway is activated when reprogramming factors are expressed (KawamuraT. et al., 2009). Because p53 causes apoptosis and senescence, it may inhibit DNA damage-related cells from being reprogrammed. The p53/p21 pathways' activation brings to light the extreme stress that cells undergo during the reprogramming process.

The somatic gene program is suppressed, and pluripotency-associated TFs are re-expressed as a result of the dynamic process of iPSC reprogramming. Initial iPSCs are the population of cells that have developed an ESC-like morphology. They are partially reprogrammed cells since the natural somatic expression profile is suppressed but pluripotency-related TFs are not expressed. Comparing iPSCs driven by BMP signaling to initial iPSCs revealed upregulation of H3K9me3 marks (Mikkelsen et al., 2008). Thus, it has been postulated that BMP associated effector proteins like Smad proteins, interact with H3K9 HMTs, such as Setdb1 and Suv39H1, to increase H3K9me3 motif (Sridharan et al., 2013). According to these results, erasing the H3K9me3 histone mark is a prerequisite for reprograming iPSCs.

A major worry of using the viral systems for reprogramming is the integration of oncogenes permanently (Higuchi et al., 2015). To establish a culture system free of animal products and lower patient dangers, several experiments have been carried out and are still ongoing (Seki Fukuda, 2015). This can be avoided by creating dependable and repeatable procedures for iPSCs that directly and effectively differentiate in the desired tissue (Cohen Melton, 2011).

Cells from patients' hiPSCs are an excellent biological model for researching various hereditary disorders. As a result, many articles in recent years have stated that hiPSCs created from patients with genetic diseases, following differentiation, are capable of recapitulating certain characteristics linked to illnesses (Sterneckert et al., 2014). Patient-specific hiPSCs are a very useful tool for the identification of patient-specific drugs (Maury et al., 2012). Researchers will be able to conduct focused preclinical toxicological in vitro experiments thanks to this advantage and their capacity to develop into a wide variety of specialized cells (Maury et al., 2012). Despite the fact that *in vitro* assays enable high-throughput screenings, they cannot mimic the complicated *in vivo* situation. The patient-specific iPSCs offer a way to avoid ethical issues that are considered as the main limitations of the therapeutic use hESCs.

1.3. Embryogenesis and Gastrointestinal Development

The formation and growth of an embryo is referred to as embryogenesis. It refers to the initial phases of fetal development in mammals. It begins with the sperm cell fertilizing the egg. When an ovum is fertilized, it becomes a zygote, which is a single diploid cell. Following mechanisms are necessary for multicellular organism development: growth, differentiation, and integration (Mahajan et al., 2018). The formation of an organism starts with several mitotic divisions and cellular differentiation. Growth is the developmental increase in cellular mass. After the basic organs are constructed, they start to develop and significantly expand in size. New cytoplasmic and nucleic protoplasm is produced during growth. Cell division is accompanied by an increase in bulk. One property that sets growth apart from other processes is cell proliferation. The organism progressively grows to be the same size as its parents . Differentiation describes the processes through which cells and other parts diverge from one another. There are two ways that it happens: first, by morphogenesis, which describes a change in the structure and arrangement of the body and its parts. Individual cells and their clusters structurally diverge from other cells and groups of cells with division and proliferation. The creation of different tissues is accomplished secondly by histogenesis, which is the term for a change in the composition and structure of the cells. Histogenesis refers to the entire process by which cells separate into discrete types and take on particular tissue characteristics. The organogenesis processes, which transform the early embryo into complete organs, are morphogenesis and histogenesis. Despite having structural unity, the new organs and organ systems still need to be transformed into cooperative working mechanisms. The neurological system and endocrine glands, which make up the main mechanism of physiological control and coordination, provide this control. A pre-functional stage will transition into a functioning stage when the organs receive enough neurological, circulatory, and hormonal inputs; this process is called the integration (Heisenberg Bellaïche, 2013 ; Keller, 2012 ; Mahajan et al., 2018).

Cleavage or segmentation refers to the succession of cell divisions that transform a single cell zygote into the multicellular embryonic stage known as the blastula. Cleavage divisions are the mitotic divisions that take place in this phase. The resultant offspring cells, known as blastomere, group together to create a dense mass known as the morula. The cleavage can be whole or partial, primarily depending on the amount of yolk. The blastomeres are clustered tightly inside the zona pellucida during the cleavage stage known as the "morula," providing the appearance of a mulberry fruit. Compaction is the term used to describe the embryo's shape change. A smaller number of interior cells and a bigger set of exterior cells make up the morula. The majority of the exterior cells develop into trophoblast cells. No embryonic structures are produced by this collection of cells. Instead, it creates the tissue of the chorion, the placenta's embryonic region. The chorion makes it possible for the fetus to receive nutrition and oxygen from the mother. The morula doesn't have an interior cavity at first. On the ring of trophoblast cells, the inner cell mass resides. The blastocyst is the resultant structure. A morula's blastomeres frequently develop an aspherical shape. The surfaces of the blastomeres that are in contact with one another are flattened by their mutual pressure, while the free surfaces of each blastomere stay to be spherical. The embryo has a layer of cells covering the yolk at the meroblastic cleavage and a hollow sphere of cells in the holoblastic kinds at the end of cleavage. Blastula is the name of this stage of development. Blastoderm refers to the layer of cells and blastocoele to the cavity. The blastocoele may initially just appear as small spaces between the blastomeres, but as the cleavage progresses, it eventually expands (Muhr Ackerman, s.d. ; Prados et al., 2012).

As the cleavage divisions conclude, the embryo attaches to uterus, where it develops. Implantation describes this connection of the embryo to uterus. The trophoblast cells carry out the implantation of the embryo. Animals exhibit two different implantation kinds. In the majority of mammals, the blastocyst attaches to the uterine wall and settles into the uterine cavity. The blastocyst penetrates deeply into the uterine wall in fewer species, such as rats and humans, and the embryo develops inside the uterine wall. At the place of penetration, the uterus' epithelial lining is damaged. The trophoblast cells' activity is what is causing this damage. Although the embryo receives some nutrition from the fluid that fills the uterus, this source of nutrients is insignificant to the food the embryo receives by diffusion from the mother's blood vessels. The uterine fluid, however, supplies the developing embryo with sustenance while the connection between the embryo and the uterine wall develops. Placentation is the process by which blood arteries between the embryo and the tissues of the mother link. The embryo is still in the blastocyst stage when it is implanted, and gastrulation doesn't begin until after the implantation. The embryonic membranes also begin to develop at this period. (Mahajan et al., 2018 ; Ochoa-Bernal Fazleabas, 2020)

Gastrulation is the collective term for the processes that change a single-layered blastula into a multi-layered gastrula. The gastrocoele/archenteron—the first known gut cavity—forms. Additionally, during this phase, the three germ layers—ectoderm , mesoderm, and endoderm —are all differentiated (Figure 1.2). This stage of development is the most critical process. Organogenesis, when specific organs grow inside the newly created germ layers, occurs after gastrulation. In a developing embryo, each one of the 3-germ layer gives rise to particular tissues. In vertebrates, the ectoderm gives rise to the neural crest, the nervous system, and the epidermis. The endoderm develops into the respiratory and digestive system epithelium as well as digestive system-related organs including the liver and pancreas. Numerous cell types, including muscle, bone, and connective tissue, are derived from the mesoderm (Muhr Ackerman, s.d.).

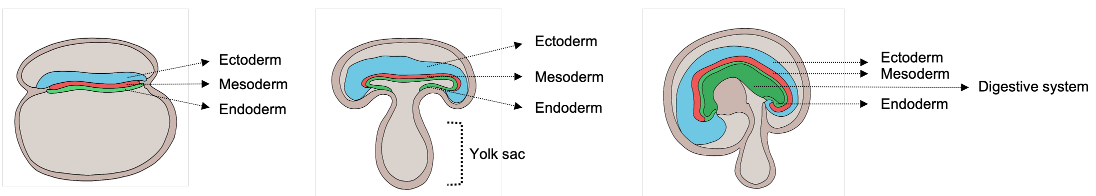

Figure 1.2: Gastrulation process and the formation of gastrocoele/archenteron.

Endoderm, mesoderm, and ectoderm are three types of germ layers that are generated during gastrulation and appear by two weeks. The germ tissues in humans serve as the building blocks for all tissues and organs. Endoderm gives rise to glands and the epithelial lining. During weeks three and four, the embryo folds craniocaudally and laterally, integrating the yolk sac into the developing primitive gut tube. The foregut, midgut, and hindgut are the three distinct portions of the tube.

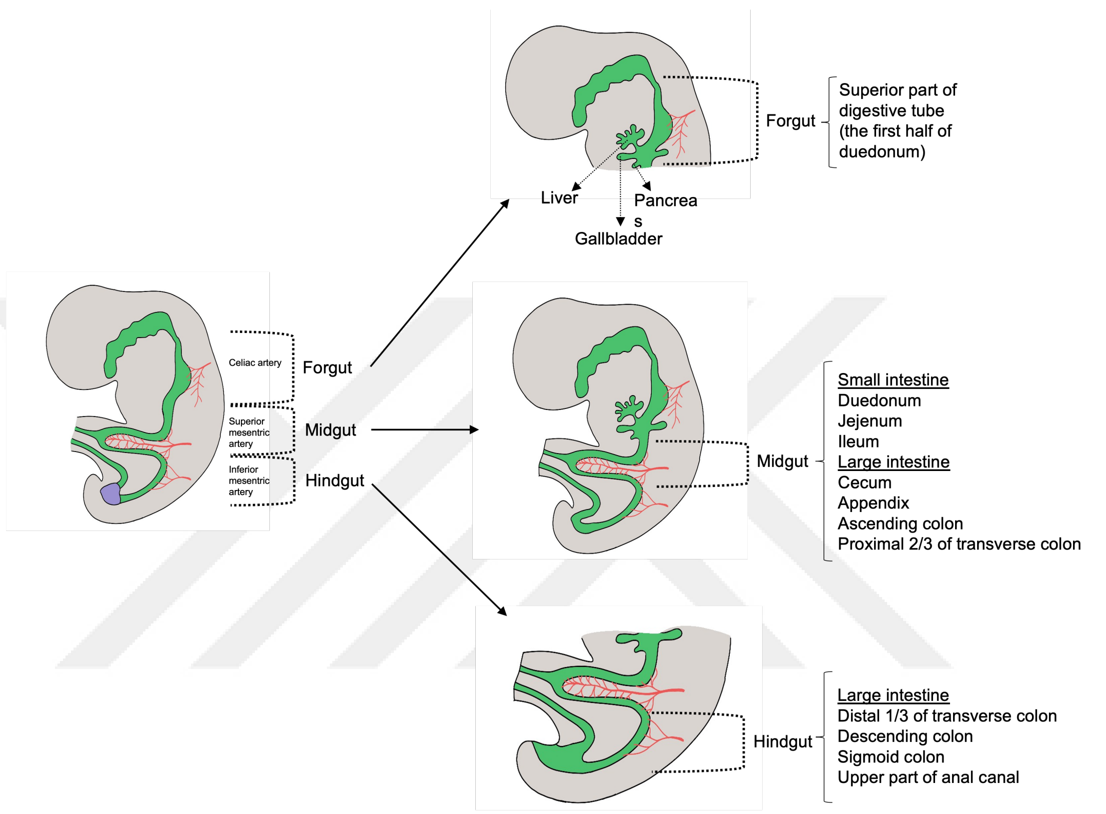

Figure 1.3: Craniocaudally and laterally folding of embryo and integrating the yolk sac into the developing primitive gut tube. Three distinct portions of the tube are formed (the foregut, midgut, and hindgut).

The ventral component of the septum develops into the respiratory system and the dorsal section into the gastrointestinal tract, dividing the respiratory and digestive tracts. During week 4, a fusiform dilation in the foregut gives rise to the stomach. Hepatic cells creating the hepatic sinusoids surround vitelline veins, the endothelial progenitor cells. Cholangiocytes and hepatocytes are both produced by bipotential hepatoblasts. In the intrahepatic portal tracts, these cells undergo remodeling to create bile ducts. Between the sixth and tenth weeks, the midgut gives rise to the detailed portions of the duodenum and colon (Grand et al., 1976 ; Osefo et al., 2009).

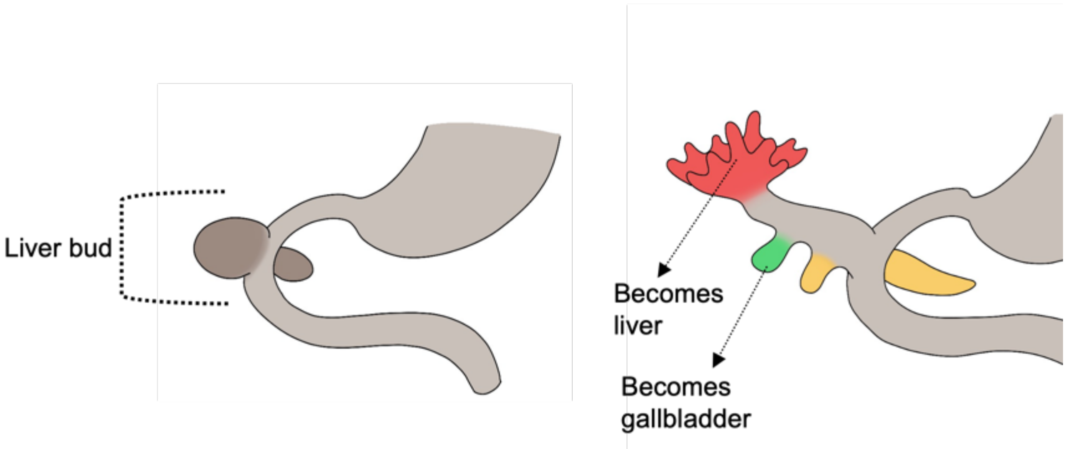

Figure 1.4: The formation of liver bud and bile duct, gallbladder formation as cystic divertcula.

1.4. Colorectal Cancer

Cancer, one of today's important health problems, is a common and multifactorial disease with a high mortality rate. Cancer causes death of approximately 9.6 million people in 2018. Gastrointestinal cancers constitute an important part of these prevalence and mortality statistics (Siegel et al., 2020). The most common type of gastrointestinal cancer worldwide is colorectal cancer. Almost 1.4 million cases are diagnosed annually and 700,000 people die due to this. The prevalence of colorectal cancer in the world is third in men and second in women (Siegel et al., 2020). Colorectal cancer (CRC) continues to be a fatal disease due to relapse and metastasis (Xu et al., 2020). CRC, which has a 5-year survival of approximately 50% of patients, is a disease with a generally poor prognosis when diagnosed late (Roxburgh et al., 2012). This situation highlights urgency of the fight against cancer.

1.5. Carcinogenesis of Colorectal Cancer

Epidemiology studies have shown that the development of colorectal cancer increases in men with advancing age. Both hereditary and environmental risk factors have major impacts on the development of colorectal cancer (Jess et al., 2012). Approximately 10-20% of patients have a family history of colon cancer (Schoen et al., 2015). Hereditary colorectal cancers are divided into two: non-polyposis and polyposis syndromes. Lynch syndrome and familial colorectal cancer belong to the non-polyposis group (Jiao et al., 2014). Syndromes classified as polyposis are often noticed by physicians because of the widespread appearance of polyps in the patient. Types of polyps are critical for the correct diagnosis of the disease. For these and similar reasons, it is extremely important to identify strong biomarkers to be evaluated in the diagnostic process.

Most CRCs arise from a polyp; the carcinogenesis begins with an abnormal crypt and evolves into a neoplastic early lesion called a polyp, eventually forms colorectal cancer over approximately 10-15-year period. The tumor initiating cell turns into colorectal cancer is thought to be a cell with stem cell characteristics (Medema, 2013 ; Nassar Blanpain, 2016). These cells are considered as the final output of the accumulated genetic and epigenetic changes which have altered oncogene and tumor suppressor gene profile.

Cancer initiating cells are thought to be located in the colonic crypt base and are the initiators of tumor formation (Medema, 2013 ; Nassar Blanpain, 2016). There are two, globally accepted, cancer initiating pathways: the chromosomal instability sequence and the neoplasia pathway leading. These two pathways include more than one genetic or epigenetic alterations (Muzny et al., 2012). Genomic changes frequently end with the chromosomal instability; APC mutation, RAS mutation (activation), p53 mutation (loss of function) are examples for this kind of genomic changes. On the other hand, the neoplasia pathway is mainly related to RAS and RAF mutations (Syngal et al., 2015). The portion of the colon which develops cancerous tissue in affects the molecular properties of the developing cancer. The side of colon cancer is important in terms of metastasis and its response to receptor-mediated drugs (Venook et al., 2016).

Cancer research mainly relies on models that maintain malignant states at the molecular and cellular level. The patient-derived models for cancer research are valuable in vitro tools for the basic and translational research. The immortalized cell lines are primarily used in vitro models for basic research, however, in recent years, iPSCs and three-dimensional organoids, are gaining importance. Unfortunately, genetic alterations and mutations have a strong effect on the reprogramming efficiency of iPSCs (Papapetrou, 2016).

1.6. Common Features of Embryogenesis and Carcinogenesis

There are many similarities between carcinogenesis and embryogenesis in terms of activated signal transduction pathways. Similar concepts between embryogenesis and carcinogenesis are: high cell proliferation rate, resistance against apoptosis, elevated angiogenesis rate, and higher migratory activity (Stoika et al., 2004). The phenomena of epithelial to mesenchymal transition (EMT) happens in both during embryogenesis and cancer development.

Cells change their configuration through migrating and fetal development proceeds. The changing in epithelial characteristics to mesenchymal characteristics, cells can enter the extracellular matrix (Kelleher et al., 2006). During gastrulation, 3 germ layers, endodermal, mesodermal, and ectodermal layers, are formed. Cells lose their apico-basal polarity through EMT and lose cell-cell adhesion (Kelleher et al., 2006).

WNTs are cytosine-rich glycoproteins, and they interact with cellular receptors to function as active molecules. The Jun N-terminal kinase as well as canonical ß-catenin pathway can all be activated by this interaction. ß-catenin is bound to the degradation complex when Wnt ligands are not present. APC and AXIN1 genes help glycogen synthase kinase 3 (GSK3) and casein kinase 1 (CK1) phosphorylate ß-catenin. The phosphorylation of ß-catenin results in the degradation of it by proteosomes. In contrast, as ß-catenin levels rise, it is translocated to the nucleus and interacts with TCF. Wnt forms the ß-catenin destruction complex to destabilize. WNTs play a role in early axial patterning, myogenesis, and nervous system development (ChenA. E. et al., 2005 ; Sarkar Sharpe, 1999 ; Shimogori et al., 2004 ; YangY., 2003). If the formation of destruction complex cannot be provided after the increase of ß-catenin, accumulation of ß-catenin causes development of certain types of cancers such as colon cancer. Almost all cases of non-hereditary colon cancer have loss of APC or increased levels of ß-catenin, both can activate the ß-catenin pathway (Tetsu McCormick, 1999).

Notch signaling pathway regulates cell fate determination, maintenance of stem cell repository (Grego-Bessa et al., 2004). Endocytosis, glycosylation, and ubiquitination are the common mechanisms that controlled by notch signaling (Lewis, 1998 ; Shawber et al., 1996). Depending on the microenvironment of cells and how other signaling pathways interacts with, Notch functions as either an oncogene or a tumor suppressor gene. The Notch receptor activation, the ligand-independent activation, or changes in the amounts of delta or other ligands can cause cancer development.

1.7. Spheroids and Organoids

In life sciences and biomedical research, animal models and established cell lines are used for in vivo or in vitro studies. These models are not completely convenient for drug studies and disease modeling as they cannot provide complex tissue and organ structures. 3D cell cultures provide better modeling to real tissues and organs in *in vitro* studies. The most important limitation in the use of experimental animals is ethical concerns. Although primitive 3D cell culture constructs do not have organ-level organization, they allow researchers to co-culture more than two cell types (Sakalem et al., 2021).

Spheroid formation is based on the cell-cell adhesion capacity of cells. Spheroids can contain a single cell type or be in a multicellular structure. Although tumor cells and cells like hepatocytes do not require a supportive extracellular environment, they can form spheroids. However, cells that can form spheroid structures cannot form advanced structures as organoids because they do not have regenerative capacity and self-assembling abilities (Kelm Fussenegger, 2004 ; Mueller-Klieser, 1997 ; Yui et al., 2012). Especially for the drug testing, monolayer cancer cells cannot reflect the actual mechanism of the drug because they are much more sensitive than cancer spheroids (Laschke Menger, 2017).

iPSC, adult stem cells (ASC), and ESCs can be used to produce organoids. Organoids require the ECM to evolve into higher organization (McCauley Wells, 2017 ; Spence et al., 2011a). Depending on the tissue type, the formation of a complex structure often takes more than two months and requires culturing in various cocktail recipes and growth agents (Spence et al., 2011a). Organoids derived from iPSC mimic ex vivo organ development, and may also include mesenchymal, epithelial, and occasionally endothelial types of cells. Organoids can be explained as tissue-specific complex cell clusters. In order for classifying a certain spheroid structure as an organoid, it has to contain at least one epithelial type and one mesenchymal type cell (Sakalem et al., 2021). Also as explained, organoid structures need a supportive extracellular matrix structure. When extracellular matrix is supplied to iPSCs or tissue-specific progenitor/stem cells, the cells can activate their self-assembling (Bartfeld et al., 2015 ; Clevers, 2016 ; Takasato et al., 2015). Numerous iPSC-derived organoids also keep fetal similarities and do not completely show the adult gene expression profile (Clevers, 2016 ; McCauley Wells, 2017).

1.8. iPSC-derived Colon Organoids as *In Vitro* Intestinal Model

The main function of intestinal system is the absorption of micro and macro nutrients. Model animals and immortalized cell lines are used to test the absorption rate of drugs, as the culturing of primary human intestinal cells *in vitro* is difficult to maintain (Di Claudio et al., 2017 ; Negoro et al., 2018 ; Taylor et al., 2010). The model animals and cell lines cannot realistically mimic the intestinal tract (Negoro et al., 2018 ; Sun et al., 2008). In iPSC studies conducted in the early 2010s, the intestinal organoids were successfully differentiated from human iPSCs (Kauffman et al., 2013 ; Spence et al., 2011a). Human intestinal organoids contain all intestinal cell types: enterocytes, goblet cells, paneth cells, and enteroendocrine cells. Especially for regenerative medicine, human intestinal organoids are efficient models. Creating and maintaining a monolayer intestinal model is very difficult because of the nature of the intestinal structure. For this reason, providing the organoid structure is important for the progression of intestinal studies.

iPSCs were differentiated into monolayer cultures of hepatocytes, pancreatic endocrine cells, and colon epithelium (Spence et al., 2011b ; Takayama et al., 2014). Embryonic development can be mimicked stepwise by directing signaling pathways with *in vitro* manipulations. The formation of colonic organoids takes place in parallel with the embryonic colon development, first as the definitive endoderm (DE) and then as the hindgut endoderm (HE). When CHIR99021 (GSK-3ß inhibitor) and activin A were used during DE differentiation of iPSCs, SRY-box 17 (SOX17) positive cells were shown to constitute 95% of the differentiated population (Crespo et al., 2017). Studies shown that WNT pathway is essential for the posterior colonic development and that the posterior marker is Cdx2 (Sherwood et al., 2011). In 2011, Spence et al. published their established three-dimensional iPSC-derived intestinal organoid model. They used human keratinocytes as the origin cell and established an efficient protocol for directed differentiation of iPSCs into intestinal organoids. They applied different combinations of growth factors temporarily to mimic embryonic development. They started with activin-induced definitive endodermal differentiation. The following step was inducing posterior endoderm using Wnt/FGF than they initiated hindgut formation, and finally pro-intestinal culture was established. They formed colonic organoid-like structures which consist of several intestinal epithelial cell types (Spence et al., 2011b). They characterized these colonic cell types with CDX2, LGR5, SOX9, KLF5, and ALB. After 14-day culture, the epithelium structure expressed intestinal transcription factors CDX2, SOX9, and KLF5. After 28-day culture, cells were still 90% positive for CDX2 and KLF5, however, SOX9 specifically localized in highly proliferative cells located in the villus basement. After 56-day culture, they showed that ASCL2 and LGR5 expressed cells were restricted in only epithelial domains. Several published studies were achieved to generate iPSC-derived intestinal models. Their protocols shared a backbone structure, they used the same growth factors and inhibitors mainly yet they used different incubation periods and concentrations (Iwao et al., 2014 ; Kondo et al., 2020 ; Ogaki et al., 2015 ; Spence et al., 2011b).

1.9. RNA Sequencing and Pathway Enrichment Analysis

Researchers can get more detailed representation of gene lists produced through genome-scale (omics) experiments. Three main processes build the protocol: creating a gene list using high-throughput data, identifying enriched pathways, and visualizing the resulting depictions/lists. Given the experimental methodology, the raw dataset typically needs bioinformatical processing (normalization and scoring.) For instance, RNA-seq data can be used to create a list of the genes that differ in expression across two groups of samples. For many academics, the processing and interpretation of omics data are significant problems. Long lists of genes produced by analyses are frequently difficult to interpret manually and require extensive literature searches. Pathway enrichment analysis condenses long gene lists into more manageable forms. For gene list enrichment, all pathways in a particular database are examined. The choice of pathway enrichment analysis method depends on the format of the gene list. For the deeper research and the better interpretation, visualization is essential. In order to discover pathways that are enriched in, gene lists are subjected to pathway enrichment analysis. The EnrichmentMap, AutoAnnotate, WordCloud, and clusterMaker2 apps of Cytoscape are used to display and understand the findings of pathway enrichment analysis.

To eliminate unneeded technical variation between samples, read counts per gene are normalized among all samples. Next, read counts for each gene are compared between sample groups to check for differential expression. Procedures for data normalization and generating differential expression lists are implemented by software programs like edgeR, DESeq, limma/voom, and Cufflinks. The p-value of the significance of differential expression, adjusted p-value has to be corrected across all genes through using the Benjamini-Hochberg false-discovery rate (BH-FDR) procedure. The trend of expression changes (upregulated genes are positive and downregulated genes are negative) are all included in the results of differential gene expression analysis. The gene list is then sorted by one or more of these parameters and examined using pathway enrichment analysis.

The standard algorithm used in g:Profiler and comparable web-based tools looks for pathways that given genes are considerably enriched, in comparison to the genome. A Fisher's exact test and multiple-correction test are used to calculate the p-value of the enrichment. Gene sets that reflect Gene Ontology (GO) terms, pathways, and disease phenotypes are searched by g:Profiler, DAVID, GeneCodis, and ShinyGo. To tailor the search, major gene set categories are chosen. The characterization of background genes is necessary for comparison when using pathway enrichment techniques that employ Fisher's exact test. Yet, the default setting frequently applies to all annotated protein-coding genes. Pathway enrichment analysis of omics data increases statistical power by condensing tens of thousands of to smaller number of pathways. The results are frequently simpler to interpret. As a result, the broad omics data is converted into refined pathways have statistical significance.

Established cell lines and primary cells are commonly used for cell-based, high-throughput studies. Unfortunately, established cell culture systems cannot mimic the tissue microenvironment. Especially stem cell and cancer studies required well-defined microenvironments to simulate their complex niches (Ranga, Gjorevski, and Lutolf 2014). Animal studies are also another strong alternative for cell culture experiments, yet the fundamental physiological differences between laboratory animals and humans make animal experiments less reliable, especially for pre-clinical studies (Pritchard et al. 2003). iPSCs can differentiate into multiple cell types under appropriate culture conditions (Sterneckert, Reinhardt, and Schöler 2014). iPSCs can be generated from the somatic cells of an individual, making it possible to generate both disease- and patient-specific models. iPSC-derived models are a useful tool for studying disease progression. iPSCs have been differentiated into monolayer cultures such as hepatocytes, pancreatic endocrine cells, and colon epithelium (Spence et al., 2011; Takayama et al., 2014). These successful efforts have therapeutic efficacy in diseases of the tissues to which they belong. iPSC-derived gut models were commonly generated from the established iPSC line Windy from the National Center for Child Health and Development (Iwao et al. 2014; Kabeya et al. 2018; Kondo et al. 2020), yet human kidney-derived cells and primary human hepatocytes were also used (Inamura et al. 2011; Kauffman et al. 2013; Takayama et al. 2014). Their protocols had a common structure; they used the same growth factors and inhibitors mainly, but they used different incubation periods to mimic embryonic intestinal development (Iwao et al. 2014; Kondo et al. 2020; Ogaki et al. 2015; Spence et al. 2011). They formed colonic models, which consist of several intestinal epithelial cell types (Spence et al. 2011). The intestinal tissue has a complex structure that includes crypts. A functional colonic *in vitro* model needs to contain all types of cells that reside in the intestinal crypt. This is the main reason why a single colonic epithelial cell type is not preferred for this kind of systemic *in vitro* model. Colon epithelial models provide a valuable tool for molecular and cellular studies (Sato et al., 2009; Yui et al., 2012). iPSC-derived gut models can be generated from intestinal epithelial stem cells (IESCs) and have a cryptic structure that contains IESCs that maintain other crypt cells (Sato et al. 2011). iPSC-derived gut models are constituted in Matrigel, which contains fibroblast growth factor 2 (bFGF), epidermal growth factor (EGF), and insulin-like growth factor (IGF), which provide an extracellular environment and support cell proliferation and spherical structure formation. As explained above, the intestinal differentiation process is based on embryonic intestinal development and is delicate to handle. Moreover, during the differentiation process, several growth factors and certain inhibitors are required. In this thesis study, we studied colorectal cancer patients;

however, we did not seek to achieve cancer cell reprogramming or create an early-stage cancer model. We planned to use erythroid progenitor cells collected from peripheral blood as the origin cells and aimed to generate patient-specific healthy intestinal models to simulate healthy intestinal tissue in CRC patients without any invasive methods such as colon biopsy. Erythroid progenitor cells were not previously used as the origin cell for iPSC-derived colon studies; this is one of the novel characteristics of this thesis study. We expected to see higher reprogramming efficiency. Also, this thesis study aimed to investigate transcriptomic patterns in healthy colon models of CRC patients as early biomarkers. iPSC and intestinal system literature are mainly focused on generating a small intestine model and drug absorption and metabolism studies. However, we generated iPSC-derived colon models as a tool for investigating early cancer biomarkers in a healthy model, which makes this thesis study novel from this perspective. We analyzed the transcriptome profiles of iPSC-derived healthy colon models to reveal whether there are specific patterns that make people susceptible to CRC development.

The main goal of this thesis study is to make an *in vitro* healthy colon model for people with colorectal cancer (CRC). CRC patients with only primary tumors and CRC patients with metastatic tumors were our experimental groups. Three patients from each group were selected according to their cancer status. As we aimed, we generated patient specific iPSC-derived intestinal organoids and analyzed their transcriptome profiles through RNA sequencing. However, we did not aim to create a cancer model from patient specific iPSC-derived intestinal organoids. Our main purpose is to reveal whether there are unknown genetic and epigenetic patterns that make people susceptible to developing CRC.

Our **first** goal was to make iPSCs from the erythroid progenitor cells (EPCs) in the peripheral blood of six CRC patients (with or without metastasis) and three control individuals. The **second** goal was differentiating patient specific iPSCs into intestinal organoids. After the validation of intestinal organoid differentiation, our **third** goal was to analyze the RNA-seq profiles of iPSC-derived intestinal organoids. As we previously explained, our main purpose was to investigate whether there is a transcriptomic pattern that makes patients susceptible before they have been diagnosed. RNA-seq was performed for iPSC-derived intestinal organoids. RNA-seq results showed that CRC and mCRC patients had different transcriptomic profiles when compared with either control donors or each other.

2. MATRIALS AND METHODS

2.1. Materials

2.1.1. General Laboratory Reagents

The alcohols and salts most commonly used in molecular experiments are from Sigma-Aldrich (Missouri, USA). These are ethanol, methanol, isopropanol, glacial acetic acid, Tris-base, glycine, sodium azide, chloroform, paraformaldehyde, sucrose, and DMSO.

2.1.2. Cell Culture Reagents

StemSpan Serum-free Expansion Medium (SFEM II), StemSpan Erythroid Expansion Supplement (100X), Ficoll Solution, TeSR-7/ReproTeSR basal medium, ReproTeSR supplement, TeSR-7 supplement, StemDiff APEL II medium, Anti-adherence rinsing solution, Aggrewell800 plates, AggreWell embryoid body formation medium, StemDiff Intestinal Organoid Kit, StemDiff Intestinal Organoid Growth Medium, and CryoStor CS10 were purchased from Stem Cell Technologies (Canada). DPBS (no calcium no magnesium), Cytotune 2.0 Sendai Vector System, Essential 8 medium, Stemflex medium, Essential 6 medium, DMEM/F12 15 mM HEPES, DMEM Low Glucose, IMDM medium, Fetal Bovine Serum (heat-inactivated), Glutamax (100X), Vitronectin, and Revitacell were purchased from Thermo Fisher Scientific (Massachusetts, USA). Tissue culture flasks, multiple well plates, serological pipettes, cryotubes were supplied from Sarstedt (Nümbrecht, Germany). Glass laboratory ware such as μ-Dish 35 mm glass bottom dish and μ-slide 8-well chambers were supplied from Ibidi GmbH (Gräfelfing, Bayern).

2.1.3. Reagents for Total RNA Isolation

Pureizol-RNA isolation reaent was supplied from Bio Rad (California, USA). Other chemicals such as chloroform, isopropanol, and ethanold were purchased from Sigma Aldrich (Missouri, USA).

2.1.4. Reagents and Primers for Conventional PCR and qRT-PCR

cDNA Synthesis kit, Taq DNA Polymerase, and SybrGreen were purchased from Bio Rad (California, USA). Primers were designed using the online database Ensemble and NCBI Primer Blast. RT-PCR plates were purchased from Roche (Mannheim, Germany). Primers were purchased from PRZ Biotech (Ankara, Turkey). All primers are listed in Table 2.1.

Table 2.1: Primers used in human conventional- and RT-PCR experiments

Gene Name Primer Sequence
hBeta-Actin_F: 5'-AAAATCTGGCACCACACCTTC-3' **hBeta-Actin_R:** 5'-AGCACAGCCTGGATAGCAAC-3'
hEndo-OCT4_F: 5'-AGTTTGTGCCAGGGTTTTTG-3' **hEndo-OCT4_R:** 5'-ACTTCACCTTCCCTCCAACC-3'
hEndo-SOX2_F: 5'-GGGAAATGGGAGGGGTGCAAAAGAGG-3' **hEndo-SOX2_R:** 5'-TTGCGTGAGTGTGGATGGGATTGGTG-3'
hNANOG_F: 5'-CTCTCCAACATCCTGAACCTC-3' **hNANOG_R:** 5'-ACACCATTGCTATTCTTCGG-3'
hc-MYC_F: 5'-GGATTCTCTGCTCTCCTCGAC-3' **hc-MYC_R:** 5'-CTTCCTCATCTTCTTGTTCCT-3'
hKLF-4_F: 5'-AAACCTACACAAAGAGTTCCCAT-3' **hKLF-4_R:** 5'-TTTCCATCCACAGCCGTCCCA-3'
hREX-1_F: 5'-AACAGGATGAAGCAGATTAACAGA-3' **hREX-1_R:** 5'-TGTAGGAGCATCTTAGTAACACC-3'
hDNMT3a_F: 5'-CCTCAAACCCAACAACACGCAAC-3' **hDNMT3a_R:** 5'-TCTGATCTTCATCCCCTCGGTCT-3'

hDNMT3a_R: 5'-TCTGATCTTCATCCCCTCGGTCT-3'
hUTF-1_F: 5'-AGTTCCTTAAAGACAAGTTTCGC-3' **hUTF-1_R:** 5'-CAGCAGCCCCATGAGCTTCC-3'
SeV_F: 5'-GGATCACTAGGTGATATCGAGC-3' **SeV_R:** 5'-ACCAGACAAGAGTTTAAGAGATATGTATC-3'
KOS_F: 5'-ATGCACCGCTACGACGTGAGCGC -3' **KOS_R:** 5'-ACCTTGACAATCCTGATGTGG-3'
KLF4_F: 5'-TTCCTGCATGCCAGAGGAGCCC-3' **KLF4_R:** 5'-AATGTATCGAAGGTGCTCAA-3'
c-myc_F: 5'-TAACTGACTAGCAGGCTTGTCG-3' **c-myc_R:** 5'-TCCACATACAGTCCTGGATGATGATG-3'

2.1.5. Agarose Gel electrophoresis

Agarose was purchased from Sigma-Aldrich (Missouri, USA), 100 bp DNA ladder was purchased from New England Biolabs (NEB Inc., Massachusetts, USA), and RedSafe Nucleic Acid Staining Solution (20,000x) was purchased from JH Science (Kirkland, WA, USA).

2.1.6. Immunostaining Reagents

BSA was purchased from Sigma (Missouri, USA). PSC-4 immunofluorescence kit used in immunocytochemistry experiments for pluripotency markers was supplied from Thermo Fisher Scientific (Massachusetts, USA).

Table 2.2: Primary and secondary antibodies used in immunostaining experiments

Primary Antibody	Secondary Antibody
Anti-Oct4 (1µL in 100µL)	Donkey anti-rabbit 555 (0.4µL+100µL)
Anti-SSEA4 (1µL in 100µL)	Goat anti-mouse IgG3 488 (0.4µL+100µL)
Anti-Sox2 (1µL in 100µL)	Donkey anti-rat 488 (0.4µL+100µL)
Anti-Tra-1-60 (1µL in 100µL)	Goat anti-mouse IgM 555 (0.4µL+100µL)
Anti-FOXA2	Goat Anti-Rabbit IgG AF488
Anti-KLF5	Goat Anti-Rabbit IgG AF488
Anti-Chromogranin A	Goat Anti-Rabbit IgG AF488
Anti-SOX9	Goat Anti-Rabbit IgG AF488
Anti-Lysozyme	Goat Anti-Rabbit IgG AF488
Anti-Villin	Goat Anti-Rabbit IgG AF488
Anti-LGR5	Goat Anti-Rabbit IgG AF488

2.1.7. Reagents for Flow Cytometry

Fix & Perm Solution used for the fixation of cells was purchased from Tonbo Bio (San Diego, CA, USA). BSA and sodium azide used in flow cytometry experiments were supplied from Sigma-Aldrich (Missouri, USA) and Merck (New Jersey, USA), respectively. All antibodies used for flow cytometry are listed in Table 2.3.

Table 2.3: Flow cytometry antibodies.

Antibody	Company (Catalog Number)
FITC mouse IgM isotype antibody	BD Technologies (BD-555583)
PE mouse anti-human CD71 antibody	BD Technologies (BD-561938)
FITC mouse anti-human GlyA antibody	BD Technologies (BD-559943)
PE Mouse IgG2a, κ Isotype Control	BD Technologies (BD-555574)

2.2. Methods

2.2.1. Peripheral Blood Mononuclear Cell Isolation

Peripheral blood samples were taken into EDTA tubes and mononuclear cell isolation was started immediately. The blood sample was diluted 1:1 with 1X DPBS (Gibco). After taking the same volume of Ficoll solution as the diluted blood sample into a 50ml tube, the blood sample was slowly spread over the Ficoll solution. The tube containing the Ficoll separation solution was tilted at an angle of approximately 45° and the diluted blood sample was gently poured onto the Ficoll solution from the tube wall. The Ficoll solution and the blood sample should remain separate to form two phases. The 50ml centrifuge tube containing the Ficoll and blood sample was placed in the centrifuge very carefully. It is centrifuged at 600 x g for 30 minutes at room temperature to separate into cell phases. Centrifuge acceleration is set to the slowest setting, and to minimize the mixing of phases during deceleration, the brake mechanism of the centrifuge is disabled. The PBMC-containing phase (interphase fraction-the buffy coat) was transferred into a new 50ml centrifuge tube. The mononuclear cell population was washed with 1X DPBS and IMDM medium. Cells are pelleted by centrifugation at 300 x g for 10 minutes at room temperature between washes. After the IMDM wash, the cell pellet was resuspended into 1ml IMDM medium and cells were counted. $3x10^5$ cells were seeded for erythroid progenitor expansion into 12-well plate ($1x10^5$ cells/well), remaining cells were frozen in erythroid progenitor freezing medium (90% FBS+10% DMSO) as $5x10^5$ cells/vial.

2.2.2. Erythroid Progenitor Cell Enrichment

StemSpan II basal medium (Stem Cell Technologies, #09695) was completed with the Erythroid Expansion Supplement (Stem Cell Technologies, #02692). PBMCs were plated at a concentration of $1x10^5$ cells/ml (day 0) in 1ml erythroid expansion medium (EEM). Cells were cultured in a humidified incubator at 37°C with 5% CO_2. The next day, cells were transferred into new wells. So, the adherent cells were removed (day 1). On day 2, 4, and 6, cells were collected into 15ml falcon tubes and centrifuged for 10 minutes at 300 x g. The cell pellet was resuspended in 1ml fresh EEM. After 7 days of culture, cells were harvested and counted for further experiments (flow cytometry characterization, RNA isolation, and Sendai virus transduction).

Characterization with flow cytometry: EPCs were pelleted by centrifugation at 300x g for 10 min. After this step, the cells were kept on ice and the solutions were used at +4°C. It was dissolved in ice-cold staining solution (150 µl of 1X PBS containing 5% BSA and 0.05% sodium azide). 50 µl containing $5x10^4$ cells as the unstained cell group was separated into a separate microcentrifuge tube, and the remaining cells were stained with conjugated flow cytometry antibodies (Table 2.3). Add 1 µl of FITC mouse anti-human GlyA (BD-559943, BD Technologies) and 1 µl PE mouse anti-human CD71 (BD-561938, BD Technologies) antibodies and isotype antibodies respectively to the cells in 100 µl of 5% BSA and 0.05% sodium azide in 1X PBS. Cells were incubated for 30 min at +4°C in the dark. 1 ml of 1X PBS was added to the stained cells and 300x g was centrifuged for 10 minutes, and the pellet was dissolved with 200 µl of 1X PBS and the reading was taken in flow cytometry (ACEA Novocyte, Agilent, California, USA).

2.2.3. Sendai Vector Transduction

Sendai viral system makes possible to integration-free transduction. 4 recombinant Sendai viral vectors (Cytotune, Life Technologies) expressing the four reprogramming factors Oct4, Sox2, Kfl4 and c-Myc were used in this thesis study. In addition to TeSR-E7 and Essential 8 media, Life technologies' homemade media recipes were also tested during the reprogramming process (Table 2.4). The protocol that was finally decided to be used is detailed below (Figure 2.1).

Table 2.1: Homemade reprogramming (ipsc) and ipsc maintenance (hesc) medium

iPSC Medium	
DMEM/F12	450ml
Defined FBS	50ml (10%)
NEAA	5ml (1%)
L-glutamine	5ml (1%)
ß- mercaptoethanol	3.5µl
b-FGF (100µg/ml)	50µl (10ng/ml)
L-ascorbic asid	50µg/ml
hESC Medium	
DMEM/F12	400ml
KOSR	100ml (10%)
NEAA	5ml (1%)
L-glutamine	5ml (1%)
ß-mercaptoethanol	3.5µl
b-FGF (100µg/ml)	50µl (10ng/ml)
L-ascorbic asid	50µg/ml

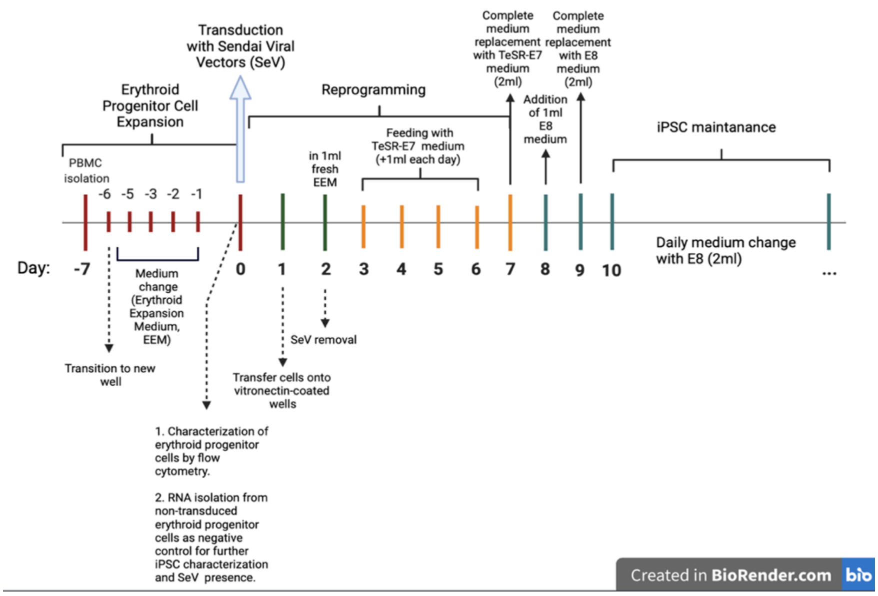

Figure 2.1: Flow chart of erythroid progenitor cell expansion and transduction with Sendai vectors by using commercial mediums.

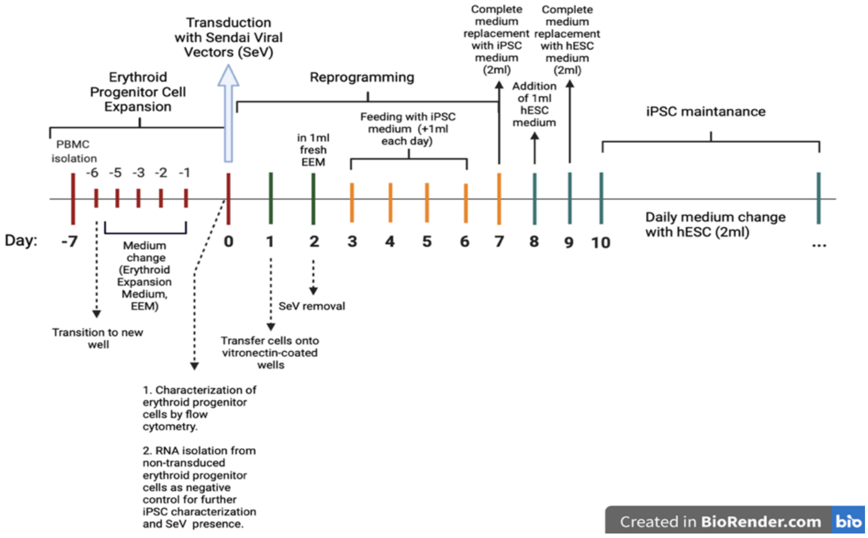

Figure 2.2: Flow chart of erythroid progenitor cell expansion and transduction with sendai vectors by using homemade mediums (table 2.4).

Day 0 (Transduction): Erythroid progenitor cells (EPCs) were collected in 15ml tubes and pelleted by centrifuging for 10 min at 300 x g. The supernatant was discarded, and cells were resuspended in 1ml supplemented StemSpan II medium. Cells were counted and resuspend in 1ml supplemented StemSpan II medium to bring the cell suspension to a concentration of 1x10^5 cells/ml and viral vectors were added vectors (transduce 1×10^5 cells with 5:5:3 MOI of hKos : hKlf4 : hc-Myc vectors). Cell suspension was transferred into a 10ml U-bottom centrifuge tube. Cells were centrifuged for 30 min at 1000 x g to increase reprogramming efficiency. Cells were seeded in 48-well plate, each well should contain 1ml cell suspension plus vectors. The plate was moved to incubator and cultured at 37°C, 5% CO_2.

Day 1 (seeded on vitronectin-coated plate): Cells were collected and seeded on vitronectin-coated 6-well plate (1x10^5 cell/well). 1ml EEM medium was added.

Day 2 (removal of viral vectors): Cells were collected in 15ml tubes and pelleted by centrifuging for 10 min at 300 x g and resuspended in 1ml fresh EEM medium.

Day 3-7 (feeding with TeSR-E7/ReproTeSR medium): 1ml of TeSR-E7 or ReproTeSR medium was added into transduced cells. Feeding was done daily until day 7. The medium was completely aspirated and changed with 2ml of TeSR-E7 or ReproTeSR medium on day 7.

Day 8-9: The cells were fed with 1ml of Essential 8 medium on day 8. The medium was completely aspirated and changed with 2ml of Essential 8 medium on day 9.

Day 10-…: The small colonies appear between day 7-10, the medium was changed daily with 2ml of Essential 8 medium. A significant amount of cell death was observed during this period. Well-defined iPSC colonies were appeared until day 15. Well-defined iPSC colonies were passaged for four times before colony picking. During the four passage, only completely reprogrammed cells could be attached and cultured on vitronectin-coated plates in Essential 8 medium. At this point, alkaline phosphatase (AP) staining, and Tra-1-60 live staining were done to validate the quality of iPSC plates. Three colonies were picked from iPSCs culture at passage 4 and expanded for characterization.

2.2.4. Induced Pluripotent Cell Culture and Characterization

In the routine follow-up culture of iPSCs, the medium was replenished daily. Essential 8 medium was used for daily medium changes. If the culture medium cannot be renewed daily, Stemflex medium was used. If it cannot be changed for one day, x2 volume was added, if it cannot be changed for two days, x3 volume medium was added.

The most critical point in iPSC passage is daily follow-up of colonies. Because their colony size expansion is logarithmic, they may need to be passaged earlier than expected. Before passage, new cell culture flasks from which iPSCs will be taken are coated with Vitronectin. Coating was done with 5 µg/ml Vitronectin in 1X DPBS, incubated for 1 hour at room temperature. After the coating was completed, the Vitronectin solution was aspirated, no washing is done, and Essential 8 medium was added to the cell flasks. Cells were removed from the incubator and used medium was removed. Cells were gently washed with 1X DPBS and Versene solution was added. It was incubated for 5-7 minutes at room temperature depending on the density of the cells. The Versene solution was aspirated in one stroke and the cells were removed by quickly squirting Essential 8 medium with a 10 ml serological pipette. The cell suspension was passaged at a ratio of 1:8 to 1:12. It should not be passaged too densely. iPSC cultures should be passaged approximately once a week, extensive passages may cause differentiation of cells.

The method used for freezing the cells is the same as for passage. Cells were frozen in 90% Essential 8 medium and 10% DMSO. While the cells were thawing, the cryovial removed from the liquid nitrogen was partially immersed in a water bath for about 30 seconds and when a small piece of ice remains, the cell suspension was transferred in 5 ml of Essential 8 containing 15 ml canonical tube. Cells were pelleted by centrifuge at 200x g for 5 min, the supernatant was removed and fresh medium containing 10 µM Revitacell was added. Cells were seeded on Vitronectin-coated cell flasks without pipetting.

For alkaline phosphatase staining, cells were seeded in an 8-well glass-bottom culture dish (#80807, Ibidi). After the colonies reached their expected morphology, they were washed 3 times with DMEM/F12 media without FBS and incubated for 30 min at 37°C with 200 µl of 1X working solution per well. After incubation, the solution was washed 2 times with DMEM/F12 without FBS, with 5 minutes holdings. After the last wash, DMEM/F12 media without FBS was added again and imaging was taken in the confocal microscope in the FITC channel.

For pluripotency gene expression analysis RT-PCR was used. In brief, total RNA isolation was completed with Pureizol RNA Isolation Reagent (Bio Rad, USA). cDNA synthesis was performed with 1 µg of RNA using the Iscript cDNA Synthesis kit (Biorad, USA). RT-PCR reactions were set up with SsoAdvanced univ SYBR Grn Suprmx (Biorad). Using the primers specified in Table 2.1.

Invitrogen Pluripotent Stem Cell 4-Marker Immunocytochemistry Kit (Invitrogen, USA) was used for the demonstration of pluripotency markers by immunochemistry and the protocol provided by the kit was applied. iPSC colonies were seeded in an 8-well glass-bottom culture dish (Ibidi, USA). Cell media was removed and incubated with fixative solution for 15 minutes at room temperature without washing. After the fixative solution was removed, the permeabilized solution was added and kept at room temperature for 15 minutes. After the permeabilized solution was removed, 100 µl of blocking solution was added and left at room temperature for 30 minutes. Primary antibodies are put directly into the blocking solution. Sox2 and Tra-1-60 antibodies were added to one group as 1 µl each. In the other group, SSEA-4 and Oct4 were added as 1 µl each. Antibodies were incubated at +4°C for 3 hours and washed 3 times with washing solution after incubation for 3 minutes. Again, secondary antibodies were added appropriately to primary antibodies in 100µl of blocking solution (Table 2.2). Secondary antibodies were incubated for 1 hour at room temperature and in the dark. After the secondary antibodies were washed 3 times with the washing solution for 3 minutes, they were covered with mounting media containing DAPI. Imaging was taken from the appropriate channels according to the em/ex values of the secondary antibodies selected in the confocal microscope.

Embryoid bodies were created using AggreWell800 (Stem Cell Technologies, Canada) plates. First, AggreWell anti-adherence rinsing solution (Stem Cell Technologies, Canada) was added to the plates and centrifuged for 5 minutes to remove the bubbles. After the solution was removed from the wells, it was washed with 2 ml of DMEM/F-12. iPSC colony cells resuspended as single cells with Accutase were seeded at $3x10^6$ per well with EB forming media (Stem Cell Technologies, Canada) containing 10 µM Revitacell. To fill the cells into the wells, they were centrifuged at 2000x g for 5 min and cultured in the incubator for 1 or 2 days. When cells are seeded into the wells, they should be as shown in Figure 2.3. After the embryoid bodies were collected from AggreWell, two different media were tried. Spontaneous differentiation was achieved using Essential 6 (Thermo, USA) or StemDiff Apel II (Stem Cell Technologies, Canada). However, daily follow-up of embryoid bodies showed that the morphology of embryoid bodies cultured in Essential 6 medium (Thermo, USA) progressed more smoothly than those in StemDiff Apel II (Stem Cell Technologies, Canada).

Immunofluorescence staining and RT-PCR were used to confirm the spontaneous differentiation of embryoid bodies. For this, on day 10 embryoid bodies were seeded on vitronectin and cultured until day 21. In the 11-day period, embryoid bodies release cells in the form of explant culture, allowing spontaneously differentiated cells to emerge. At the end of the 21st day, the cells were passaged using Versene solution and transferred to glass-bottom dishes. GATA4 was used for endodermal differentiation, Desmin for mesodermal differentiation, and Nestin for ectodermal differentiation (Table 2.5). Primers MAP2, alpha-SMA, and SOX17 were used for confirmation by RT-PCR (Table 2.1).

Karyotyping experiments completed by acquisition of services from the Microgen Genetic Diagnostics Company (Ankara)

2.2.5. Colon Organoid Formation

The StemDiff Intestinal Organoid kit from Stem Cell Technologies was used for colon organoid formation (05140, Stem Cell Technologies, Canada). Stepwise differentiation method was followed, monolayer iPSCs were differentiated into the definitive endoderm first and then the hindgut endoderm. In the hindgut differentiation process, spheroids were budding from monolayer endodermal cells. The collected hindgut spheroids were cultivated in Matrigel to obtain mature intestinal organoids.

The differentiation process was maintained in 24-well plates until the maturation phase of intestinal organoids. iPSCs were seeded as 4000, 5000, and 6000 clump/well. Optimization was done by trying different clump numbers. The most efficient starting number was found to be 6000 clump/well. Two wells were seeded for each iPSC line. Definitive endoderm differentiation was initiated when cells reached 85-90% confluency.

Definitive Endoderm Differentiation

Definitive endoderm (DE) Medium (1.98 ml StemDiff™ Endoderm Basal Medium + 20 ul StemDiff Definitive Endoderm Supplement CJ) used during Day 0 (0.7 ml), Day 1 (0.5 ml), and Day 2 (0.5 ml) 2 ml/well was prepared. On Day 0, 0.7 ml of DE medium was added dropwise onto the cells. In Day 1 and Day 2, the used medium was removed, and 0.5 ml of DE medium was added dropwise. One well of iPSCs was taken to flow cytometry to confirm definitive endoderm differentiation on Day 3 and hindgut differentiation was initiated in the other well. The increase in CXCR4 and CD117 markers was examined for confirmation of definitive endoderm differentiation.

Hindgut Differentiation

Mid-/Hindgut (MH) medium (2.94 ml StemDiff™ Endoderm Basal Medium + 30 µl StemDiff™ Gastrointestinal Supplement PK+ 30 µl StemDiff™ Gastrointestinal Supplement UB) was used during Day 3-8, 3 ml/well was prepared. Daily MH medium was changed (0.5 ml/day). The formation of hindgut spheroids began to be observed on the fourth day and it was observed that the spheroids were released in the medium in the following days. For this reason, care was taken to avoid loss of hindgut spheroids while medium changes were made from the fourth day. The hindgut spheroids collected on the seventh and eighth days, when spheroid secretion is most intense, were taken into Matrigel for intestinal organoid formation. After spheroids were harvested, the remaining monolayer cells were used to confirm hindgut differentiation.

Colonoid Formation

After all the collected spheroids were taken into 15 ml canonical tubes, they were left to settle on ice for 5-10 minutes depending on the spheroid density. The supernatant was carefully removed. 1 ml of DMEM/F12 with 15 mM HEPES was added onto the spheroids and centrifuged at 300 x g for 15 min at room temperature. As much supernatant as possible was removed. Matrigel was added to canonical tubes at 50 µl/dome. Bubble-free spheroids were provided by pipetting evenly dispersed in Matrigel. The Matrigel-spheroid mixture was deposited as a droplet on the 24-well plate, neither too slowly nor too quickly. At this stage it is critical to keep the pipettor upright and only press down to the first stop of the pipette. For the polymerization of the Matrigel, 0.5 ml/well OGM medium was added slowly after incubation for 5 minutes at room temperature and 10 minutes at 37°C. The medium was changed every four days and passaged once a week.

2.2.6. Bioinformatics Analysis

IlluminaSeq6000 platform was used for RNA sequencing and Illumina RNA library prep set (Illumina, #20040525) was used for the library preparation according to the manufacturer's protocol. RNA sequencing completed by service acquisition from AgriBio (Ankara). FastQC (v 0.11.5), Fastq screen (v0.9.3), and MultiQC were used to assess sequencing quality control (v1.8dev). TrimGalore! (v0.6.4) was used to remove adapters and low-quality bases from reads before aligning them to the human genome (GRCh38) with HISAT2 (v2.2.1), with a mean of 90.4 percent reads uniquely mapping and a mean of 56 M paired reads/sample. HTSeq-Counts were used to determine gene quantification (v0.6.1p1). Counts extracted with HTSeq-counts were used in R (version 3.5.2) to perform differential gene analysis with the package DESeq2 (v.1.22.2).

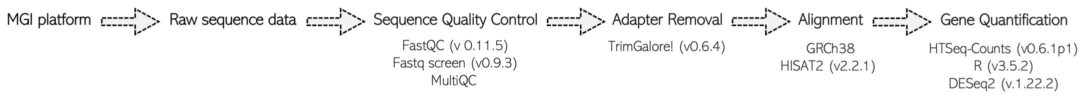

Figure 2.3: Flowchart of RNA sequencing analysis.

There were no overlaps between our gene lists (P value < 0,05). The read counts were normalized based on the estimated size factors. All genes were subjected to Principal Component Analysis (PCA) using log-transformed count data. GO and Kegg pathway analysis were performed on DEGs with absolute log2 fold change >1 and adjusted P value 0.05 using the clusterProfiler package (v.3.10.1). The Wang lab (16) provided the data matrix for the RNA-seq data. The regularized log transformation function (from the DESeq2 package) was used to calculate heatmap counts. Heatmaps were created using the R package 'ComplexHeatmap' (v 1.20.0). The differentially expressed genes on heatmaps were chosen based on their significance (lowest adjusted P value) and absolute log2 fold changes. The RcisTarget R package was used to investigate potential placental regulatory networks (v.1.2.1).

2.2.7. Statistical Analysis

Results are given as mean SD. For independent samples t-test was used to compare the experimental groups with control (GraphPad Inc.). For the p-value, $p < 0.05$ was considered statistically significant.

3. RESULTS

We used human PBMCs as the starting material for iPSC reprogramming. At the beginning, we isolated PBMCs from peripheral blood sample of healthy donors, colorectal cancer (CRC) patients, and CRC patients with metastasis (mCRC). To prepare more potent cell population to ease reprogramming process, all PBMC samples were enriched for erythroid progenitor cells, and characterized with erythroid markers. Then, reprogramming procedure was initiated with Sendai viral vector system. After the confirmation experiments were completed for pluripotency characteristics of iPSC-lines, intestinal organoid differentiation was started. Organoid formation is a stepwise procedure, all three main steps of intestinal tissue development were successfully accomplished, total RNA isolation was done for RNA sequencing. Illumine MGI system was used for RNA sequencing.

3.1. Erythroid Progenitor Cell Enrichment and Characterization

The erythroid progenitor expansion kit suggests that after 14 days of culture, the erythroid cells will reach the appropriate density for transduction. The first experiment was completed according to the manufacturer's protocol by culturing Control #1 in EEM for 14 days. However, at the end of the 14th day, there were significant deteriorations in the morphology of the cells. Subsequent Sendai virus transduction was unsuccessful. In addition, 50.000 and 100.000 cells/ml concentration were tried as the kit's recommended cell number range. As flow cytometry, total RNA isolation and Sendai vector transduction are must for further with the cells obtained at the end of erythroblast expansion, 50.000 cells could not reach the sufficient number at the end of the expansion period. Other expansion procedures were started with at least

100.000 cells.

At the end of the 7th day of expansion, cell morphologies were as expected. Flow cytometry characterizations of erythroid progenitor cells were performed on either day 7 or day 8 as the cell morphologies were not affected by an additional 24-hour (Figure 3.1). In addition, total RNA was isolated from cells as a non-transduced control. The non-transduced control will be used both as a control to demonstrate removal of Sendai vectors in advanced passages (passages 20-25) and as a non-reprogrammed control for iPSC characterization.

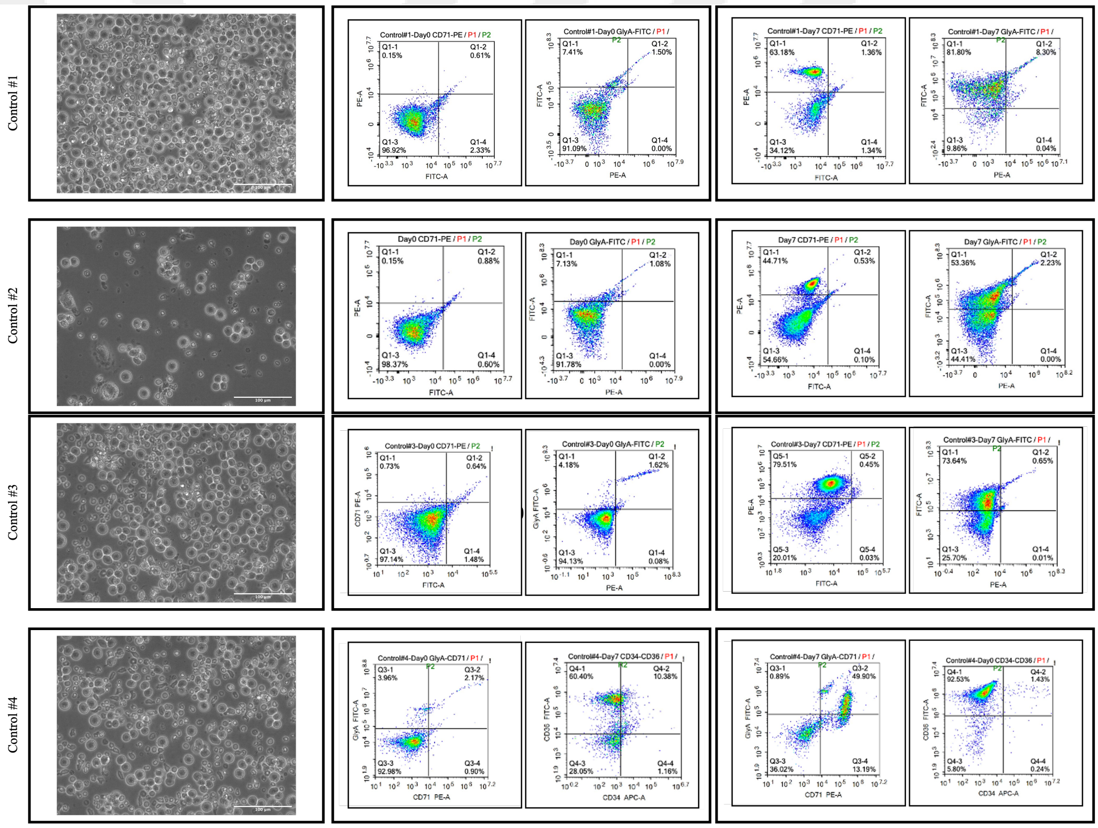

Figure 3.1: Healthy donors' EPC morphology (left panel) and erythroid markers expression change after the enrichment process. Flow cytometry results for CD71 and GlyA are shown. Expression levels were compared between day 0 (middle panel) and day 7 (right panel).

For erythroid characterization, CD71 and CD235a (GlyA) surface markers were chosen. Enrichment process took 7 days long and marker comparison was done between day 0 and day 7 samples. All samples were characterized with CD71 and GlyA but Control #4 and all mCRC samples were also examined for CD34 and CD36 markers. In fact, it was planned to examine the expressions of the four markers in all samples. However, due to a delay in the delivery of CD34 and CD36 antibodies, four markers could be studied for the last five samples taken. Since all the samples used in the thesis study were human samples, it was not possible to collect blood samples retrospectively during the process, so CD34 and CD36 expressions of other donors could not be examined.

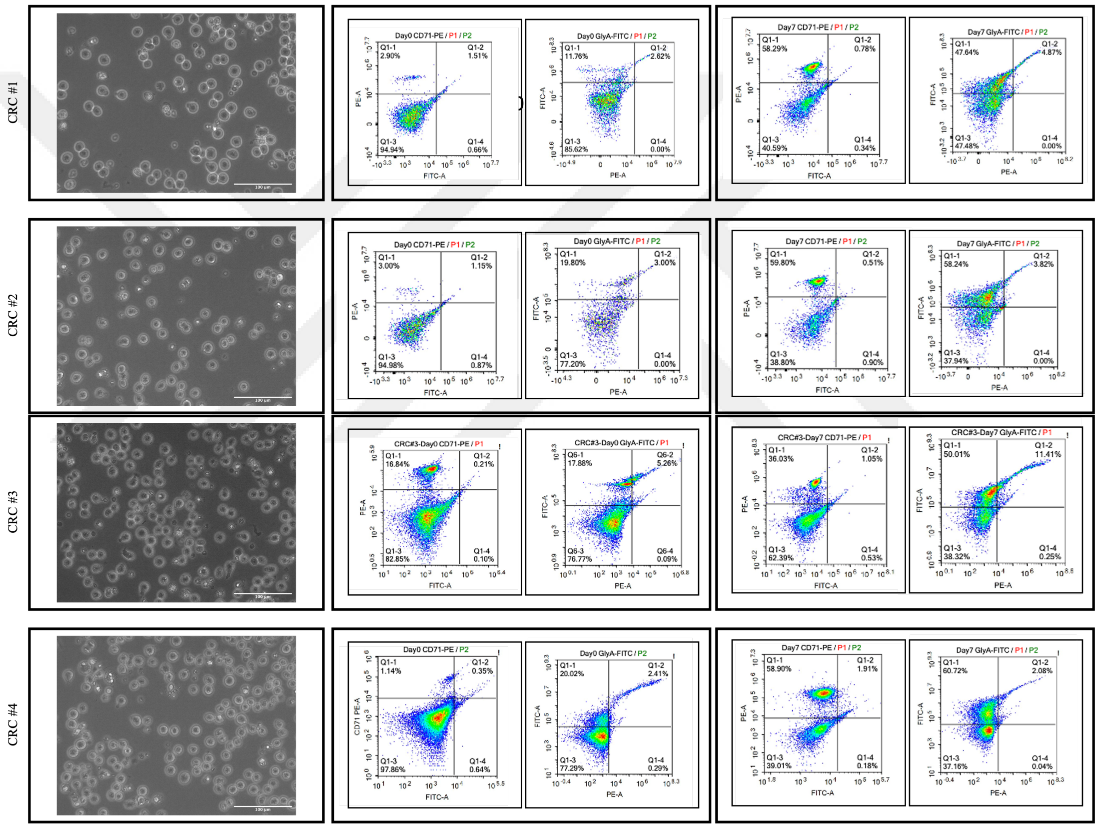

Figure 3.2: CRC donors' EPC morphology (left panel) and erythroid markers expression change after the enrichment process. Flow cytometry results for CD71 and GlyA are shown. Expression levels were compared between day 0 (middle panel) and day 7 (right panel).

Our expression analysis has shown erythroid marker expression change was varied among the groups after the enrichment (Table 3.1). Healthy donors had higher expression increase in GlyA and CD71 (Figure 3.1). The fold increase of GlyA varied among CRC donors but the fold change in CD71 expression was quite similar between donors (Figure 3.2). The increase in CD36 expression was less than the other two markers. CD36 increases of CRC and mCRC donors have close values (Figure 3.2 and 3.3).

Table 3.1: Representation of increase in erythroid markers as fold difference after 7 days of enrichment.

	GlyA	CD71
Control #1	55,63	10,11
Control #2	43,9	6,22
Control #3	58,36	12,8
CRC #1	13,39	3,65
CRC #2	14,53	2,67
CRC #3	2,17	2,65
CRC #4	40,8	2,8

	GlyA-CD71	CD36
Control #4	9,1	1,53
mCRC #1	8,53	1,5
mCRC #2	1,67	1,46
mCRC #3	1,6	1,64
mCRC #4	6,05	1,69

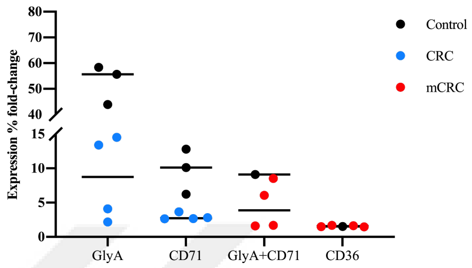

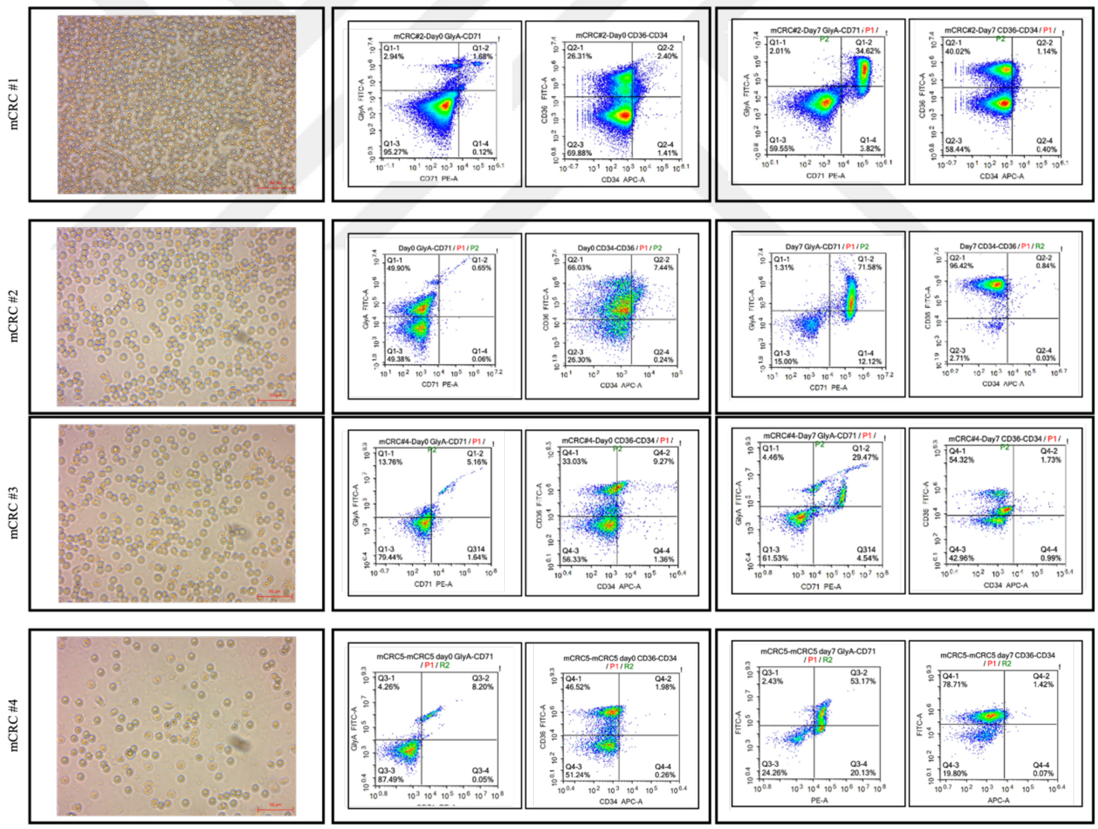

Figure 3.3: mCRC donors' EPC morphology (left panel) and erythroid markers expression change after

the enrichment process. Flow cytometry results for CD71 and GlyA (middle panel); CD36 and CD34 (left panel) are shown. Expression levels were compared between day 0 and day.

The system used for reprogramming in this study is the Sendai viral vector system. The recommended MOI values for hKOS:hc-myc:hKlf4 in the manufacturer's protocol are 5:5:3, respectively. It has been shown in the literature that these values can be optimized and reduced (Yilmazer-Aktuna et al., 2017). Initially, two different MOI ratios were tried: 5:5:3 and 3:1:2. Also, the recommended starting cell count in the manufacturer's protocol is between $2.5x10^5$ and $5x10^5$. As in this study, human samples were studied, reducing the initial cell number was done to prevent re-sampling for possible repetitions of experiments. For this reason, the initial reprogramming experiments were completed with $5x10^4$ and 10^5 cell numbers for the first donor. Finally, regarding the reprogramming procedure, both commercial media and homemade recipes. Four experimental groups were planned for the conditions to be optimized (Figure 3.4).

The kit's protocol recommends transduction in a 12-well plate. There are publications in the literature that seed 10^4 cell/well into a 96-well plate on the day of transduction to increase efficiency (Ye et al., 2013). We used 48-well plate for the transduction because the 96-well plate would be too narrow for $5x10^4$ and 10^5 cells (Day 0). In the standard Sendai transduction protocol, centrifugation is recommended on Day 1 to remove the Sendai vectors. However, some PBMC-reprogramming protocols suggesting that washing should be done on the second day to increase reprogramming efficiency. In addition, although the protocol recommends seeding cells on vitronectin on day 3, we observed that seeding cells on Day 1 increased the efficiency. While the cells were taken into vitronectin-coated wells, 1ml EEM medium was added to reduce the toxic effect of the vectors.

iPSC colonies were obtained from the four optimization setups; however, the fastest reprogramming was seen in Group D (Figure 4.4). The MOI values (5:5:3) and the initial cell number (10^5) were kept constant, only the efficiency of the mediums used was tested in the second iPSC reprogramming experimental setup as we confirmed that homemade mediums are also suitable for reprogramming.

Homemade mediums were found to be more efficient in reprogramming when compared to commercial mediums. However, after the formation of iPSC colonies, commercial mediums were found to be more suitable for maintaining the stability of the colonies without differentiation and keeping them healthy after passaging. Early colonies appeared in four days late in cells cultured in commercial mediums (data not shown). Experiments were continued with commercial media as there was no problem with the formation of colonies even if the reprogramming were completed in homemade medium. The main reason why homemade media were tested, especially during the reprogramming process, was that the ReproTeSR medium ordered has not yet been delivered when the experiments started. We had TeSR-E7 medium which is especially used for reprogramming adherent cells. However, TeSR-E7 has also been shown to work in erythroid progenitors.

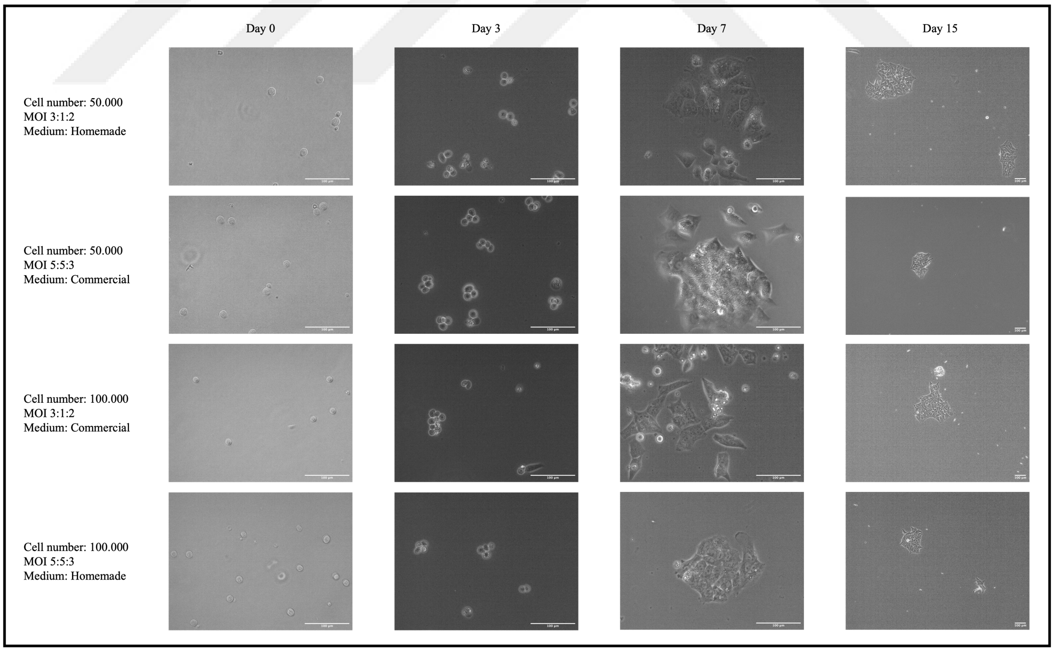

Figure 3.4: The effects of different transduction conditions on cell morphology and reprogramming efficiency. Day 0/3/7/10 photos are shown for the same donor.

3.2. iPSC Characterization

Colonies began to appear from the 7th day after transduction into erythroid precursor cells. Both donor and patient iPSC colonies were observed to have cobble-like structure, round shape, large nucleus, and compact multicellular colonies at day 10. After the colonies were formed, four total passages were performed. In passage 4, ALP activity was confirmed by live alkaline phosphatase staining prior to colony selection (Figure 3.5). Colonies with expected ALP activity and appropriate morphology were selected by microdissection method. At least 3 healthy colonies were selected from each donor, expanded and frozen. However, due to the large sample size of the study, further experiments were advanced with one clone for each donor. Clones passaged two more times after colony selection were tested in passage 7 by immunofluorescent staining and qRT-PCR for markers of pluripotency (Figure 3.6-3.8).

The expression of pluripotency factors (OCT4, SSEA4, TRA1-60 and SOX2) for one of each selected clone was studied at protein level. It was observed that all colonies were positive for the stated pluripotency factors (left and middle panel of Figure 3.6-3.8). No significant difference was observed between colonies.

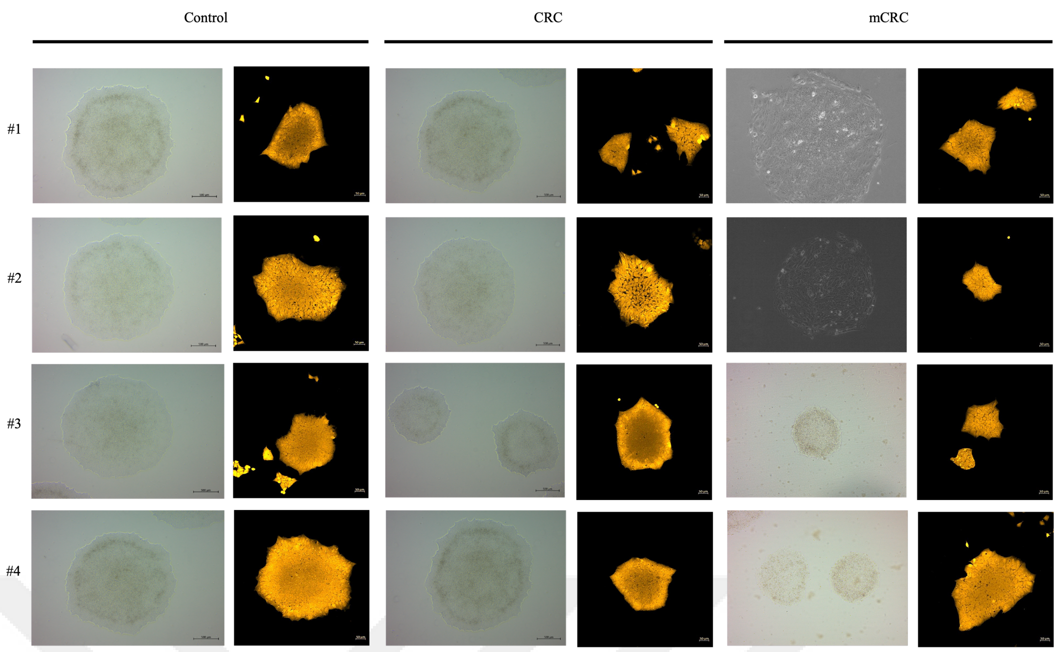

Figure 3.5: The representative photographs of passage 4 iPSC colonies and alkaline phosphatase staining of each donor. Colony picking was performed after ALP staining.

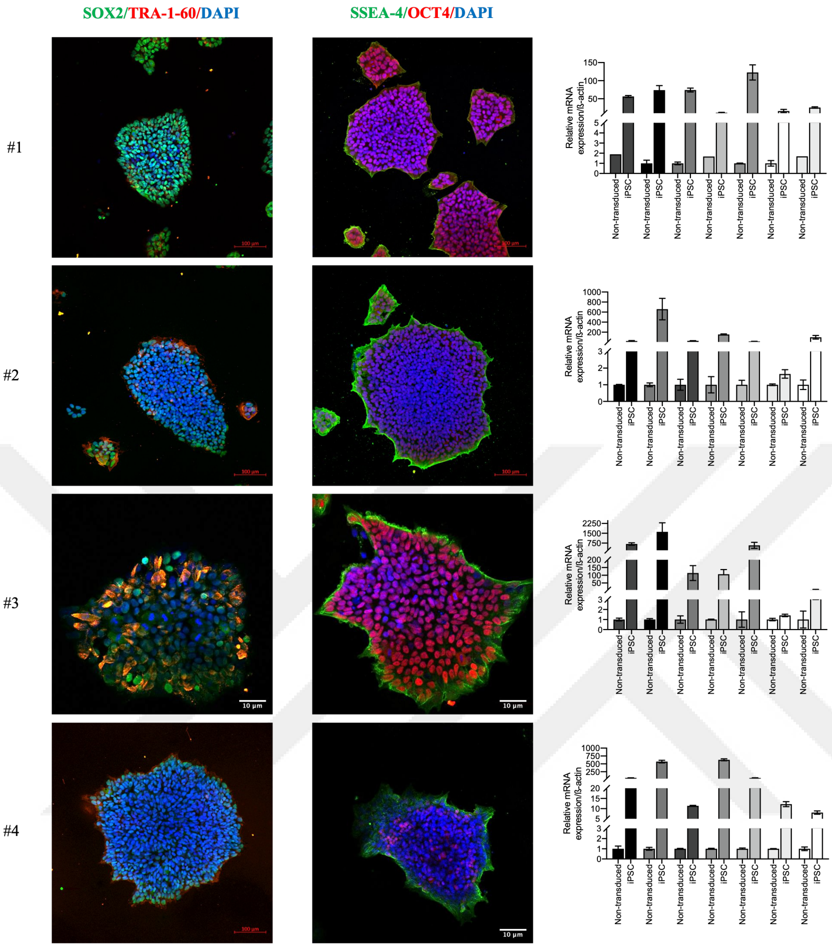

Figure 3.6: Pluripotency validation of control iPSCs derived from healthy donors. SOX2 and TRA-1-60 staining (left panel), SSEA4 and Oct4 staining (middle panel) were shown. Reactivation of the endogenous pluripotency genes and other regulators in erythroblast-derived iPSCs (passage 7). Total RNA from parental cells and reprogrammed iPSCs were isolated, reverse transcribed and analyzed by qRT-PCR for relative transcript levels of the endogenous pluripotency markers and other regulator genes (SOX2, OCT4, NANOG, DNMT3A, REX1, CDH1, UTF1). Expression levels were normalized to ß-actin.

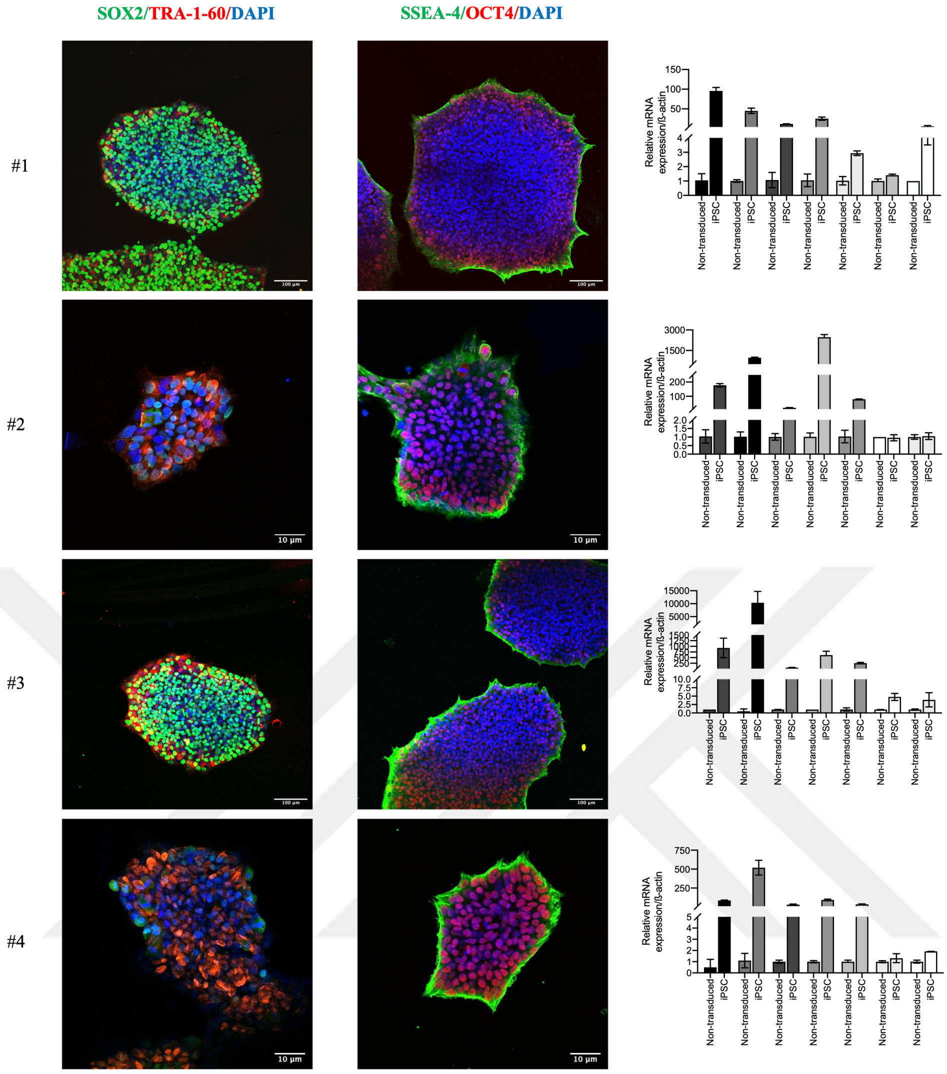

Figure 3.7: Pluripotency validation of CRC iPSCs derived from colorectal cancer patients. SOX2 and TRA-1-60 staining (left panel), SSEA4 and Oct4 staining (middle panel) were shown. Reactivation of the endogenous pluripotency genes and other regulators in erythroblast-derived iPSCs (passage 7). Total RNA from parental cells and reprogrammed iPSCs were isolated, reverse transcribed and analyzed by qRT-PCR for relative transcript levels of the endogenous pluripotency markers and other regulator genes (SOX2, OCT4, NANOG, DNMT3A, REX1, CDH1, UTF1). Expression levels were normalized to ß-actin.

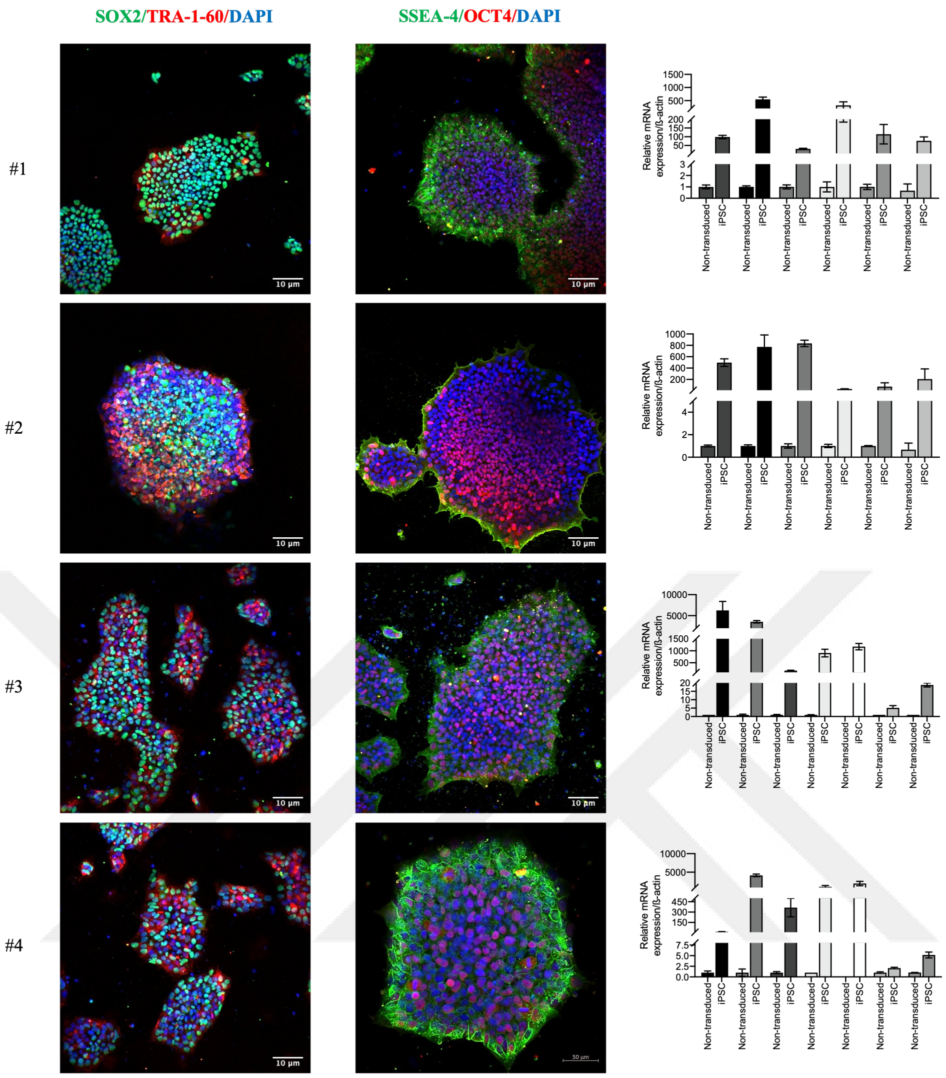

Figure 3.8: Pluripotency validation of mCRC iPSCs derived from colorectal cancer patients with metastasis. SOX2 and TRA-1-60 staining (left panel), SSEA4 and Oct4 staining (middle panel) were shown. Reactivation of the endogenous pluripotency genes and other regulators in erythroblast-derived iPSCs (passage 7). Total RNA from parental cells and reprogrammed iPSCs were isolated, reverse transcribed and analyzed by qRT-PCR for relative transcript levels of the endogenous pluripotency markers and other regulator genes (SOX2, OCT4, NANOG, DNMT3A, REX1, CDH1, UTF1). Expression levels were normalized to ß-actin.

The differentiation potential of spontaneously differentiated embryoid bodies (EB) into three germ layers was evaluated. In order to evaluate the *in vitro* differentiation potential of iPSCs, the EB formation assay was conducted from iPSC colonies in passage 20 with prominent edges and a compact structure, and embryoid bodies were obtained with AggreWell plates. After EBs were allowed to differentiate spontaneously, significant morphological changes (increased in size, prominent in three-dimensional spheroid appearance, different density areas, cystic formations, and proliferating inner cell mass) were observed from the first day to the 21st day, similar to the early period of embryogenesis. The change in the morphology of EBs has been shown in Figure 3.9.

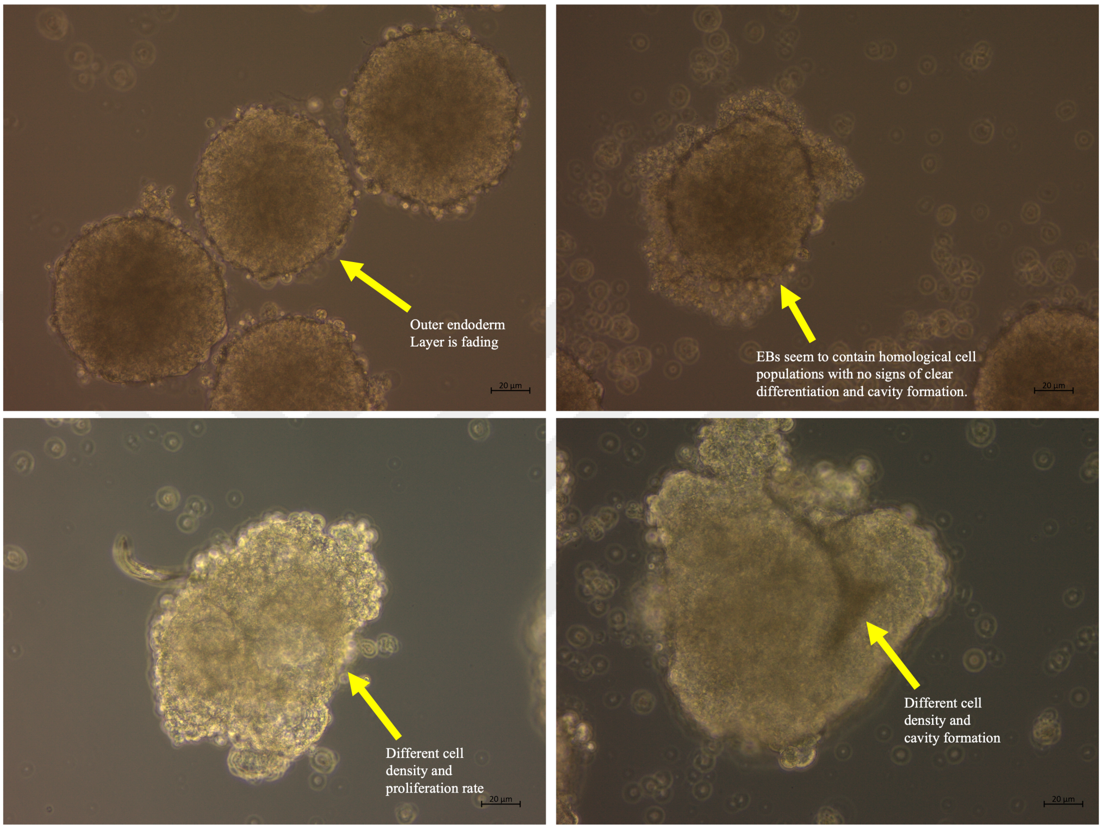

Figure 3.3: Morphological changes of EBs during spontaneous differentiation for 21 days.

The differentiation potential of clones from four healthy donor and eight patients into three germ sheets (ectoderm, endoderm, mesoderm) was demonstrated by immunofluorescent staining at the protein level. On day 21, each of the EBs showed positive signal in triple staining with anti-GATA4 (endoderm), anti-Nestin (ectoderm), anti-Desmin (mesoderm) antibodies (Figure 3.10-3.12).

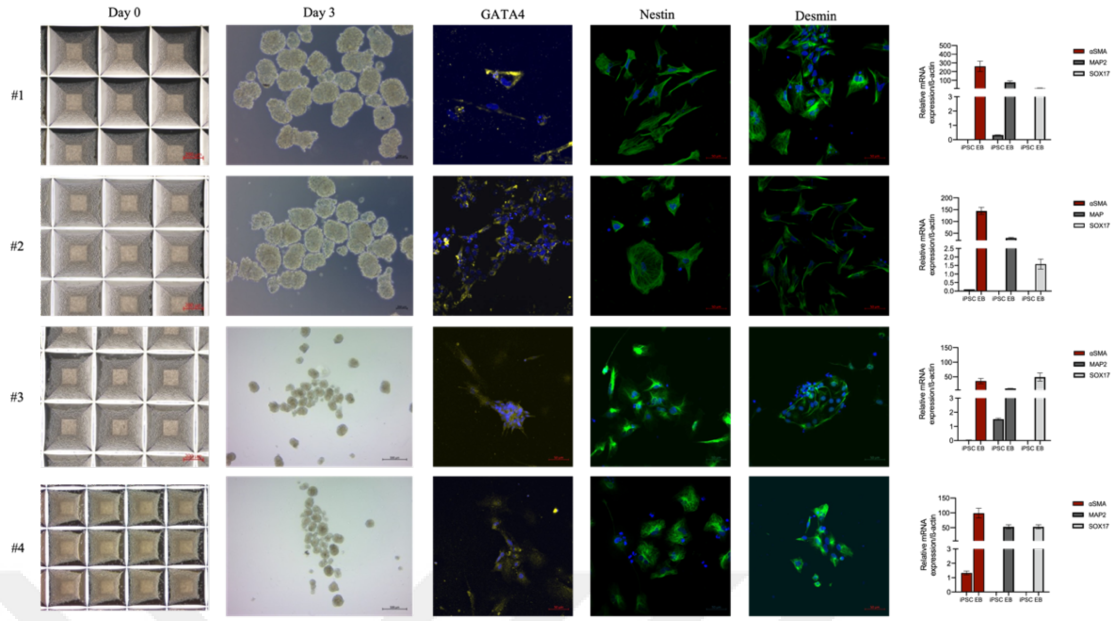

Figure 3.4: Evaluation of the in vitro differentiation potential of healthy donors iPSCs by spontaneous differentiation of EBs. Day 0 and 3 images of EBs in the AggreWell (first two columns from the left). From the 7th day onwards, differences began to be observed between embryonic bodies. Reactivation of the selected 3-germ layer genes in iPSC-derived EBs (day 21). GATA4, Nestin, and Desmin were stained for each distinct germ layer. Total RNA of iPSCs and EBs were isolated, reverse transcribed and analyzed by qRT-PCR for relative transcript levels of MAP2, aSMA and SOX17 (The right column). Expression levels were normalized to ß-actin.

The potential for iPSCs to differentiate into three germ sheets was demonstrated at the mRNA level by qRT-PCR. The endogenous control gene β-actin was used. Undifferentiated iPS cells of each donor was used as control and $2^{-\Delta\Delta CT}$ value was calculated by normalizing according to these values. On day 14, ectodermal MAP2, endodermal SOX17 gene expression, and mesodermal α-SMA gene expression were examined (the right column of Figure 3.10-3.12). The representative karyotype analysis was given in Figure 3.13.

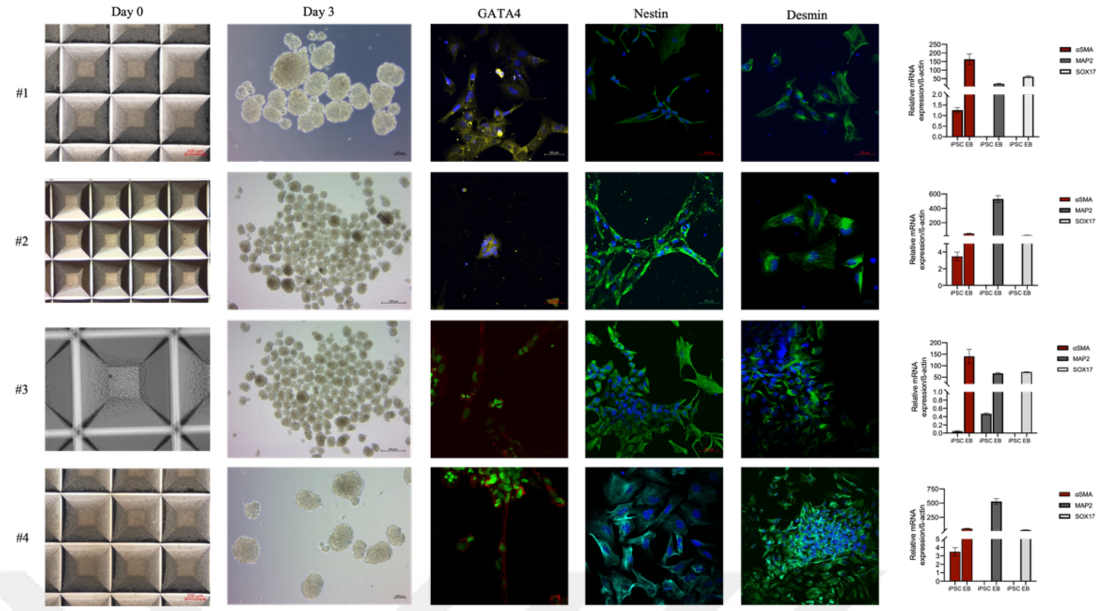

Figure 3.5: Evaluation of the in vitro differentiation potential of CRC patients-derived iPSCs by spontaneous differentiation of EBs. Day 0 and 3 images of EBs in the AggreWell (first two columns from the left). From the 7th day onwards, differences began to be observed between embryonic bodies. Reactivation of the selected 3-germ layer genes in iPSC-derived EBs (day 21). GATA4, Nestin, and Desmin were stained for each distinct germ layer. Total RNA of iPSCs and EBs were isolated, reverse transcribed and analyzed by qRT-PCR for relative transcript levels of MAP2, aSMA and SOX17 (The right column). Expression levels were normalized to ß-actin.

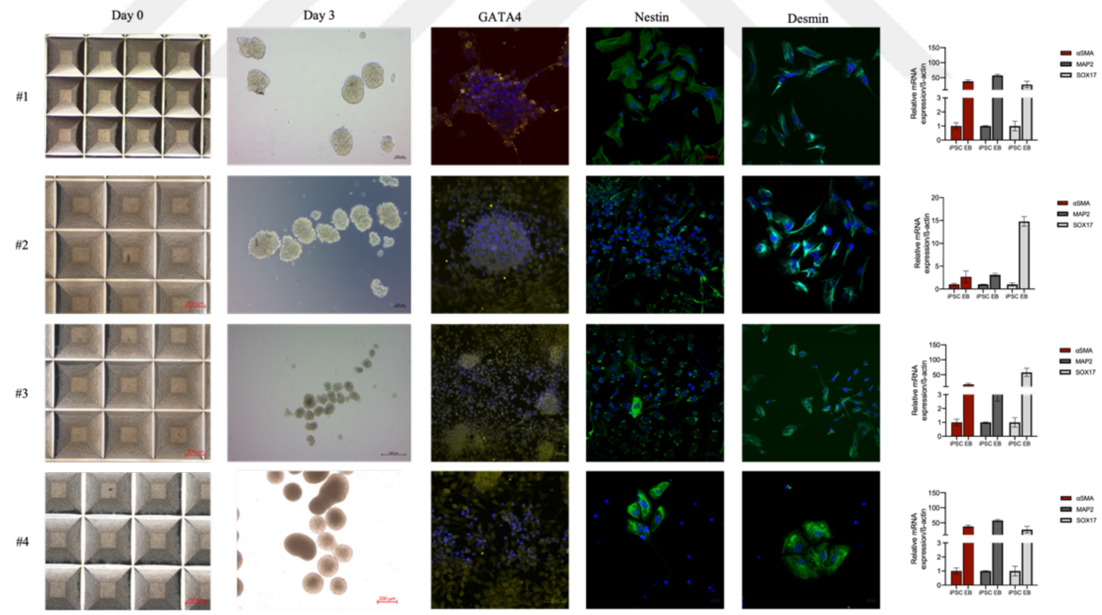

Figure 3.6: Evaluation of the in vitro differentiation potential of metastatic CRC patients-derived iPSCs by spontaneous differentiation of EBs. Day 0 and 3 images of EBs in the AggreWell (first two columns from the left). From the 7th day onwards, differences began to be observed between embryonic bodies. Reactivation of the selected 3-germ layer genes in iPSC-derived EBs (day 21). GATA4, Nestin, and Desmin were stained for each distinct germ layer. Total RNA of iPSCs and EBs were isolated, reverse transcribed and analyzed by qRT-PCR for relative transcript levels of MAP2, aSMA and SOX17 (The right column). Expression levels were normalized to ß-actin.

A.

B.

C.

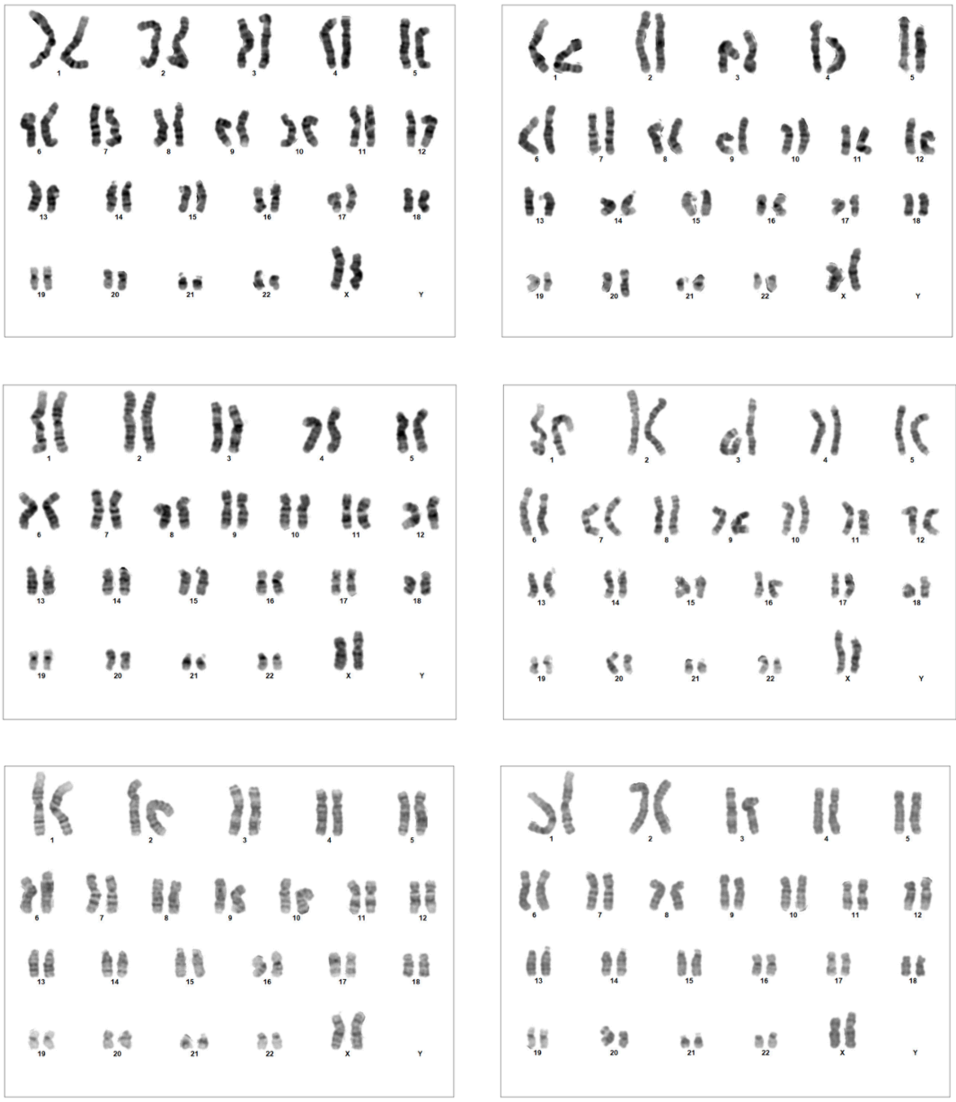

Figure 3.13: Chromosome karyotyping images after chromosome banding was performed for contro (A)l, CRC (B), mCRC (C) donors.

3.3. Intestinal Organoid Differentiation

Intestinal organoid differentiation is a stepwise differentiation process: definitive endoderm (DE) differentiation (DED), hind/mid-gut (HD) differentiation (HGD), and intestinal organoid (IO) formation (IOD). Each step has to be tested for its own specific markers with either flow cytometry or immunofluorescence staining.

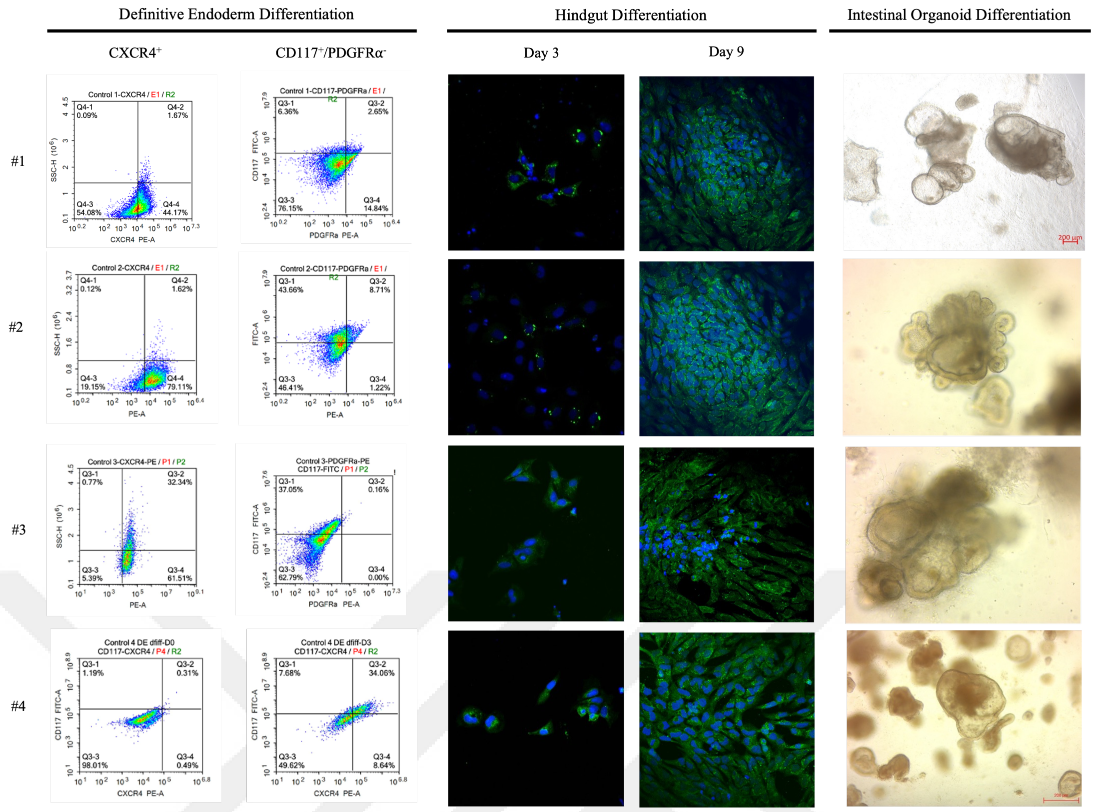

Figure 3.14: Evaluation of the in vitro differentiation of healthy donors' iPSCs into intestinal organoids. The definitive endoderm differentiation process was confirmed with flow cytometry analysis for CXCR4, CD117, and PDGFRa (the left column). The hindgut differentiation was confirmed with CDX2 protein expression (the middle column) and the intestinal organoid formation was tracked by morphological evaluation until the passage number 10 (the right column).

CXCR4 and CD117 were examined for definitive endoderm characteristics after the 3-day of DED, PDGFRa is also a common negative marker for DE cells. All groups were examined for these three markers with flow cytometry (Figure 3.14-16). All flow cytometry experiments were set as two separate groups: CXCR4 and CD117-PDGFRa. Only Control #4 and mCRC #2 were examined for the DE markers on day 0 and day 3. These samples are the very first samples that differentiated into DE and day 0 to day 3 comparison was must at the beginning. Additionally, PDGFRa cannot be evaluated for Control #4 and mCRC #2 samples as the antibody delivery was delayed and DE differentiation process was done before the delivery. Unfortunately, because of the sample size Control #4 and mCRC #2 cannot be differentiated again in order to get another flow cytometry result for DE markers. The expression of DE markers as percentage showed in Table 3.2.

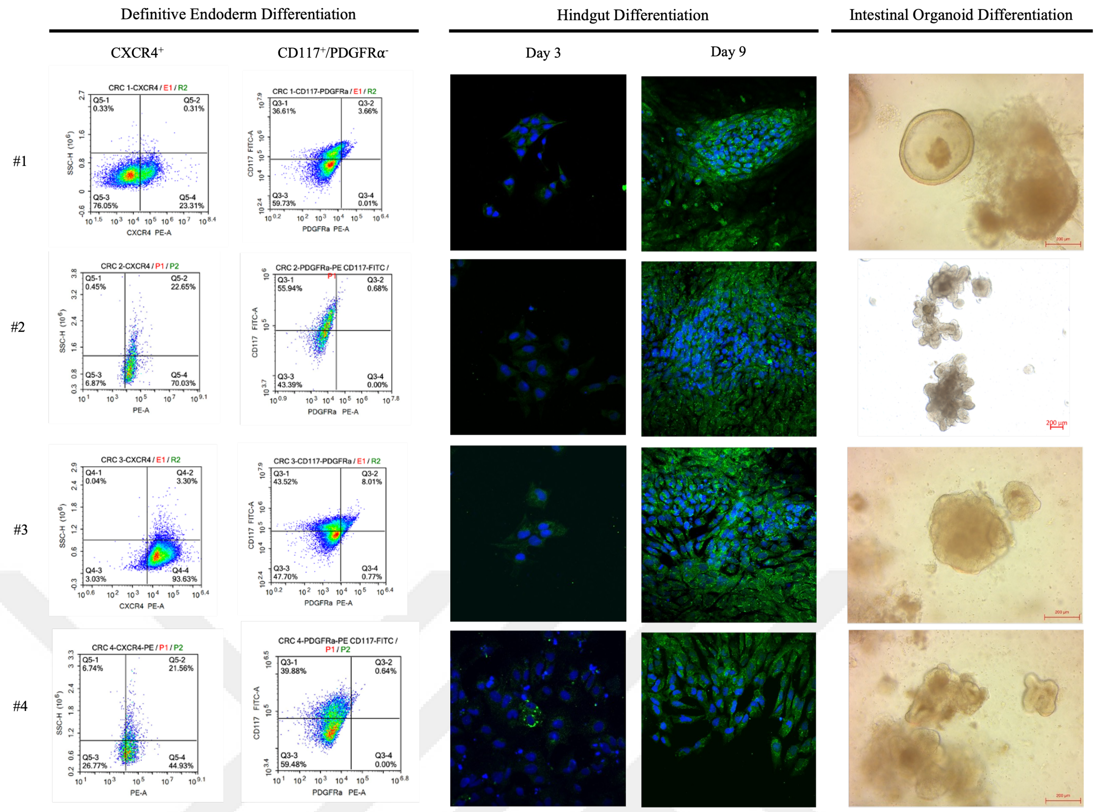

Figure 3.15: Evaluation of the in vitro differentiation of CRC patients' iPSCs into intestinal organoids. The definitive endoderm differentiation process was confirmed with flow cytometry analysis for CXCR4, CD117, and PDGFRa (the left column). The hindgut differentiation was confirmed with CDX2 protein expression (the middle column), and the intestinal organoid formation was tracked by morphological evaluation until the passage number 10 (the right column).

CDX2 is a well-known and most commonly used HD cell marker. CDX2 protein expression levels were examined with immunofluorescence staining and the difference between the CDX2 expression was dramatically increased at the end of HDD (Figure 3.14-16).

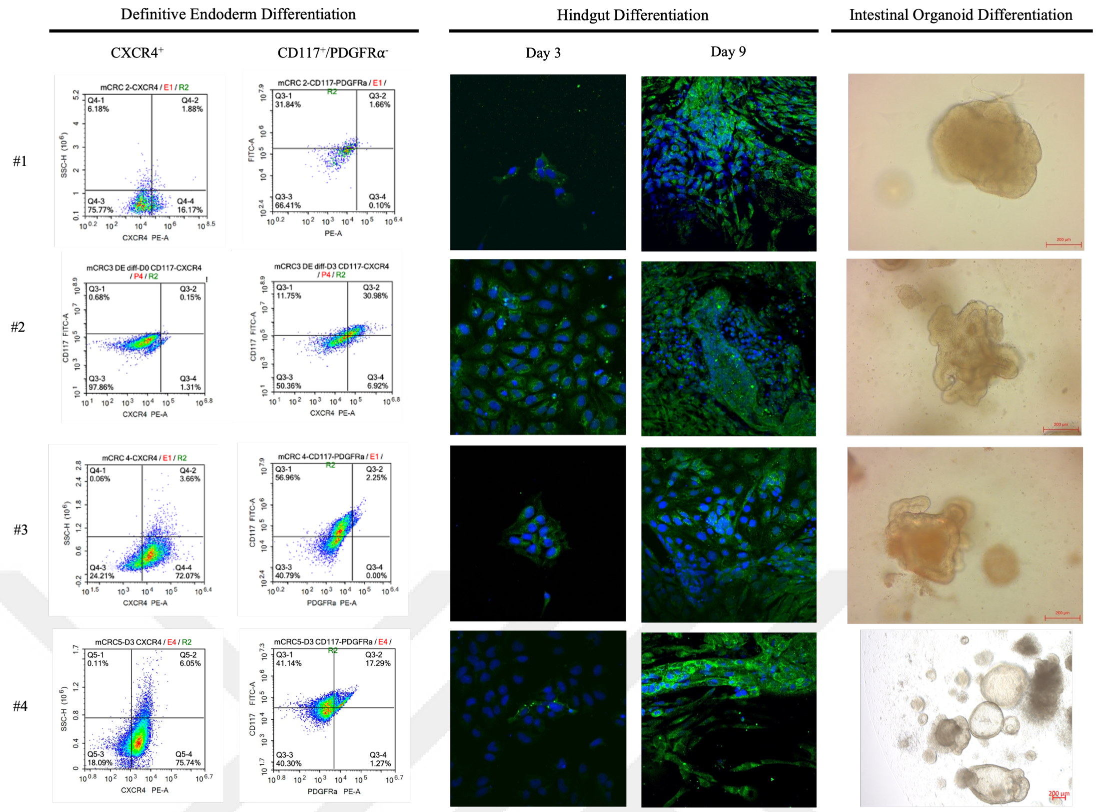

Figure 3.16: Evaluation of the in vitro differentiation of metastatic CRC patients' iPSCs into intestinal organoids. The definitive endoderm differentiation process was confirmed with flow cytometry analysis for CXCR4, CD117, and PDGFRa (the left column). The hindgut differentiation was confirmed with CDX2 protein expression (the middle column), and the intestinal organoid formation was tracked by morphological evaluation until the passage number 10 (the right column).

Table 3.2: Expression of definitive endoderm markers as percentage after 3 days of differentiation.

	CXCR4	CD117	PDGFRa
Control #1	45,84	9,01	17,49
Control #2	80,73	52,37	9,93
Control #3	93,85	37,19	0,16
CRC #1	23,62	40,27	3,67
CRC #2	92,68	56,62	0,68
CRC #3	96,93	51,53	8,78
CRC #4	66,49	40,52	0,64
mCRC #1	18,05	33,5	1,76
mCRC #3	75,73	59,21	2,25
mCRC #4	81,79	52,43	18,56

	CXCR4 (Day 0-3)		CD117 (Day 0-3)	
Control #4	1.5	52,8	0,8	9,93
mCRC #2	1,46	37,9	0,83	42,7

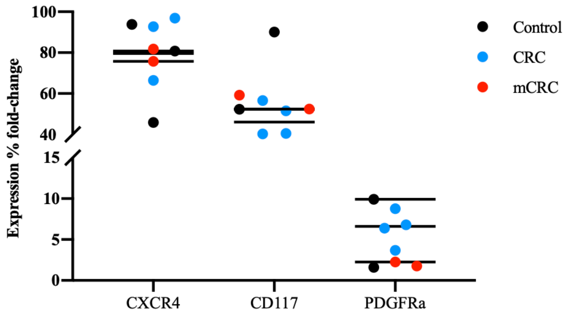

Intestinal organoid differentiation is a long process that can be extended for unlimited time period. In this thesis study, all organoid samples were passaged weekly and characterization analysis and RNA sequencing done at the passage number 10. IOs' morphology set after the passage number 3 and did not change at this point. Chromogranin A, KLF5, FOXA2, Villin, lysozyme, LGR5, and CDX2 were examined as intestinal cell population markers (Figure 3.17).

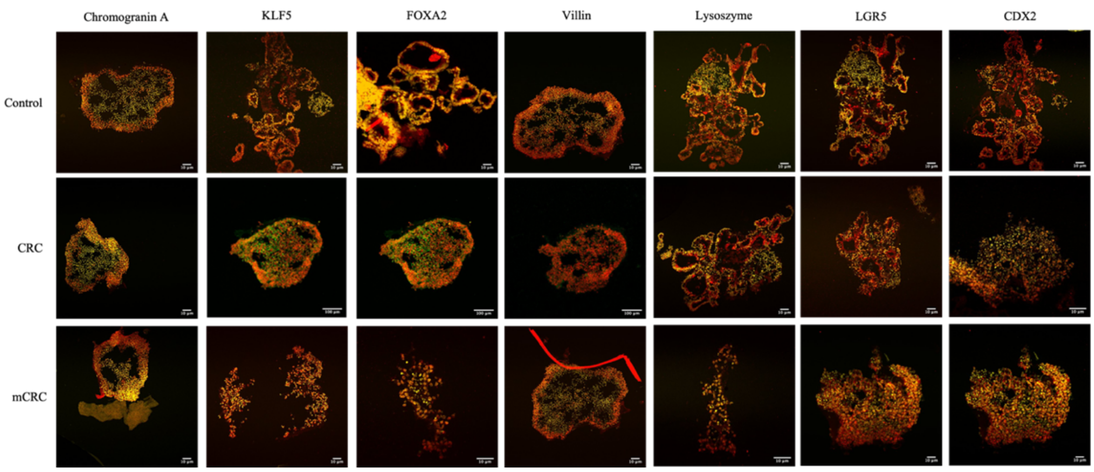

Figure 3.17: Chromogranin A, KLF5, FOXA2, Villin, lysozyme, LGR5, and CDX2 were examined as intestinal cell population markers. Intestinal organoids were frozen sectioned (4 µm) and stained.

3.4. RNA Sequencing and Enrichment Analysis

Total RNA isolation was done for three samples from each group. RNA concentrations were measure before RNA samples were processed for library preparation. Additionally, RNA integrity was checked by gel electrophoresis (Table 3.3).

Table 3.3: RNA concentrations of intestinal organoids after total RNA isolation with trizol and RNA gel image for the evaluation of RNA integrity.

	260/280	ng/µl	2% agarose gel
Control #1	2.084	169.586	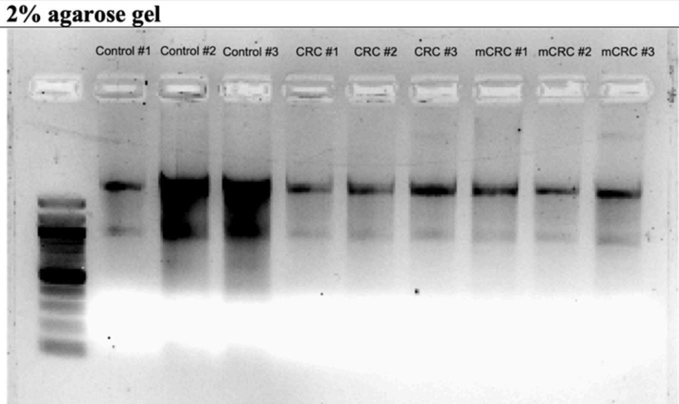
Control #2	2.15	352.16	
Control #3	2.05	669.215	
CRC #1	2.1	162.413	
CRC #2	2.1	178.71	
CRC #3	2.07	218.464	
mCRC #1	2.1	252.422	
mCRC #2	2.1	192.06	
mCRC #3	2.1	184.701	

Illumina platform was used for RNA sequencing, quality control analysis results of each sample were in Appendix 1. Differential gene expression analysis and all calculations were done for Control vs CRC, Control vs mCRC, and CRC vs. mCRC groups.

The data obtained after the initial analysis and normalization of the RNA sequence results are in figures 3.18. The variance plot obtained by comparing the RNA sequence results are also shown in figure 3.19. In figure 3.19, each dot symbolizes a gene, the blue dots indicate statistically significant genes with p value. Those above the midline indicate genes that are upregulated, and those below the midline indicate genes that are downregulated.

Differential expression analysis was completed from the bulk RNA-seq results. Genes obtained were filtered according to the p-values of log_2FC, and genes with a p-value less than 0.05 were loaded into GeneCodis4. All comparisons were analyzed separately (Control vs CRC, Control vs mCRC and CRC vs mCRC).

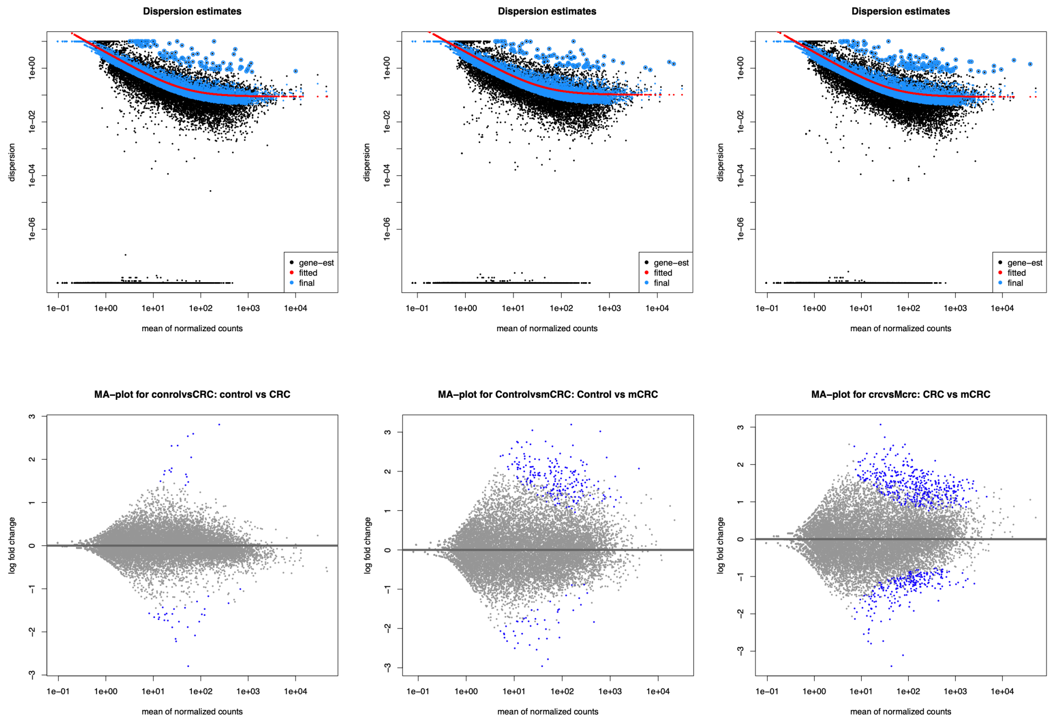

Figure 3.18: The dispersion estimates and MA-plots of RNA sequence data comparison between control, CRC, and mCRC groups. The left panel shows control vs CRC comparison, the middle panel shows control vs mCRC comparison, and the right panel shows CRC vs mCRC comparison.

Gene lists obtained after p-value cut off was determined as 0.05 showed that mCRC group has greater number of differentially expressed genes. CRC has 309 and mCRC has 572 differentially expressed genes. Gene lists submitted to GeneCodis, and enriched pathways were listed from Reactome, KEGG, and WikiPathways databases. Cell type specific enrichment analysis was also done for each gene list through online WebCSEA tool (bioinfo.uth.edu/webcsea). All obtained graphs and comparisons were listed under the related section.

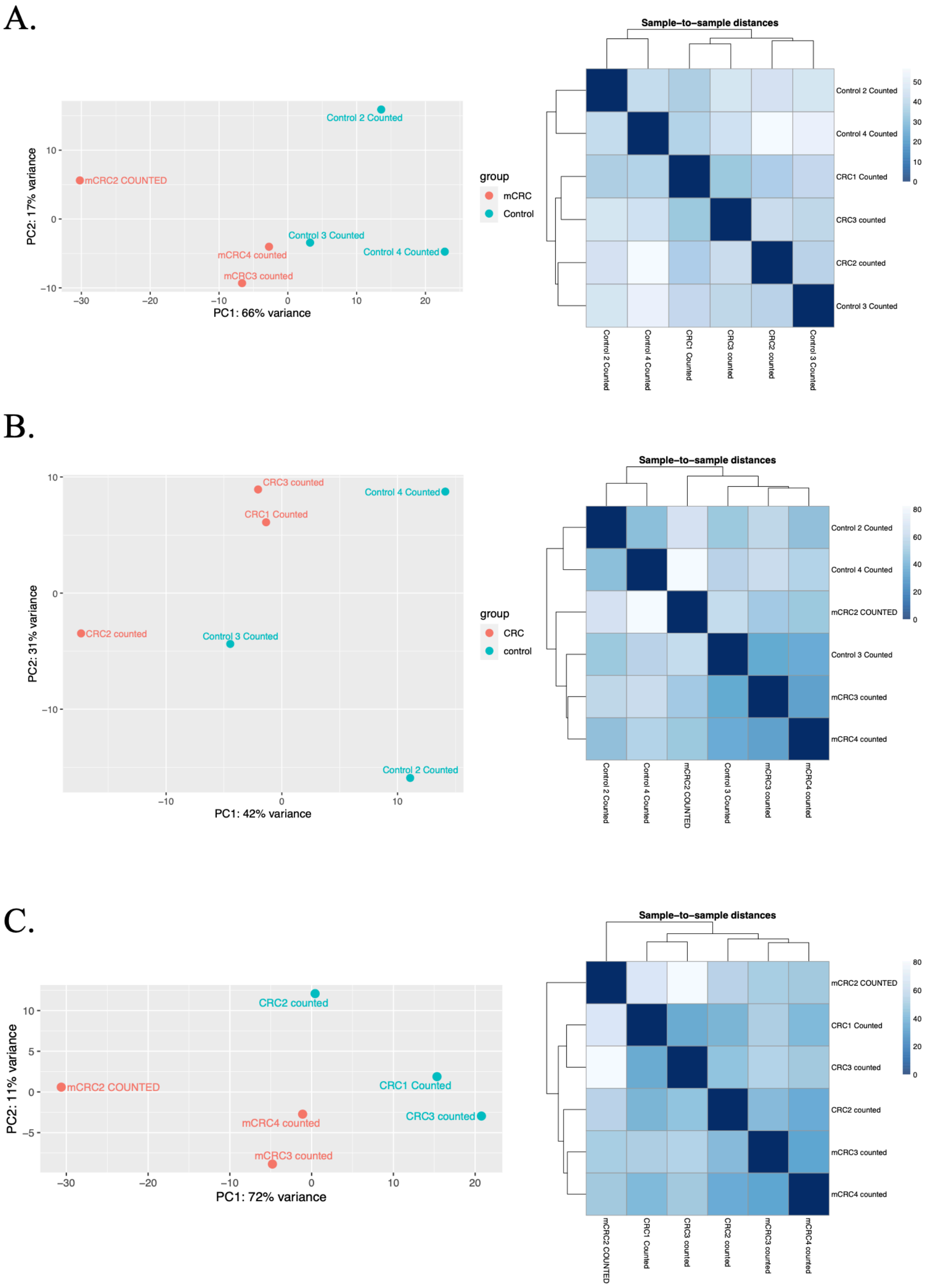

Figure 3.19: The variance distribution and sample-to-sample distance between control and CRC (A), control vs mCRC (B), and CRC vs mCRC (C) individuals.

Terms are given color by automatically detected clusters that were calculated using the TF-IDF values and the Leiden algorithm (Figure 3.20, left panel). The phrase is more considerably enriched the point assigned darker and larger. The p-value obtained from the enrichment computation.

The relevance of each gene set from the chosen library is displayed against its odds ratio using a volcano graphic (Figure 3.20, right panel). The x-axis measures the odds ratio (0, inf) calculated for the gene set, and the y-axis displays the gene set's -log(p-value). Each point represents a single gene set. Statistically significant terms are shown by larger blue dots (p-value 0.05), whereas non-significant phrases are represented by smaller gray points.

NAD+ metabolism, Focal adhesion and Wnt signaling pathway, GPRCs, glycogen synthesis, TGF-ß signaling pathway, and Hippo-Merlin signaling pathway were enriched in control vs CRC plots in Figure 3.20A. For control vs mCRC, eicosanoid synthesis, Hippo-Merlin dysregulation, dopamine metabolism, HIF1A regulation of glycogenesis, lipid metabolism, Ras signaling, EMT in colorectal cancer, and regulation of microtubule cytoskeleton were enriched (Figure 3.20B). Amplification and expansion of oncogenic pathways as metastatic traits, Wnt ß-catenin signaling by small molecules, regulation of microtubule cytoskeleton, and oxysterols-derived from cholesterol were enriched in CRC vs mCRC gene list (Figure 3.20C).

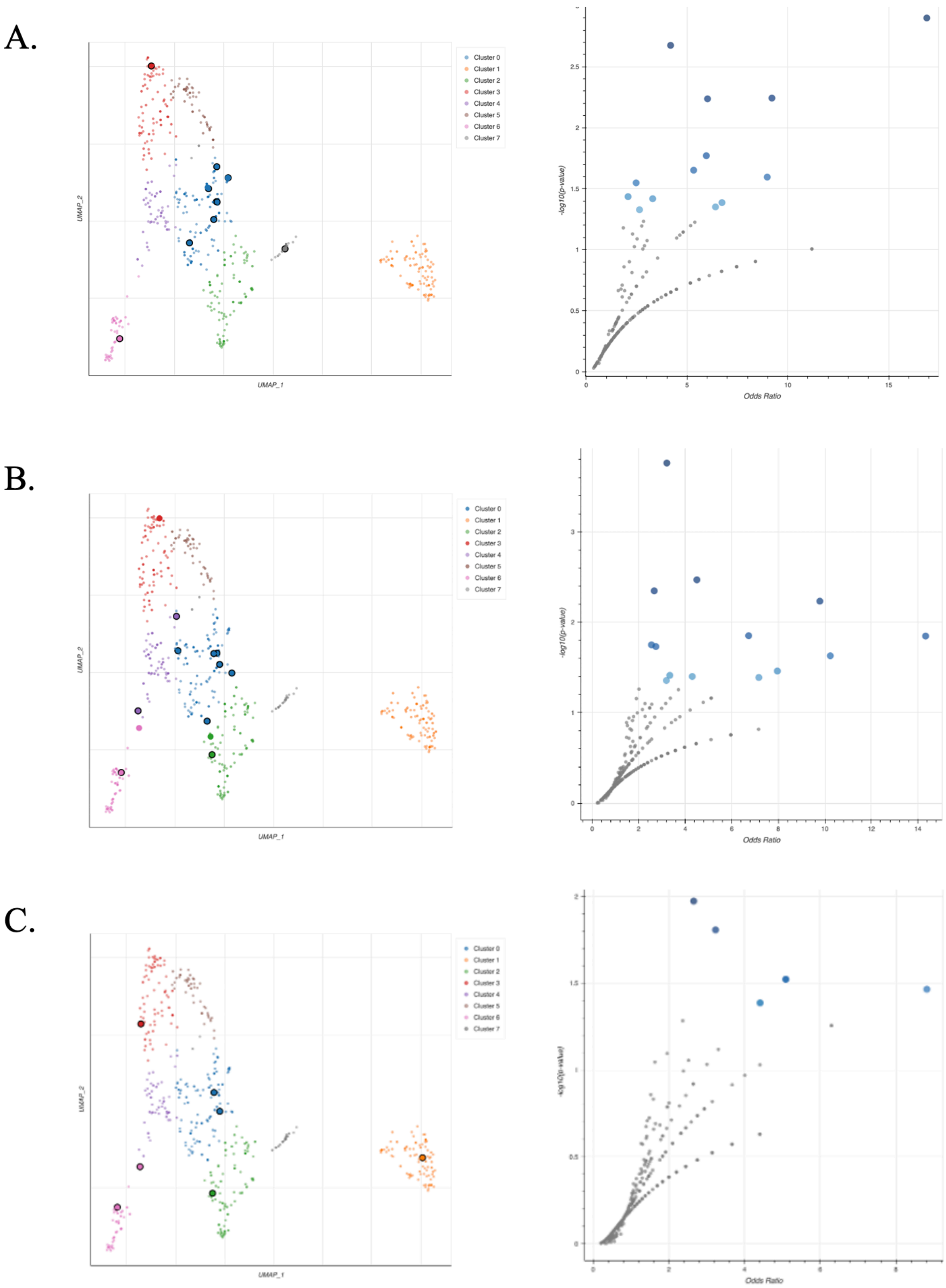

Figure 3.20: A term from the library is represented by each point. For the gene set corresponding to each term, term frequency-inverse document frequency (TF-IDF) values were calculated, and UMAP was then applied to the resulting values (Left panel). Terms from the WikiPathways 2019 Human gene collection are plotted in a volcano shape (Right panel). According to the enrichment findings of the input query gene set, each point represents a single term and is plotted by the associated odds ratio (x-position) and -log10(p-value) (y-position). The input gene set is considerably enriched for the phrase if the point is larger and darker in color. Control and CRC (A), control vs mCRC (B), and CRC vs mCRC (C) individuals.

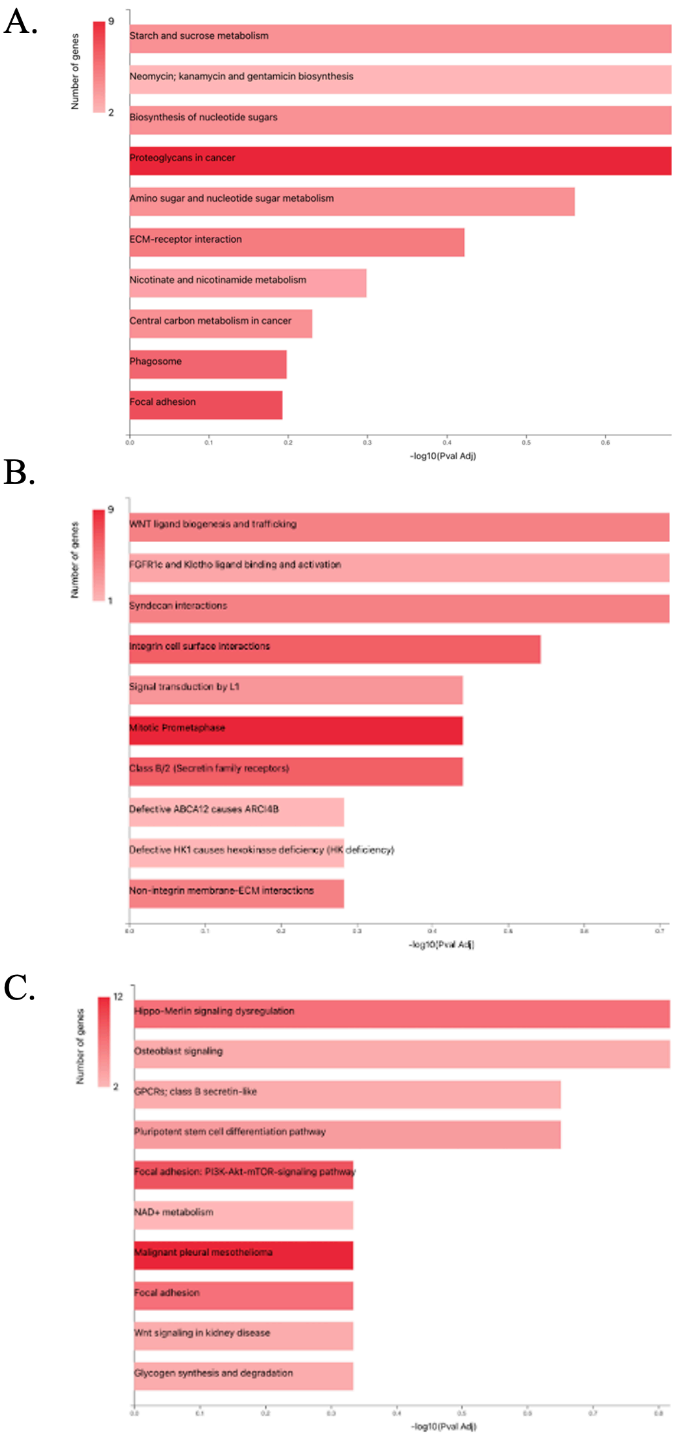

Figure 3.21: The pathway enrichment bar graph for control vs. CRC gene list obtained from GeneCodis; Reactome (A), KEGG (B), and WikiPathway (C) database results.

Starch and sucrose metabolism, biosynthesis of nucleotide sugars, proteoglycans in cancer, amino sugar and nucleotide sugar metabolism, ECM-receptor interaction, nicotinate and nicotinamide metabolism, central carbon metabolism in cancer, phagosome, and focal adhesion are nine of the first 10 Reactome results (Figure 3.21A). WNT ligand biogenesis and trafficking, integrin cell surface interactions, mitotic prometaphase, secretin family receptors, and non-integrin membrane-ECM interactions are five of the first 10 KEGG pathway results (Figure 3.21B). Hippo-merlin signaling dysregulation, focal adhesion: PI3K-Akt-mTOR signaling pathway, NAD+ metabolism, glycogen synthesis and degradation are four of the first 10 Wikipathways results (Figure 3.21C). Metabolism and metabolic pathways were enriched in control vs CRC differential expression gene set. The enrichment map was shown in Figure 3.22 for metabolic pathways.

Figure 3.22: The enrichment map of “metabolism” and “metabolic pathways” related genes in control vs CRC differentially expressed gene set.

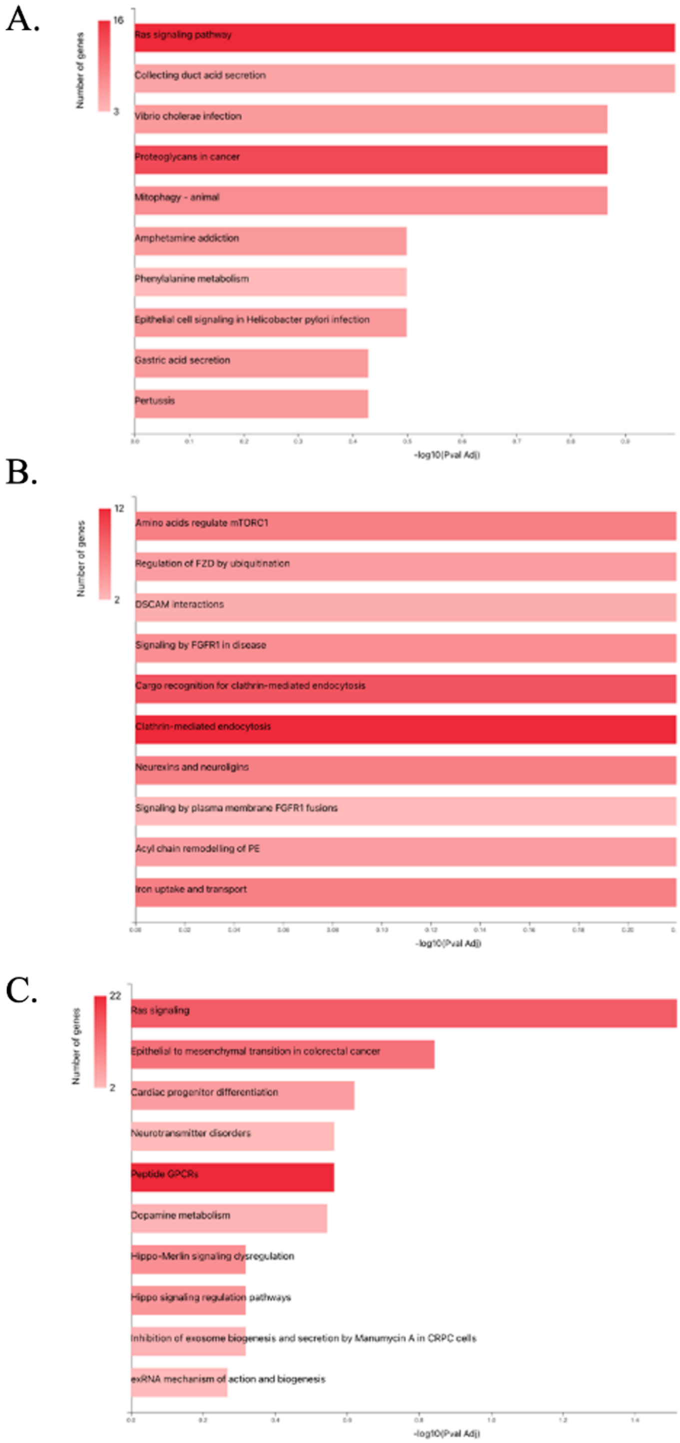

Figure 3.23: The pathway enrichment bar graph for control vs. mCRC gene list obtained from GeneCodis; Reactome (A), KEGG (B), and WikiPathway (C) database results.

Ras signaling pathway, collecting duct acid secretion, proteoglycans in cancer, mitophagy, phenylalanine metabolism, epithelial signaling in H. Pylori infection, and gastric acid secretion are seven of the top 10 Reactome pathway results (Figure 3.23A).

Regulation of FZD by ubiquitination, amino acids regulate mTORC1, signaling by FGFR1 in disease, clathrin-mediated endocytosis, cargo recognition dor clathrin-mediated endocytosis, and peroxisomal protein import are six of the top 10 KEGG pathway results (Figure 3.23B). Ras signaling, epithelial to mesenchymal transition in colorectal cancer, peptide GPRCs, and Hippo-merlin signaling dysregulation are four of the top 10 Wikipathways results (Figure 3.23C). Clathrin-mediated endocytosis, mTORC1 regulation, Ras signaling, MAPK signaling pathways were enriched in control vs mCRC differential expression gene set. The networks were shown in Figure 3.24.

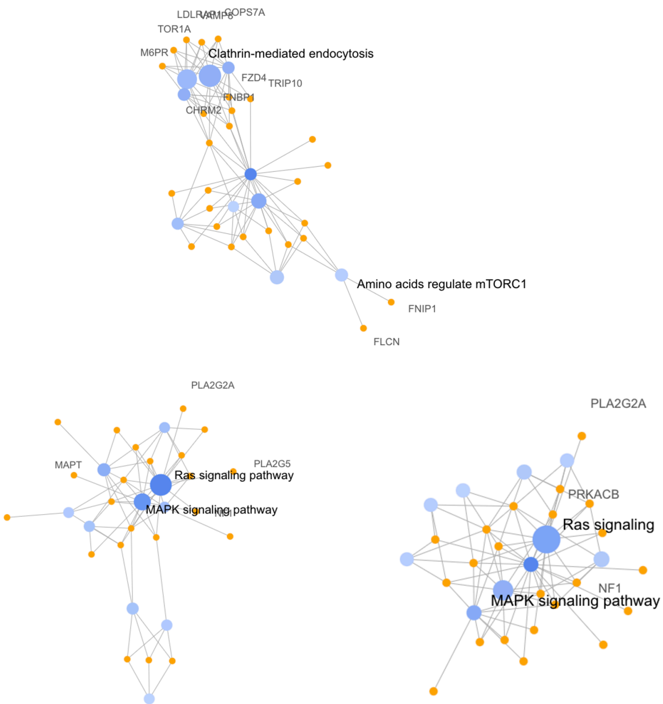

Figure 3.24: The enrichment map of endocytosis and signaling pathways related genes obtained from the gene list of control vs mCRC differential expression analysis.

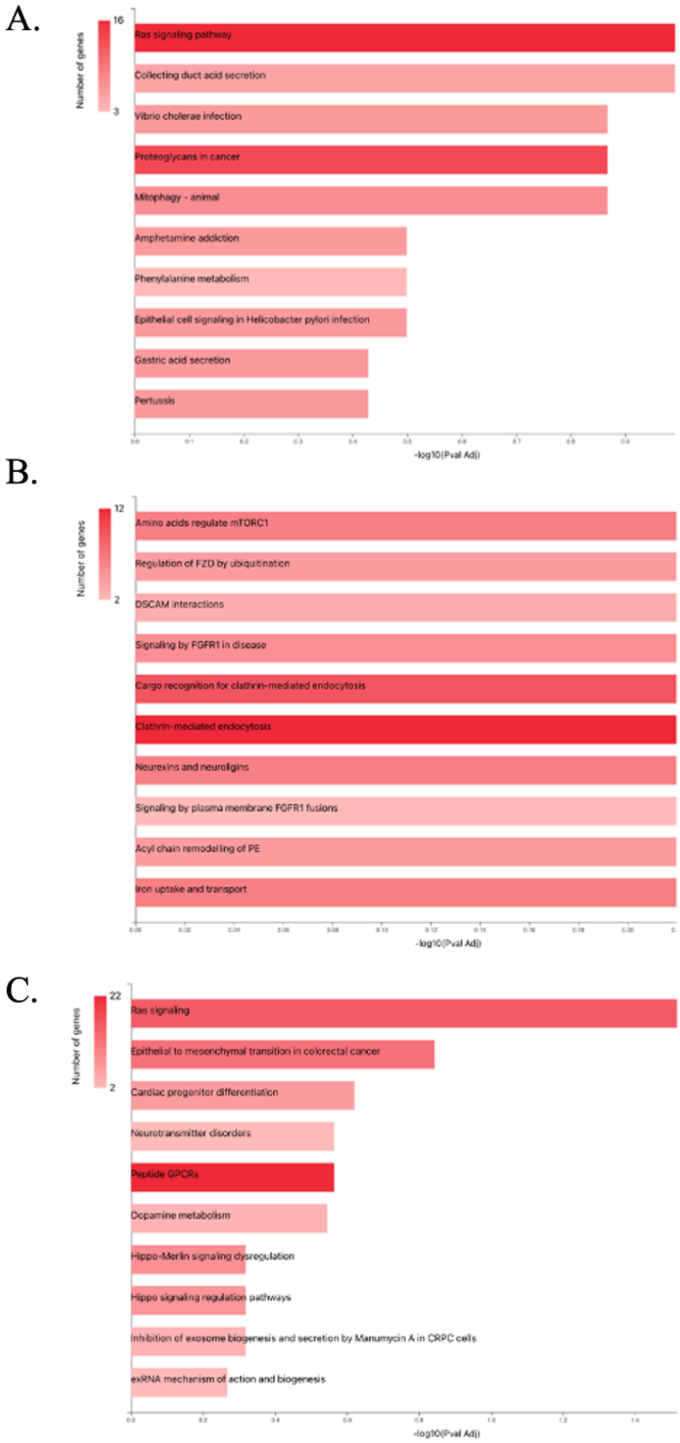

Figure 3.25: The pathway enrichment bar graph for CRC vs. mCRC gene list obtained from GeneCodis; Reactome (A), KEGG (B), and WikiPathway (C) database results.

Biosynthesis of nucleotide sugars, primary bile acid biosynthesis, bile secretion, and sphingolipid metabolism are four of the top 10 Reactome results (Figure

3.25A). RND3 GTPase cycle, vitamin B6 activation, and lysosomal oligosaccharide catabolism are three of the top 10 KEGG pathway results (Figure 3.25B). Glycine metabolism, CCL18 signaling pathway, methylation pathways, and epithelial to mesenchymal transition in colorectal cancer are four of the top 10 WikiPathways results (Figure 3.25C).

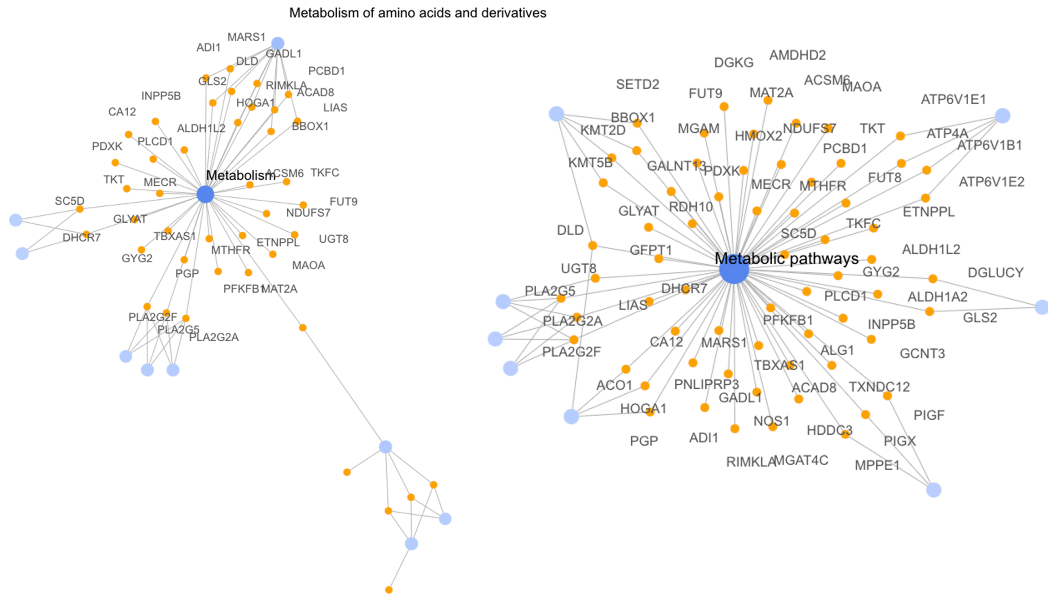

Figure 26: The enrichment map of metabolism and metabolic pathways related genes obtained from the gene list of CRC vs mCRC differential expression analysis.

Metabolism and metabolic pathways were enriched in CRC vs mCRC differential expression gene set. The enrichment map was shown in Figure 3.26 for metabolic pathways.

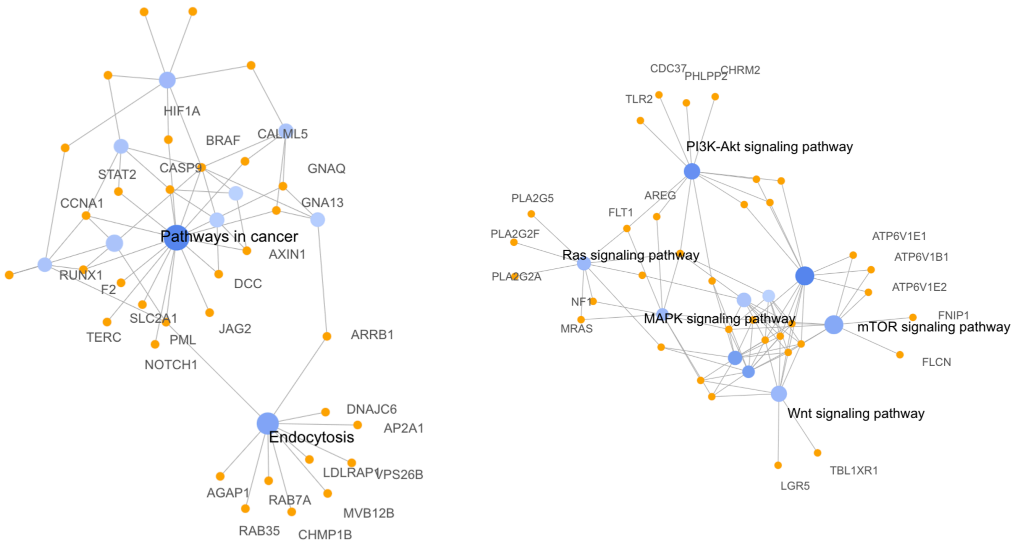

Figure 3.27: The enrichment map of pathways in cancer, endocytosis, and signaling pathways related genes obtained from the gene list of CRC vs mCRC differential expression analysis.

Pathways in cancer, Ras signaling, MAPK signaling, PI3K-Akt signaling, mTOR signaling, and Wnt signaling pathways were enriched in control vs mCRC differential expression gene set. The enrichment maps were shown in Figure 3.27.

3.4.1. Colorectal Cancer and Proteoglycans in Cancer

Results from databases like KEGG, Reactome, and WikiPathways were filtered using FDR values less than 0.05 in pathway analyses of differential gene expression lists using webtools like DAVID, g:Profiler, and GeneCodis. Afterward, from the findings of the three databases for all three gene lists, genes categorized as "Colorectal Cancer" and "Proteoglycans in Cancer" were picked (Table 3.4).

Table 3.4: Gene lists obtained from the pathway analysis of total differential expression lists for colorectal cancer and proteoglycans in cancer.

A.

COLON/COLORECTAL CANCER		
PROTEOGLYCANS in CANCER		
Control vs CRC	Control vs mCRC	CRC vs mCRC
FGFR1	CLDN1	ANK1
ITGA2	DCC	ANK2
ITGA5	EZR	AREG
ITGAV	FGFR1	AXIN
KDR	FZD4	BRAF
MAPK8	GAB1	CASP9
PRKACB	HIF1A	CLDN1
THSB1	ITGA5	CSNK1A1
WNT2	KDR	CXXC4
WNT7B	MAPK8	DCC
	MRAS	DDX5
	NANOG	FZD4
	NOTCH2	GAB1
	PAK1	HIF1A
	PKP1	HJAG2
	PRKACB	HSPG2
	RRAS2	MRAS
	SLC7A14-AS	NOTCH1
	STRAP	NOTCH2
	TMPRSS4	PKP1
	WNT3	PPP1R12A
		PPP1R12B
		STRAP
		TLR2
		TMPRSS4
		WNT2
		WNT3

B.

	Control vs CRC	Control vs mCRC	CRC vs mCRC
FGFR1	1,1310	1,8950	
ITGA5	-1,3353	-1,8349	
KDR	-1,7629	-1,6720	
MAPK8	-1,4414	-2,0159	
PRKACB	0,9980	1,8258	
CLDN1		1,8956	1,9871
DCC		-0,8796	-0,7599
FZD4		0,8898	1,0627
GAB1		1,9759	1,2629
HIF1A		1,4472	1,5358
MRAS		0,8371	0,9631
NOTCH2		3,0175	1,5835
PKP1		2,0708	1,5385
STRAP		1,6300	1,3313
TMPRSS4		1,6870	0,1738
WNT3		1,4253	1,6857

3.4.1.1. Control vs. CRC Results

Genes listed in Table 3.4 were analyzed in ShinyGo webtool for detailed information about their genomic and functional identity. The first graph obtained is showed the first 20 pathway related to these 10 genes (Figure 3.28). Pathways in cancer, Wnt signaling pathway, PI3K-Akt signaling pathway, and focal adhesion are shown to be enriched. Fold enrichment dot plot of associated pathways (Figure 3.28), the hierarchical clustering tree shows correlation between enriched pathways (Figure 3.29) and network depiction of relation between enriched pathways (Figure 3.30) are shown below.

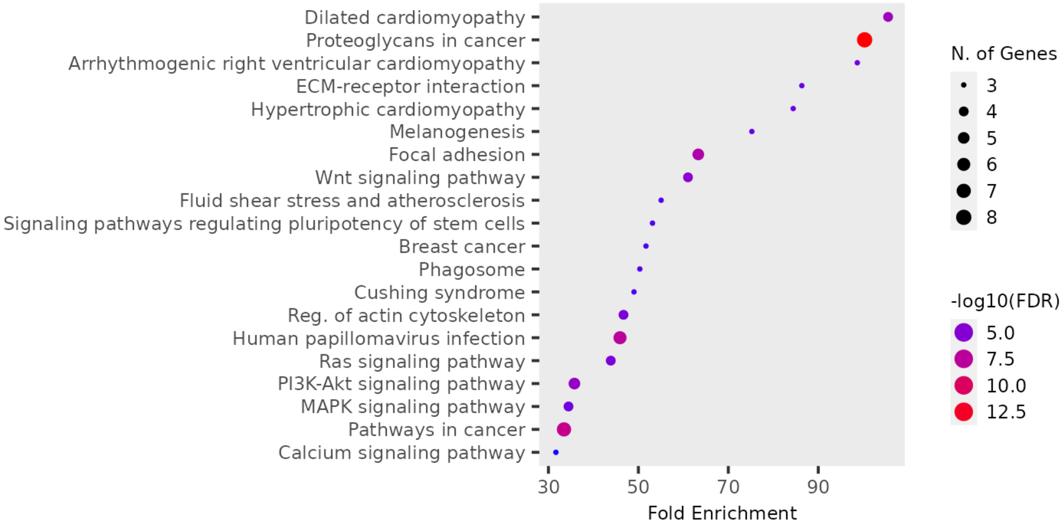

Figure 3.28: Fold enrichment dot plot of associated pathways for control vs CRC comparison. Bigger dots indicate higher number of genes included.

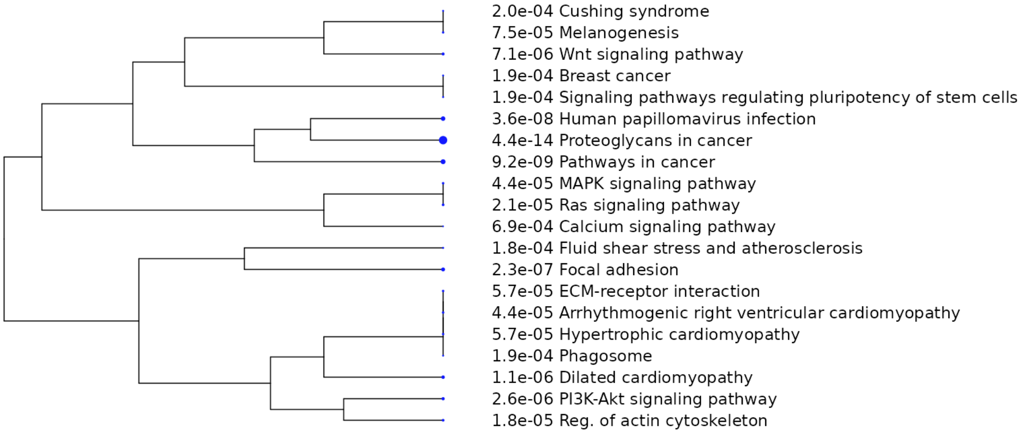

Figure 3.29: A hierarchical clustering tree which summarizes the correlation among significant pathways listed in Figure 3.19. Bigger dots indicate signifiant p-values.

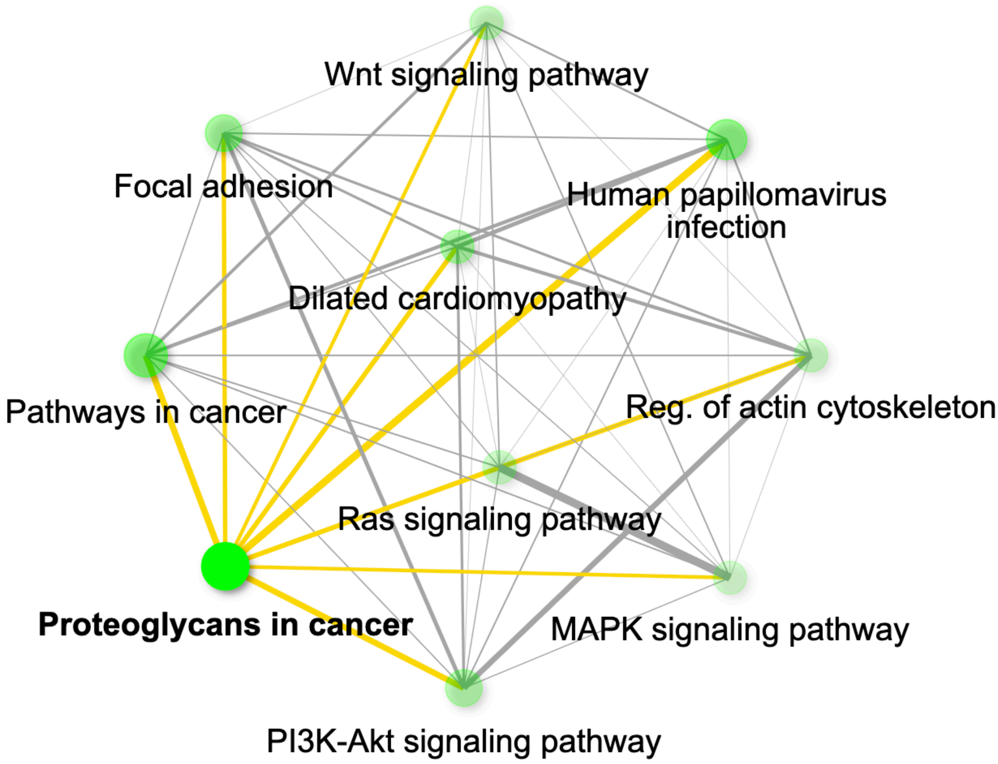

Figure 3.30: This network shows the relationship between enriched pathways for control vs CRC filtered gene list for colorectal cancer and proteoglycans in cancer.. Two nodes are connected if they shared 20% or more genes. Bigger and darker nodes indicate significantly enriched gene sets. Thicker edges represent more overlapped genes.

3.4.1.2. Control vs. mCRC Results

Genes listed in Table 3.4 were analyzed in ShinyGo webtool for detailed information about their genomic and functional identity. The first graph obtained is showed the first 10 pathway related to these 21 genes (Figure 3.31). Pathways in cancer, MAPK signaling pathway, RAS signaling pathway, and regulation of actin cytoskeleton are enriched. Fold enrichment dot plot of associated pathways (Figure 3.31), the hierarchical clustering tree shows correlation between enriched pathways (Figure 3.32) and network depiction of relation between enriched pathways (Figure 3.33) are shown below.

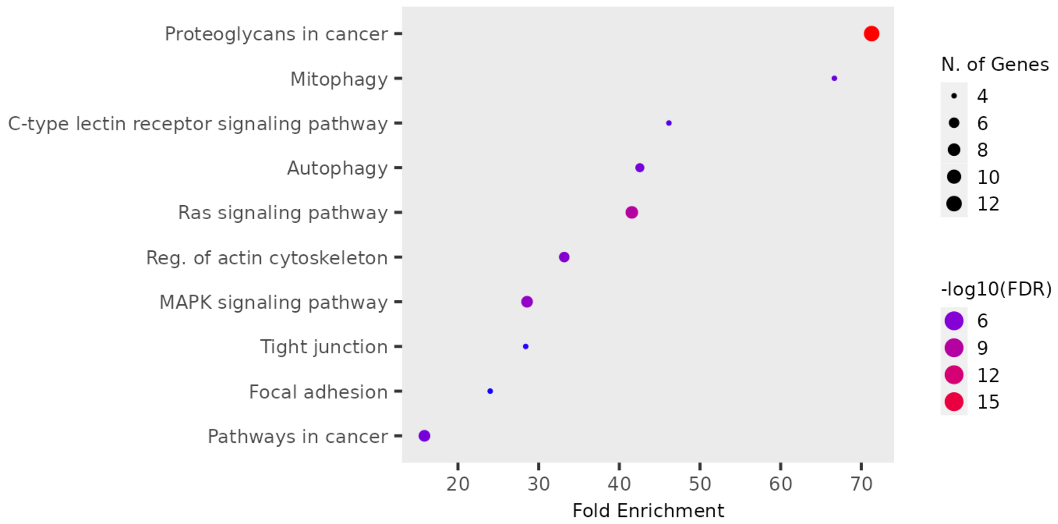

Figure 3.31: Fold enrichment dot plot of associated pathways for control vs mCRC comparison. Bigger dots indicate higher number of genes included.

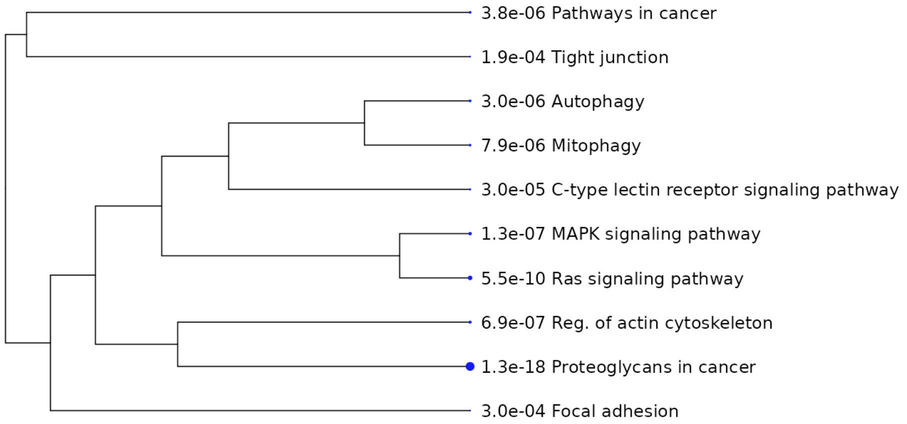

Figure 3.32: A hierarchical clustering tree which summarizes the correlation among significant pathways listed in Figure 3.31. Bigger dots indicate signifiant p-values.

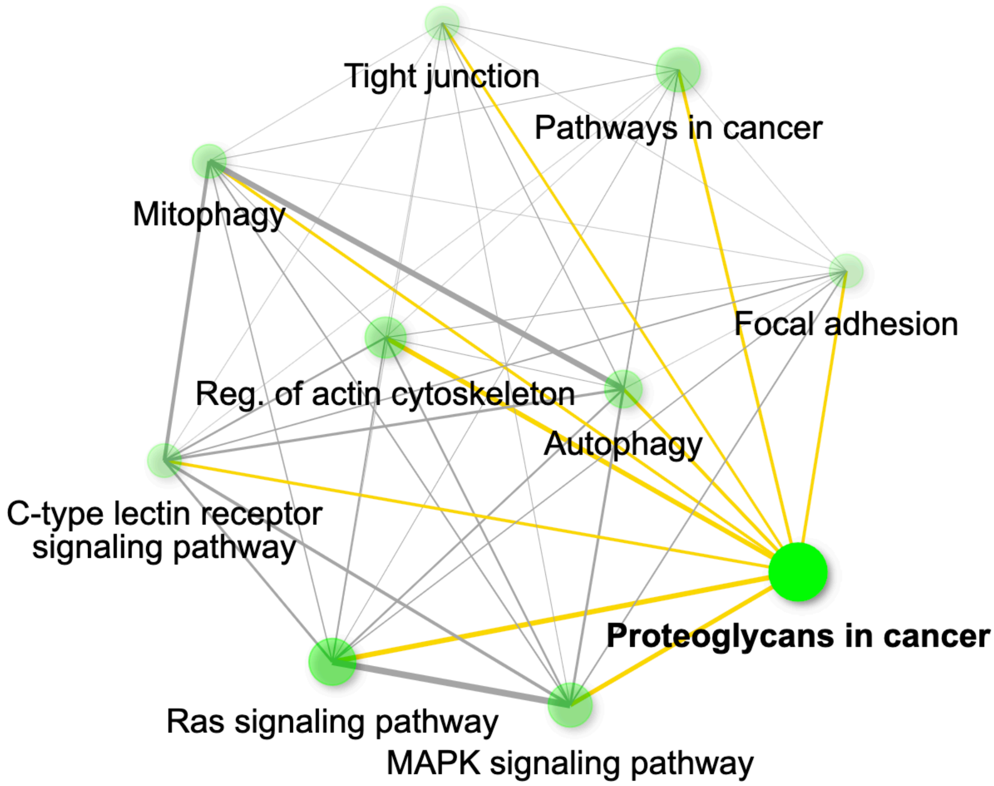

Figure 3.33: This network shows the relationship between enriched pathways for control vs mCRC filtered gene list for colorectal cancer and proteoglycans in cancer.. Two nodes are connected if they shared 20% or more genes. Bigger and darker nodes indicate significantly enriched gene sets. Thicker edges represent more overlapped genes.

The “Colorectal Cancer” and “Proteoglycans in Cancer” genes of control vs mCRC comparison listed in Table 3.4 inclued several transcription factors (TFs). Genecodis selects TFs among the list and analyzed the association of genes as TFs in pathways. These TFs have role in pathways in cancer. Moreover, metabolic pathways such as starch ans sucrose metabolism, carbon metabolism ad fructose metabolism were enriched (Figure 3.34). These pathways also enriched in total differential gene list analysis.

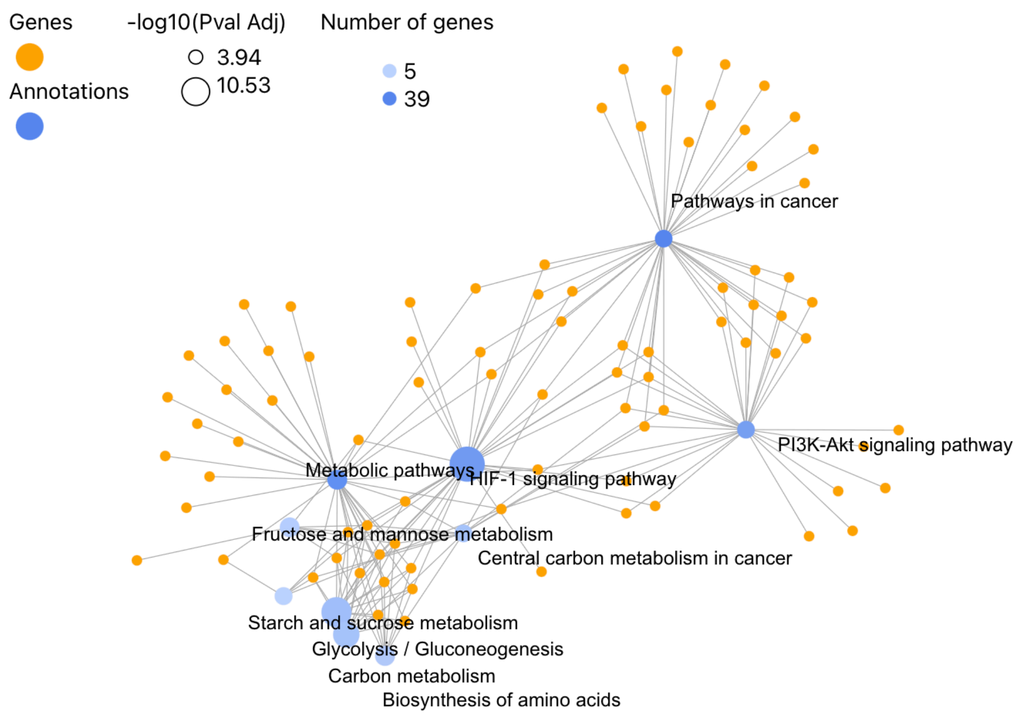

Figure 3.34: The enrichment map of pathways in cancer, endocytosis, and signaling pathways related genes obtained from the gene list of control vs mCRC differential expression analysis.

3.4.1.3. CRC vs. mCRC Results

Genes listed in Table 3.4 were analyzed in ShinyGo webtool for detailed information about their genomic and functional identity. The first graph obtained is showed the first 10 pathway related to these 27 genes (Figure 3.35). Pathways in cancer, colorectal cancer, and hepatocellular carcinoma are enriched. Fold enrichment dot plot of associated pathways (Figure 3.36), the hierarchical clustering tree shows correlation between enriched pathways (Figure 3.37) and network depiction of relation between enriched pathways (Figure 3.38) are shown below.

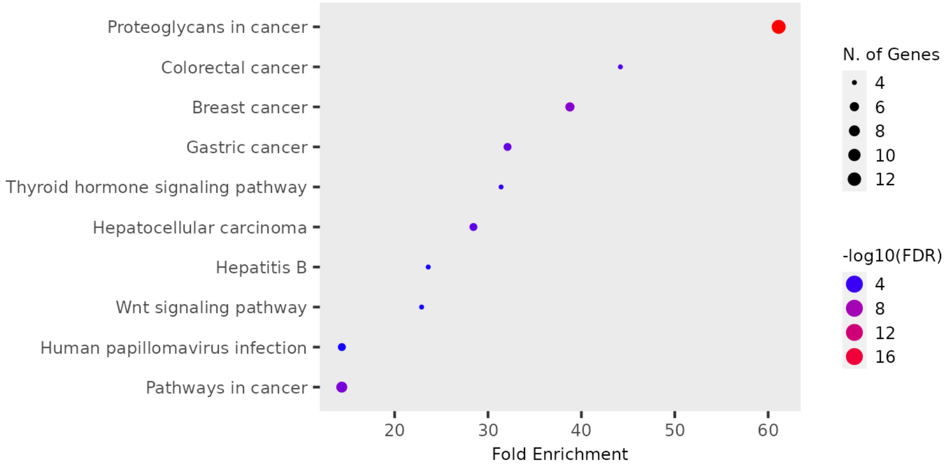

Figure 3.35: Fold enrichment dot plot of associated pathways for CRC vs mCRC comparison. Bigger dots indicate higher number of genes included.

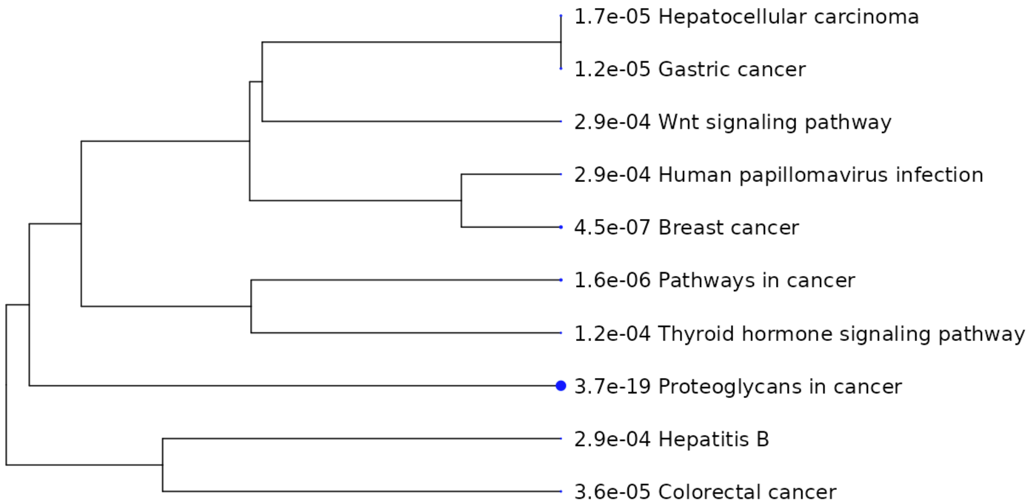

Figure 3.36: A hierarchical clustering tree which summarizes the correlation among significant pathways listed in Figure 3.35. Bigger dots indicate signifiant p-values.

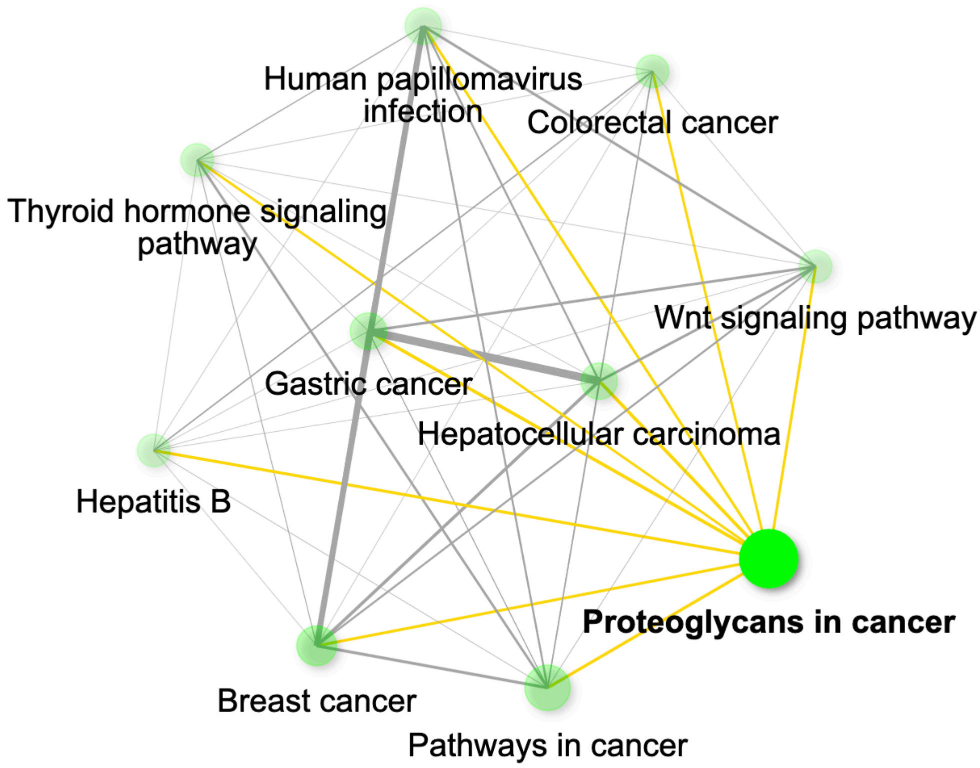

Figure 3.37: This network shows the relationship between enriched pathways for CRC vs mCRC filtered gene list for colorectal cancer and proteoglycans in cancer. Two nodes are connected if they shared 20% or more genes. Bigger and darker nodes indicate significantly enriched gene sets. Thicker edges represent more overlapped genes.

The "Colorectal Cancer" and "Proteoglycans in Cancer" genes of control vs mCRC comparison listed in Table 3.4 included several transcription factors (TFs). Genecodis selects TFs among the list and analyzed the association of genes as TFs in pathways. These TFs have role in pathways in cancer. Moreover, metabolic pathways such as starch ans sucrose metabolism, carbon metabolism ad fructose metabolism were enriched (Figure 3.38). The PI3K-Akt signaling pathway and glycolysis-glucogenesis metabolism have both been enriched among the requires the listed TFs, unlike the control vs. mCRC comparison. These pathways also enriched in total differential gene list analysis.

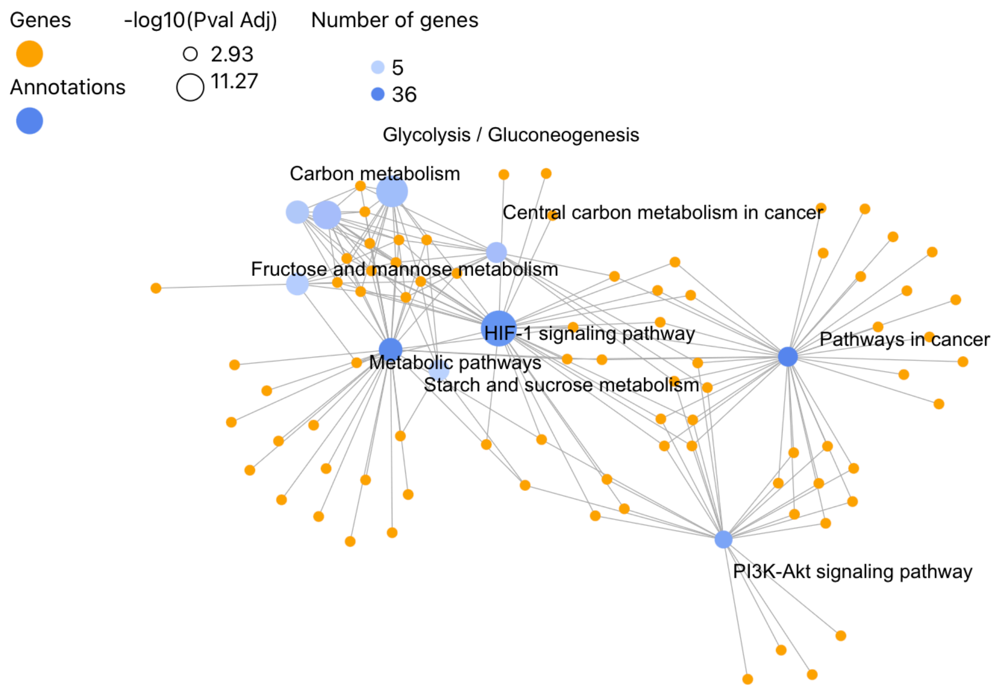

Figure 3.38: The enrichment map of pathways in cancer, endocytosis, and signaling pathways related genes obtained from the gene list of CRC vs mCRC differential expression analysis.

3.4.2. Lipid Metabolism

Results from databases like KEGG, Reactome, and WikiPathways were filtered using FDR values less than 0.05 in pathway analyses of differential gene expression lists using webtools like DAVID, g:Profiler, and GeneCodis. Afterwards, from the findings of the three databases for all three gene lists, genes categorized as "Lipid metabolism", "Metabolism of lipids", and " Metabolism of steroids" were picked (Table 3.5).

Table 3.5: Gene lists obtained from the pathway analysis of total differential expression lists for lipid metabolism and steroid metabolism.

A.

Lipid Metabolism		
Control vs CRC	**Control vs mCRC**	**CRC vs mCRC**
ABCA12	ACSBG2	ACMS6
ABCB4	ACSM6	ACOT7
ACSM6	ALDH3B2	ALG1
ALG5	CYP2R1	AMDHD2
CYP2U1	CYP46A1	ARSJ
CYP7B1	DHCR7	CASP9
FUT9	DLD	CYP46A1
GNPNAT1	ECH1	DGKG
GPD2	ETNPPL	DHCR7
HSD3B1	GDE1	DLD
INSIG1	GDPD5	ESYT3
INSIG2	GNAQ	ETNPPL
ITGAV	HSD3B1	FDXR
MAPK8	LDLRAP1	FUT9
PGM3	MAPK8	GFPT1
PLPP1	MED22	GNA13
PPP1R14C	ORM1	GNAQ
PRKACB	OSBP	HS3ST1
SGMS2	OSBPL9	HSPG2
SIRT1	PLA2G2A	INSIG2
TERT	PLA2G2F	LIPE
THSB1	PLA2G5	LYPLA2
TSPOAP1	PLAAT1	MECR
	PRKACB	MECR
	PROCA1	MED25
	PTGES	NCOA6
	SLC27A2	NLRP7
	ST8SIA3	ORM1
	TBL1XR1	OSBP
	TERT	OSBPL9
		PLA2G15
		PLA2G2A
		PLA2G2F
		PLA2G5
		PLA2R1
		PLPPP2
		PNLIPRP3
		PPP2R2A
		PROCA1
		PRR29
		SC5D
		SLC10A1
		SP3
		TBL1XR1
		TBXAS1
		TKFC
		TNFRSF1A
		UGT8

B.

	Control vs CRC	Control vs mCRC	CRC vs mCRC
ACSM6	-0,61855	1,21310	1,84940
FUT9	0,88507		-1,15270
HSD3B1	-2,00000	-2,32140	
INSIG2	1,07700		-1,06550
PRKACB	0,99805	1,82581	
TERT	0,94180	2,75521	
MAPK8	-1,44140	-2,01591	
CYP46A1		1,50710	1,76250
DHCR7		2,66180	1,92900
DLD		-0,90336	-0,91410
ETNPPL		1,67590	1,29360
GNAQ		2,00000	1,79180
ORM1		1,34350	1,30960
OSBP		1,33860	1,44140
OSBPL9		1,72270	1,48350
PLA2G2A		1,66493	1,88370
PLA2G2F		2,32112	2,19580
PLA2G5		1,82672	1,82490
PROCA1		0,94119	1,09320
TBL1XR1		2,31330	2,41430

3.4.2.1. Control vs. CRC Results

Genes listed in Table 3.5 were analyzed in ShinyGo webtool for detailed information about their genomic and functional identity. The first graph obtained is showed the first 10 pathway related to these 23 genes (Figure 3.39). Metabolic pathways, pathways in cancer, cortisol synthesis, nucleotide sugar biosynthesis and metabolism are enriched. Fold enrichment dot plot of associated pathways (Figure 3.39), the hierarchical clustering tree shows correlation between enriched pathways

(Figure 3.40) and network depiction of relation between enriched pathways (Figure 3.41) are shown below.

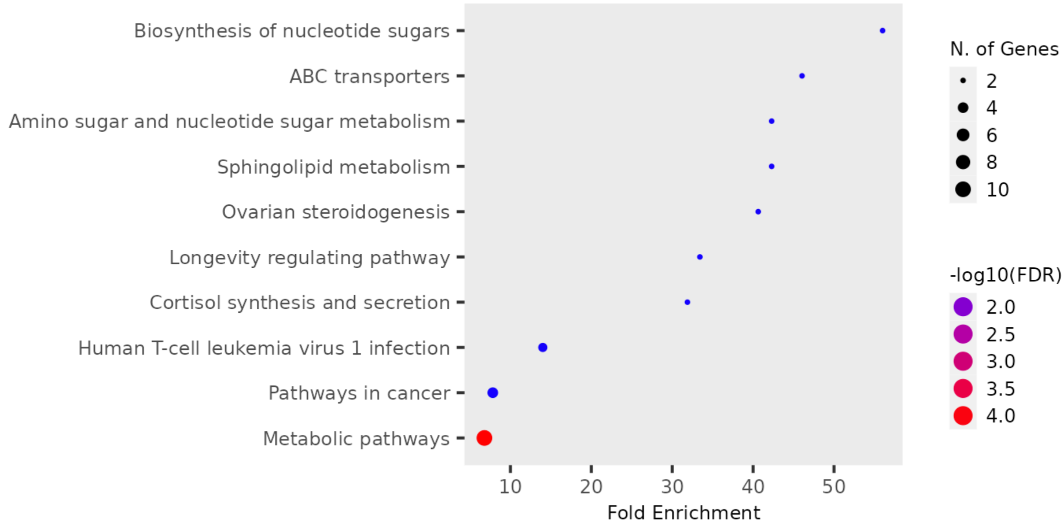

Figure 3.39: Fold enrichment dot plot of associated pathways for control vs CRC comparison. Bigger dots indicate higher number of genes included.

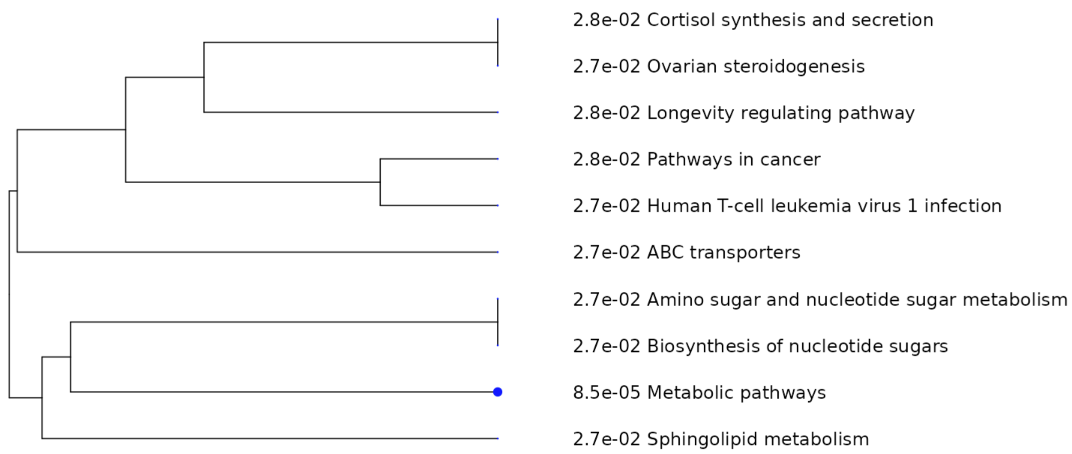

Figure 3.40: A hierarchical clustering tree which summarizes the correlation among significant pathways listed in Figure 3.39. Bigger dots indicate signifiant p-values.

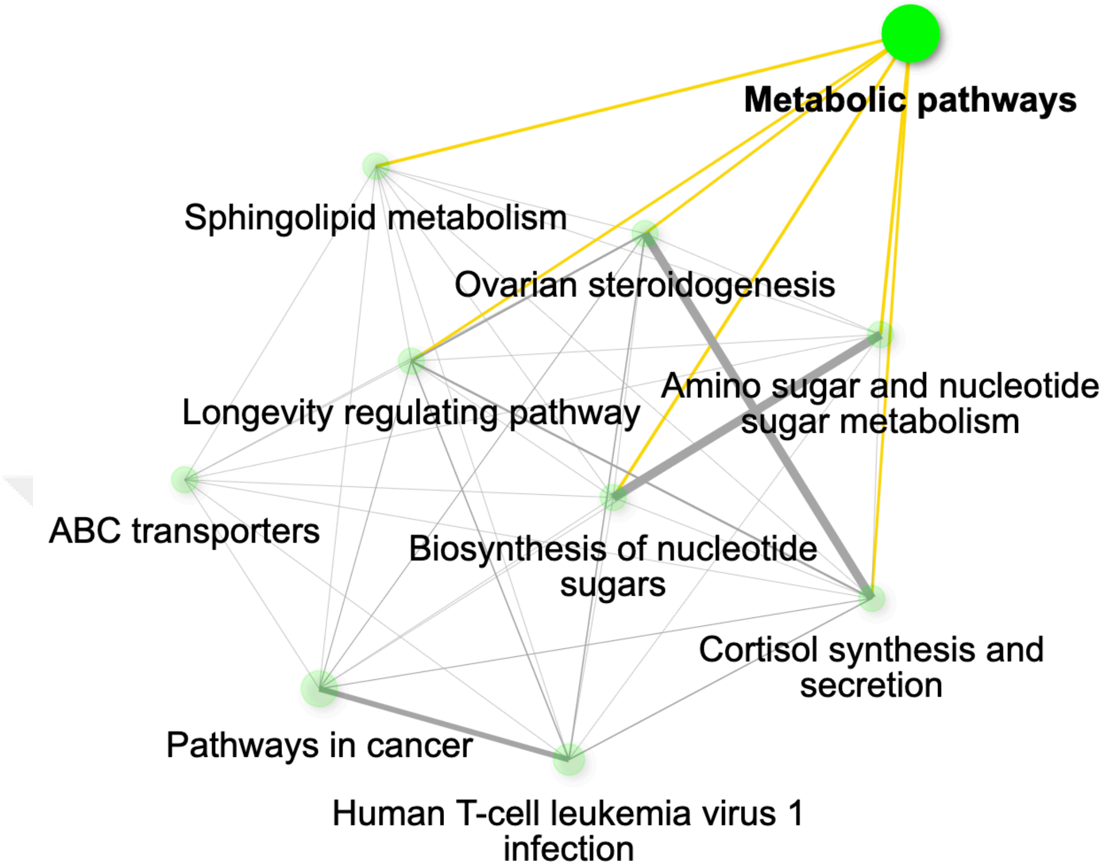

Figure 3.41: This network shows the relationship between enriched pathways for control vs CRC filtered gene list for colorectal lipid metabolism and fat digestion and absorption. Two nodes are connected if they shared 20% or more genes. Bigger and darker nodes indicate significantly enriched gene sets. Thicker edges represent more overlapped genes.

3.4.2.2. Control vs. mCRC Results

Genes listed in Table 3.5 were analyzed in ShinyGo webtool for detailed information about their genomic and functional identity. The first graph obtained is showed the first 10 pathway related to these 30 genes (Figure 3.42). Metabolic pathways, Ras signaling pathway, fat digestion and absorption, linoleic acid metabolism and ether lipid metabolism are enriched. Fold enrichment dot plot of associated pathways (Figure 3.42), the hierarchical clustering tree shows correlation between enriched pathways (Figure 3.43) and network depiction of relation between enriched pathways (Figure 3.44) are shown below.

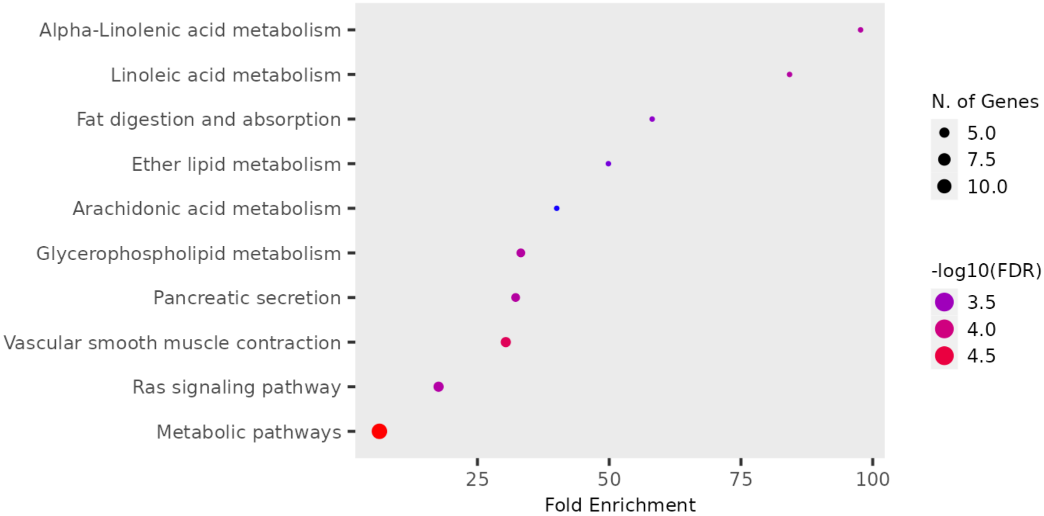

Figure 3.42: Fold enrichment dot plot of associated pathways for control vs mCRC comparison. Bigger dots indicate higher number of genes included.

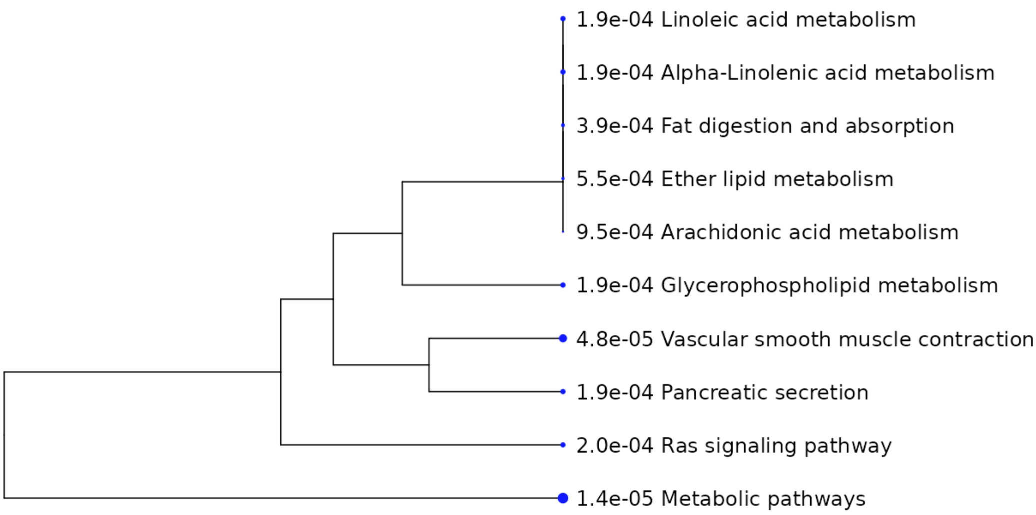

Figure 3.43: A hierarchical clustering tree which summarizes the correlation among significant pathways listed in Figure 3.40. Bigger dots indicate signifiant p-values.

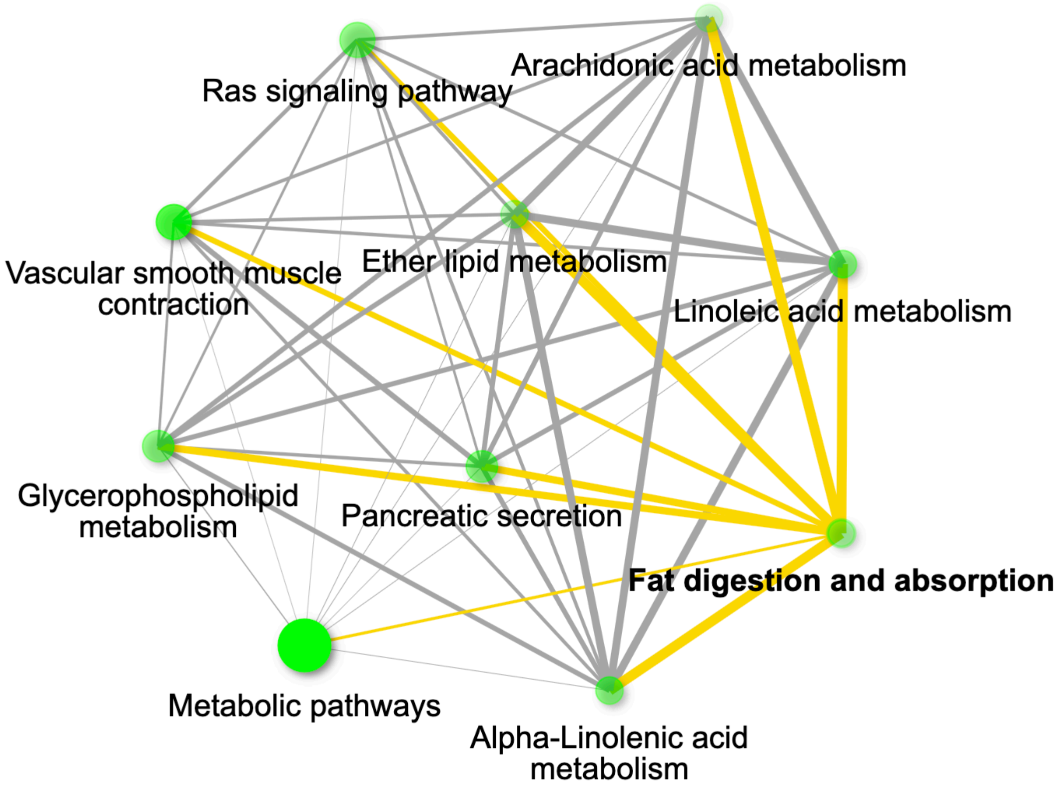

Figure 3.44: This network shows the relationship between enriched pathways for control vs mCRC filtered gene list for lipid metabolism and fat digestion and absorption. Two nodes are connected if they shared 20% or more genes. Bigger and darker nodes indicate significantly enriched gene sets. Thicker edges represent more overlapped genes.

3.4.2.3. CRC vs. mCRC Results

Genes listed in Table 3.5 were analyzed in ShinyGo webtool for detailed information about their genomic and functional identity. The first graph obtained is showed the first 10 pathway related to these 48 genes (Figure 3.45). Metabolic pathways, sphingolipid signaling pathway, fat digestion and absorption, linoleic acid metabolism and ether lipid metabolism are enriched. Fold enrichment dot plot of associated pathways (Figure 3.45), the hierarchical clustering tree shows correlation between enriched pathways (Figure 3.46) and network depiction of relation between enriched pathways (Figure 3.47) are shown below.

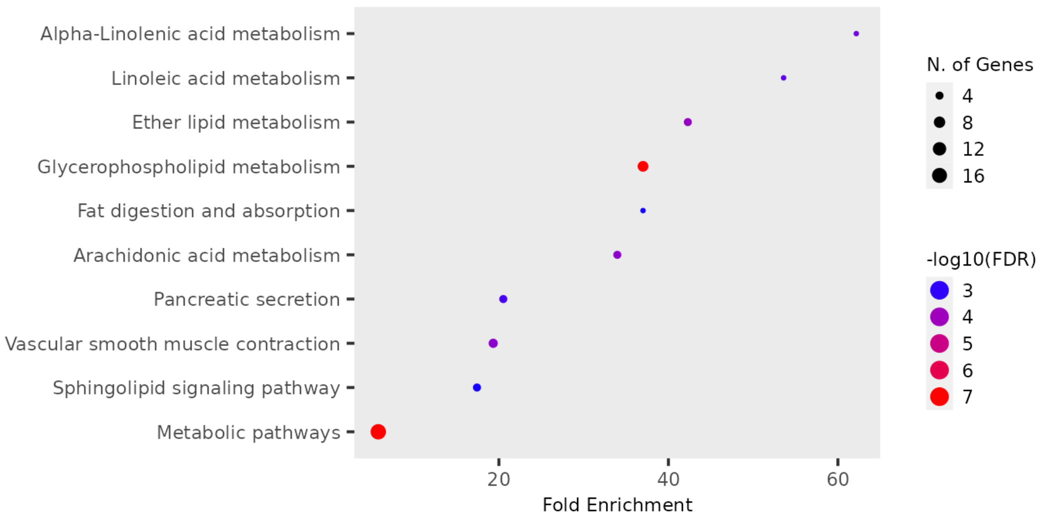

Figure 3.45: Fold enrichment dot plot of associated pathways for CRC vs mCRC comparison. Bigger dots indicate higher number of genes included.

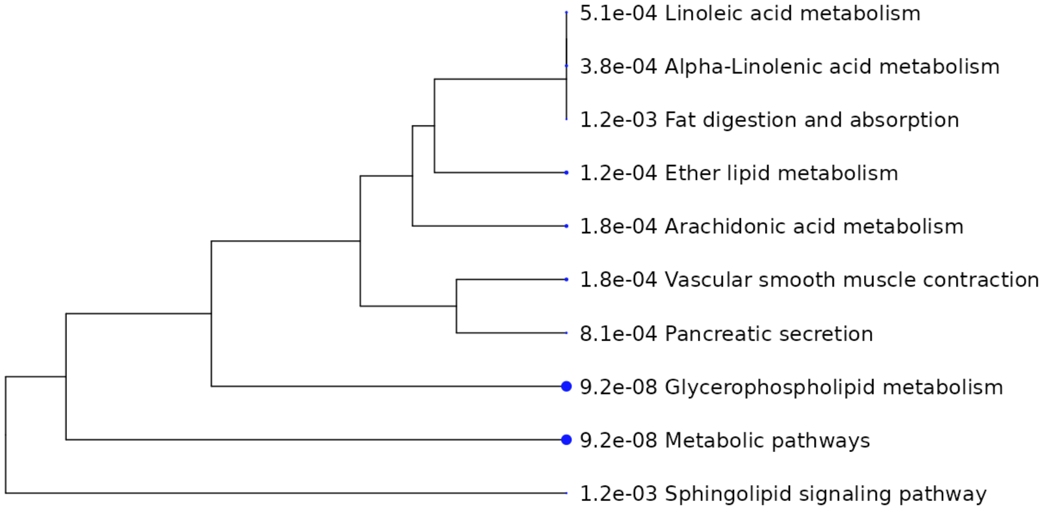

Figure 3.46: A hierarchical clustering tree which summarizes the correlation among significant pathways listed in Figure 3.45. Bigger dots indicate signifiant p-values.

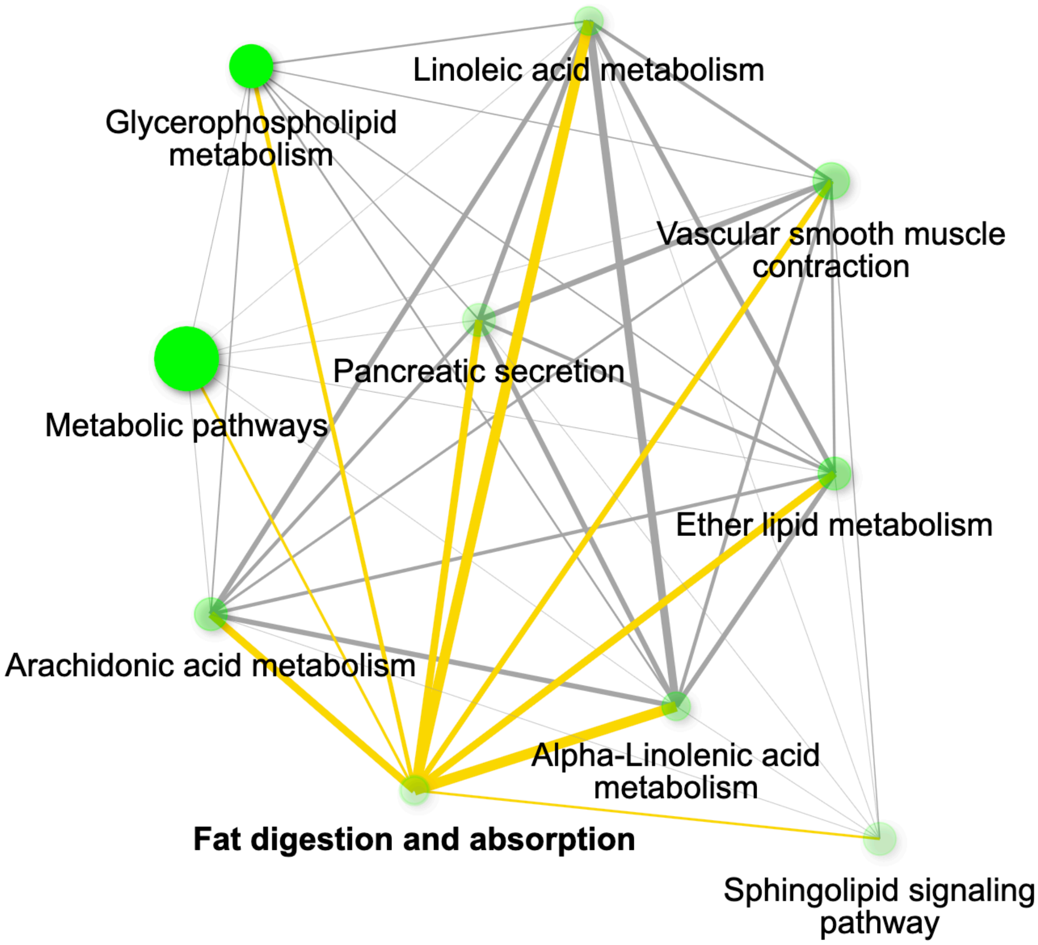

Figure 3.47: This network shows the relationship between enriched pathways for CRC vs mCRC filtered gene list for lipid metabolism and fat digestion and absorption. Two nodes are connected if they shared 20% or more genes. Bigger and darker nodes indicate significantly enriched gene sets. Thicker edges represent more overlapped genes.

3.4.3. Rho GTPase Signaling

Results from databases like KEGG, Reactome, and WikiPathways were filtered using FDR values less than 0.05 in pathway analyses of differential gene expression lists using webtools like DAVID, g:Profiler, and GeneCodis. Afterwards, from the findings of the three databases for all three gene lists, genes categorized as " Rho GTPase signaling ", " Signaling by Rho GTPases ", and “ Rho GTPase effectors” were picked (Table 3.6).

Table 3.6: Gene lists obtained from the pathway analysis of total differential expression lists for Rho GTPase signaling and signaling by Rho GTPases
.

A.

Rho GTPase Signaling		
Control vs CRC	**Control vs mCRC**	**CRC vs mCRC**
CENPF	CDC37	ARHGAP2
CKAP5	DENND1C	ARHGEF5
CLASP2	DOCK7	CDC37
CPSF7	EIF3L	CFTR
DLG5	EIF5B	CKAP5
MYO6	FNBP1	CLASP1
MYO9A	KALRN	DLG5
NDUFA5	LIN7B	DOCK7
PKP4	MRTFA	EIF3I
PRC1	MYO6	EIF3L
RANBP2	NET1	FMNL3
RHOT1	OSBPL11	FNBP1
SKA2	PAK1	GNA13
STK10	PKN2	HMOX2
WASL	RHOT1	IL32
	RND3	LIN7B
	RPS13	MAPRE1
	RRAS2	MCF2
	SHERF1	MRTFA
	SNAP23	NISCH
	TRIP10	PCDH7
	VRK2	PKP4
		PLXNB1
		PPP1R12A
		PPP1R12B
		PRC1
		RAB7A
		RANBP2
		RND3
		SEMA4F
		SH3RF1
		SKA2
		SNAP23
		SRGAP1
		TRIP10
		VIM
		ZWILCH

B.

	Control vs CRC	Control vs mCRC	CRC vs mCRC
MYO6	-2,0832	-2,2586	
DLG5	-0,8912		1,5678
CKAP5	-1,3077		1,5827
PKP4	-0,7553		0,9592
PRC1	-0,6121		1,0471
RANBP2	-1,5929		1,9402
RHOT1	1,3458	2,3420	
SKA2	0,7872		-1,3369
STK10	0,9451		-0,8140
CDC37		1,4232	1,7760
DOCK7		1,2229	1,3278
EIF3I		1,1706	1,2582
FNBP1		1,1212	0,9980
LIN7B		1,5646	1,4282
MRTFA		1,3486	1,2547
RND3		1,9979	1,3738
SH3RF1		1,6299	1,8533
SNAP23		0,7577	0,8692
TRIP10		1,7127	1,9460

3.4.3.1. Control vs. CRC Results

Genes listed in Table 3.6 were analyzed in ShinyGo webtool for detailed information about their genomic and functional identity. The first graph obtained is showed the first 10 pathway related to these 15 genes (Figure 3.48). Signaling by RHO GTPases, RHO GTPase effectors, RHO GTPases activate formins, mitotic anaphase and mitotic spindle checkpoints are enriched. Fold enrichment dot plot of associated pathways (Figure 3.48), the hierarchical clustering tree shows correlation between enriched pathways (Figure 3.49) and network depiction of relation between enriched pathways (Figure 3.50) are shown below.

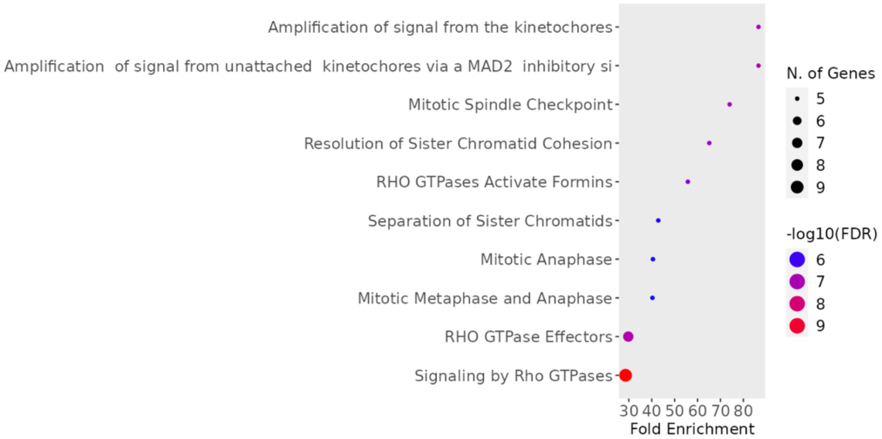

Figure 3.48: Fold enrichment dot plot of associated pathways for control vs CRC comparison. Bigger dots indicate higher number of genes included

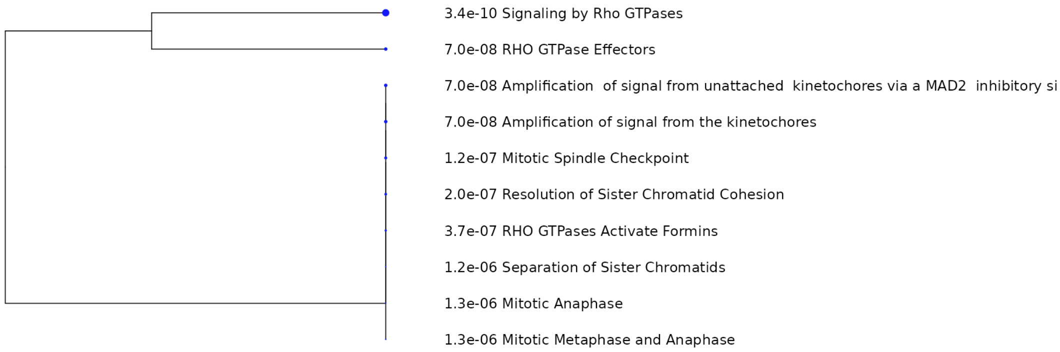

Figure 3.49: A hierarchical clustering tree which summarizes the correlation among significant pathways listed in Figure 3.48. Bigger dots indicate signifiant p-values.

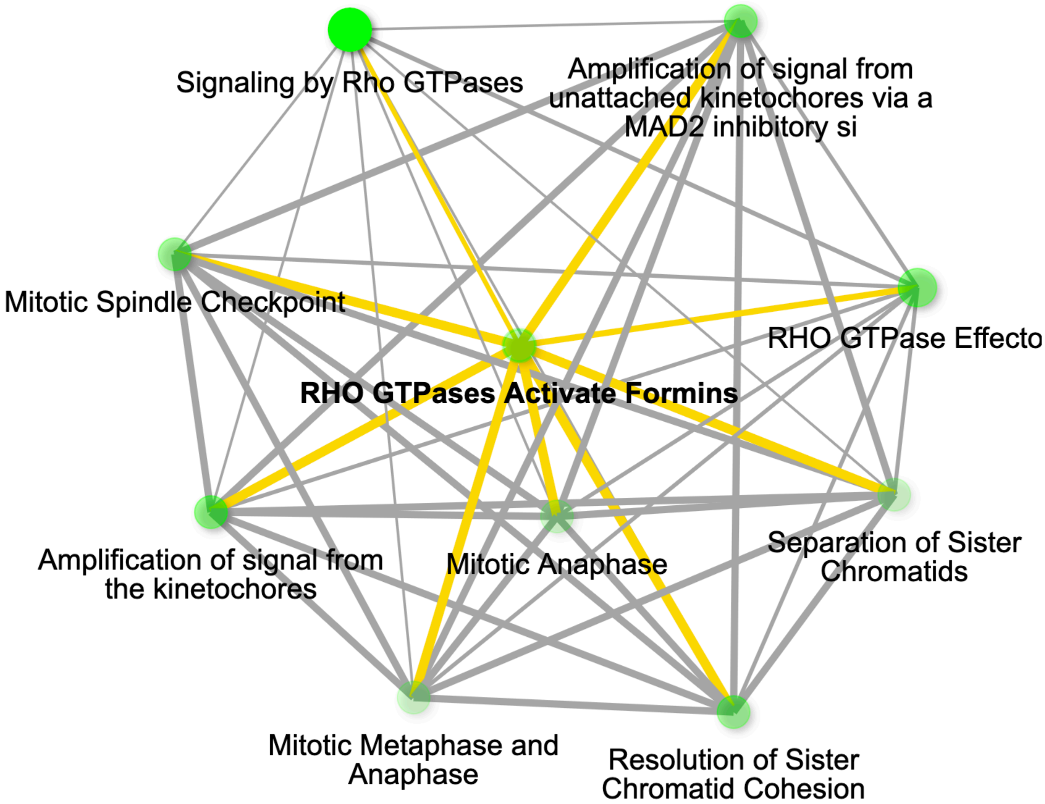

Figure 3.50: This network shows the relationship between enriched pathways for control vs CRC filtered gene list for signaling by RHO GTPases and RHO GTPase activate formins . Two nodes are connected if they shared 20% or more genes. Bigger and darker nodes indicate significantly enriched gene sets. Thicker edges represent more overlapped genes.

3.4.3.2. Control vs. mCRC Results

Genes listed in Table 3.6 were analyzed in ShinyGo webtool for detailed information about their genomic and functional identity. The first graph obtained is showed the first 10 pathway related to these 15 genes (Figure 3.51). Signaling by RHO GTPases, RHO GTPase effectors, RHO GTPase cycle, membrane trafficking and GTP hydrolysis are enriched pathways. Fold enrichment dot plot of associated pathways (Figure 3.51), the hierarchical clustering tree shows correlation between enriched pathways (Figure 3.52) and network depiction of relation between enriched pathways (Figure 3.53) are shown below.

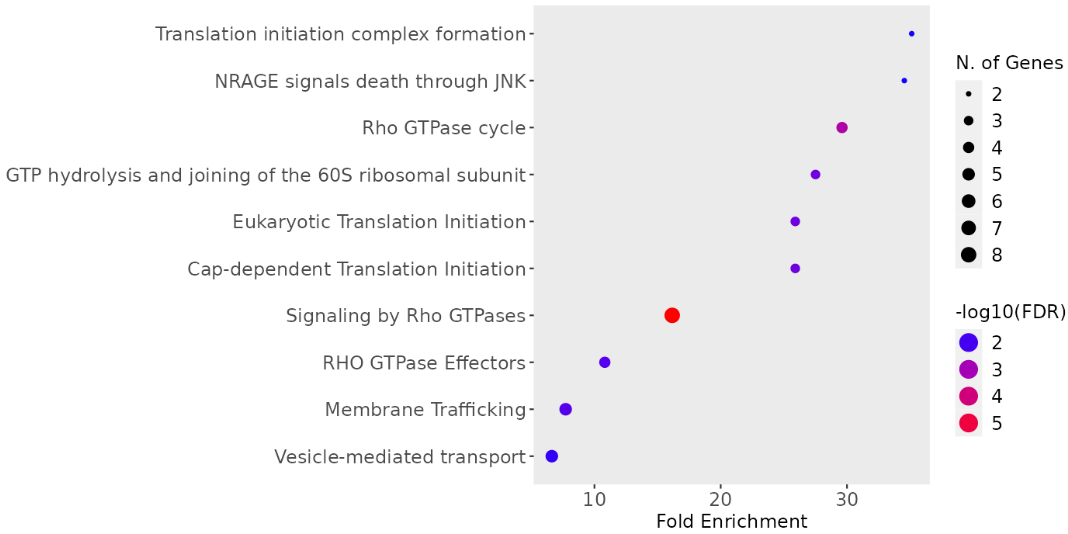

Figure 3.51: Fold enrichment dot plot of associated pathways for control vs mCRC comparison. Bigger dots indicate higher number of genes included

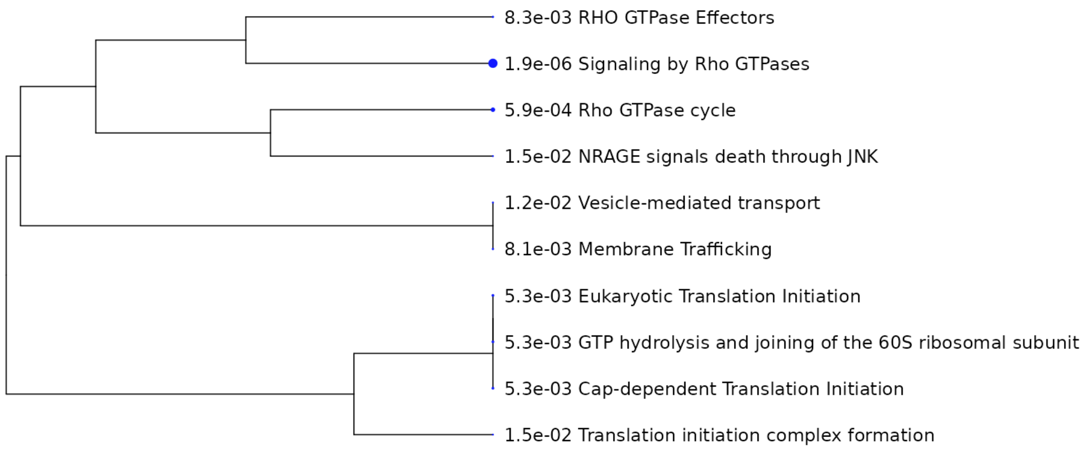

Figure 3.52: A hierarchical clustering tree which summarizes the correlation among significant pathways listed in Figure 3.51. Bigger dots indicate signifiant p-values

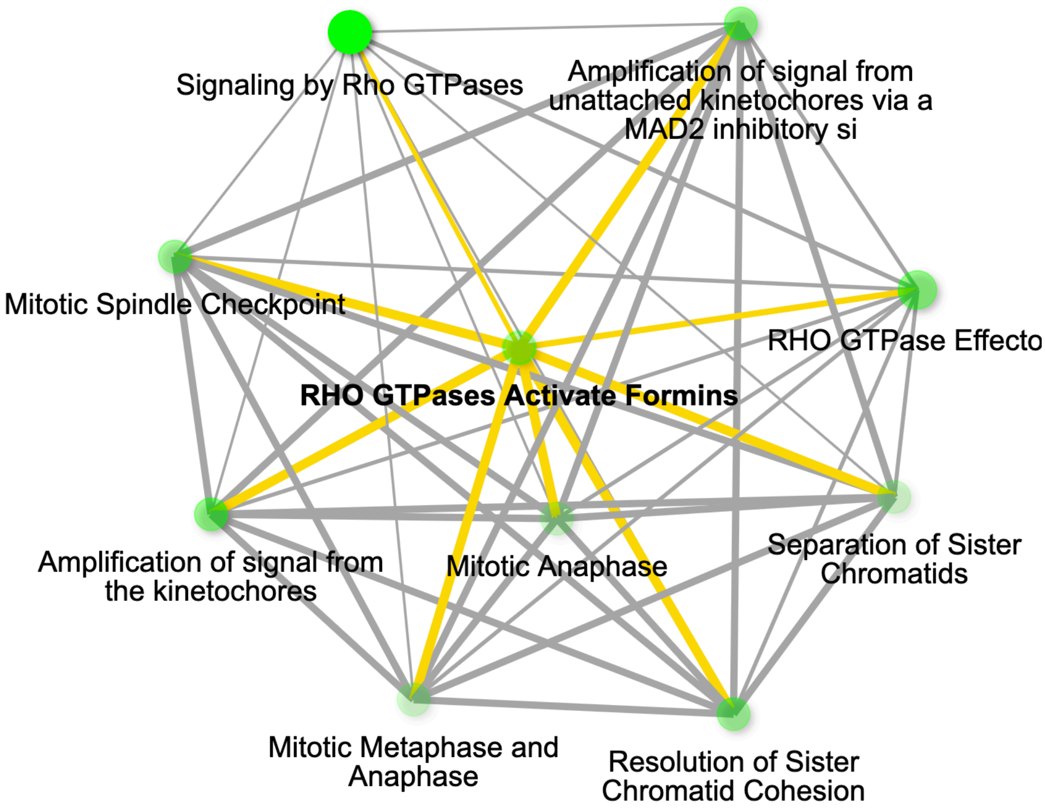

Figure 3.53: This network shows the relationship between enriched pathways for control vs mCRC filtered gene list for signaling by RHO GTPases and RHO GTPase activate formins . Two nodes are connected if they shared 20% or more genes. Bigger and darker nodes indicate significantly enriched gene sets. Thicker edges represent more overlapped genes.

3.4.3.3. CRC vs. mCRC Results

Genes listed in Table 3.6 were analyzed in ShinyGo webtool for detailed information about their genomic and functional identity. The first graph obtained is showed the first 10 pathway related to these 15 genes (Figure 3.54). Signaling by RHO GTPases, RHO GTPase effectors, RHO GTPases activate formins, mitotic metaphase and anaphase and mitotic spindle checkpoints are enriched. Fold enrichment dot plot of associated pathways (Figure 3.54), the hierarchical clustering tree shows correlation between enriched pathways (Figure 3.55) and network depiction of relation between enriched pathways (Figure 3.56) are shown below.

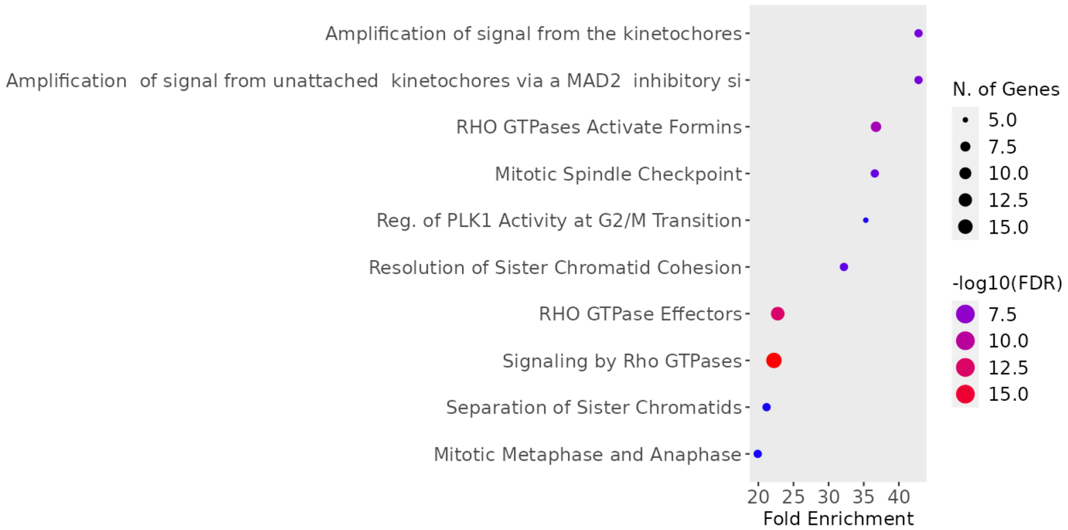

Figure 3.54: Fold enrichment dot plot of associated pathways for CRC vs mCRC comparison. Bigger dots indicate higher number of genes included

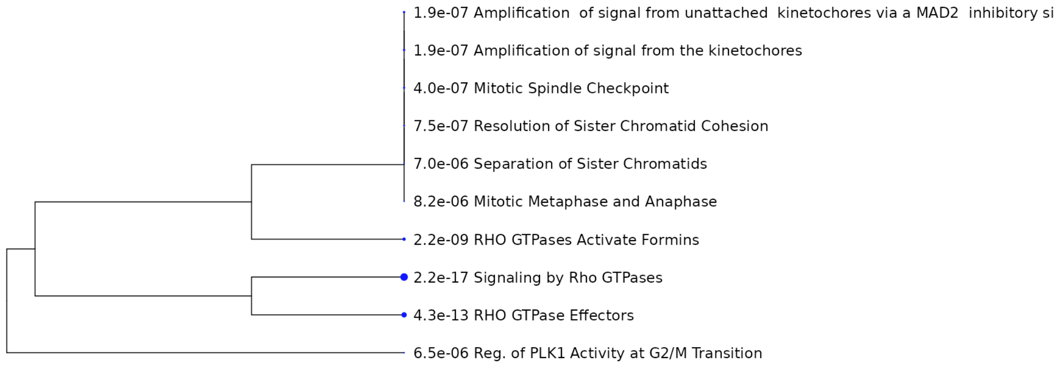

Figure 3.55: A hierarchical clustering tree which summarizes the correlation among significant pathways listed in Figure 3.54. Bigger dots indicate signifiant p-values

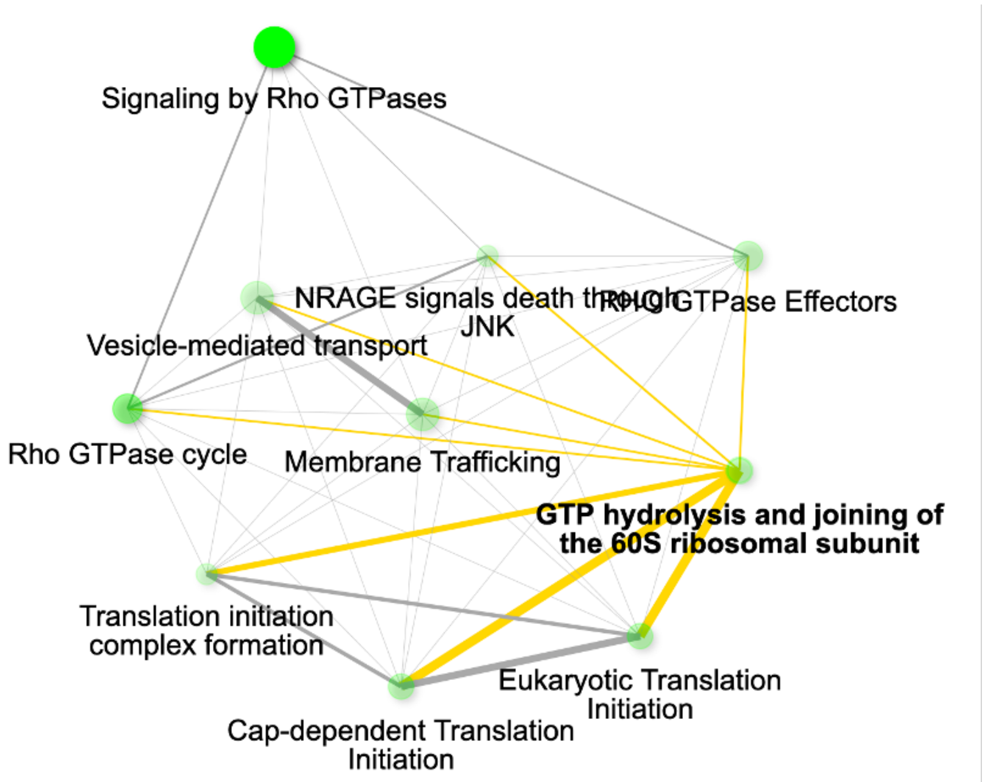

Figure 3.56: This network shows the relationship between enriched pathways for control vs mCRC filtered gene list for signaling by RHO GTPases and RHO GTPase activate formins . Two nodes are connected if they shared 20% or more genes. Bigger and darker nodes indicate significantly enriched gene sets. Thicker edges represent more overlapped genes.

Genes listed in Table 3.6B were analyzed in ShinyGo webtool for detailed information about their genomic and functional identity. The first graph obtained is showed the first 10 pathway related to these 15 genes (Figure 3.57). Signaling by RHO GTPases, membrane trafficking, clathrin-mediated endocytosis, and vesicle-mediated transport are enriched pathways. Fold enrichment dot plot of associated pathways is shown below.

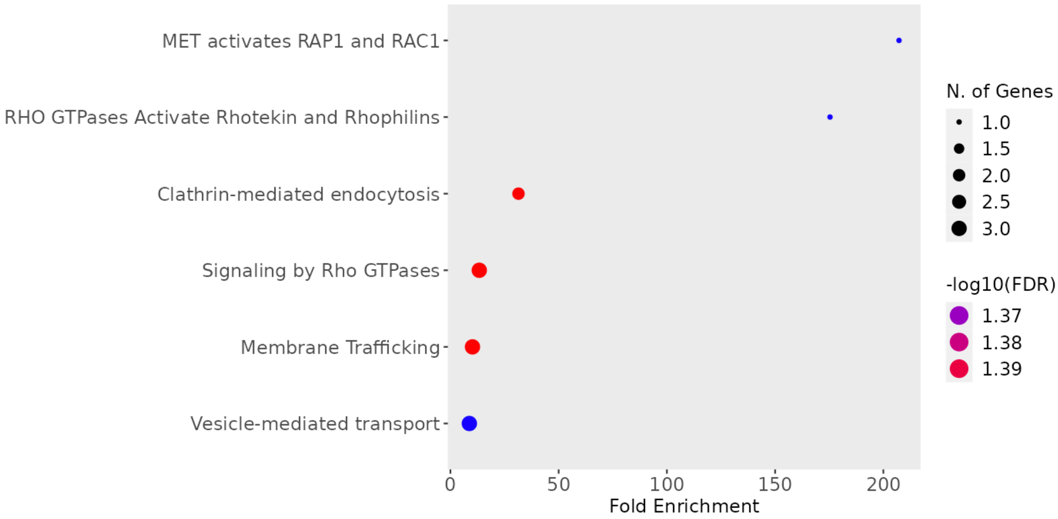

Figure 3.57: Fold enrichment dot plot of associated pathways with the shared genes in Table 3.6.. Bigger dots indicate higher number of genes included

3.4.4. microRNA Enrichment Analysis

microRNAs that differentially expressed according to our RNA-seq results were listed (Table 3.7). miRNAs were individually entered in miRPathDB (mpd.bioinf.uni-sb.de/) to get detailed information about them. miRTargetLink (ccb-compute.cs.uni-saarland.de/mirtargetlink2) was used to obtain associated network with the interested miRNAs. Only strong and validated pathways were drawn. Targets of miRNAs were retrieved from miRPathDB. The list of target genes and the initial differential expression genes (Appendix 2) were uploaded into Set Comparison Appyter (appyters.maayanlab.cloud/#/CompareSets) to get the venn diagram for the shared genes. The shared genes were uploaded into Genecodis and ShinnyGo web tools for pathway enrichment analysis.

Table 3.7: The list of differentially expressed miRNAs in RNA sequencing differential expression gene lists (Appendix 2).

microRNAs		
Control vs CRC	**Control vs mCRC**	**CRC vs mCRC**
hsa-mir-455	hsa-mir-3157	hsa-mir-548
	hsa-mir-548	hsa-mir-4495
		hsa-mir-3187
		hsa-mir-4307
		hsa-mir-4455
		hsa-mir-3945
		hsa-mir-4746
		hsa-mir-3157
		hsa-mir-4527
		hsa-let-7d

hsa-miR-3157 (UUCAGCCAGGCUAGUGCAGUCU) was differentially expressed in mCRC samples in comparison with both control and CRC samples. The shared genes among its target genes and the initial differentially expressed genes were uploaded into Set Comparison Appyter and the below venn diagram was obtained (Figure 3.58). The shared genes were TIRAP, DYRK1A, POLL, OSBP, BRIX1, GDE1, UBOLN4, and KNSTRN. The only associated pathways with has-mir-4495 was shown in figure 3.59. However, the only enriched pathway for the shared genes was the non-homologous end joining pathway.

Figure 3.58: This Venn diagram compares the inputted gene sets (0: hsa-mir-3157 target genes; 1: control vs mCRC differential expression gene list; 2: CRC vs mCRC differential expression gene list) and displays the intersections between them.

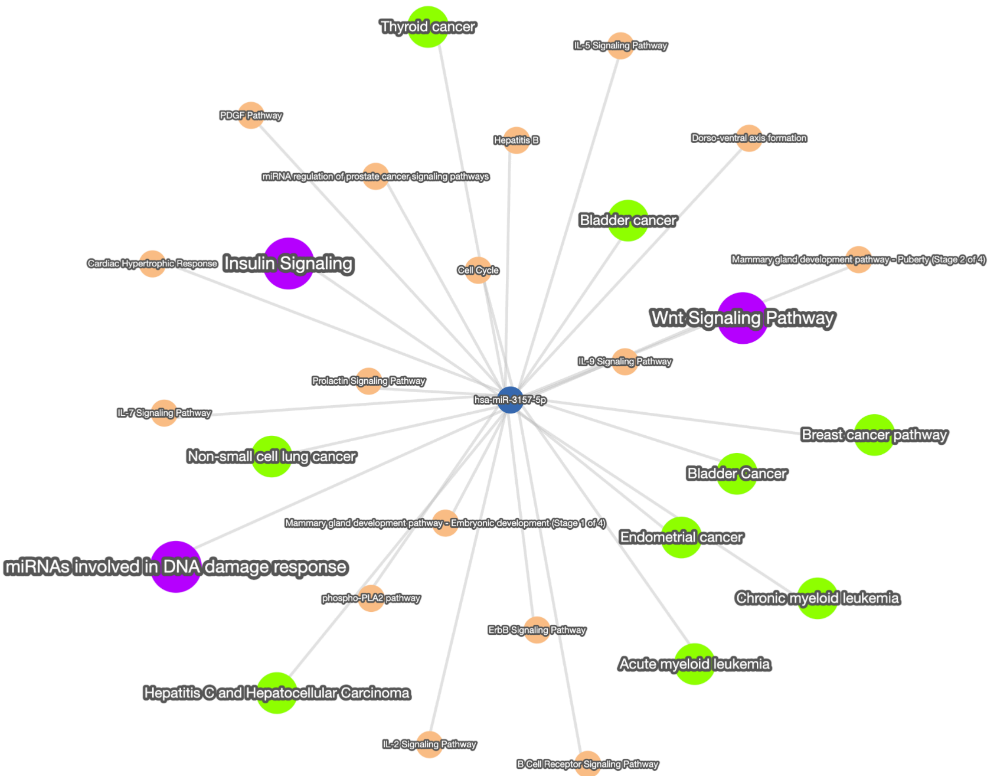

Figure 3.59: The network depiction of associated pathways with hsa-mir-3157. Purple nodes represent signaling pathways and DNA damage response related pathways. Green nodes represent the related cancer types.

hsa-miR-4495 (AAUGUAAACAGGCUUUUUGCU) was differentially expressed in mCRC samples in comparison with CRC samples. The shared genes among its target genes and the initial differentially expressed genes were uploaded into Set Comparison Appyter and the below venn diagram was obtained (Figure 3.60). The shared genes were SLC14A2, ZMYM1, CNGA1, LGR5, CHMP1B, RBM41, SLC7A2, TBC1D10B, RCAN3, SIGLEC9, CFAP44, PCM1, PCDHB7, FGFBP3, CYTIP, NF1, SLC7A6, UBR7, CYB5R4, CSRNP3, DNAIC6, TOR1A, KDM7A, CD47, NUP62CL, ESCO1, ERLIN2, TTF2, RIMKLA, TBC1D9, CBLN3, STXBP4, COPS7A, GFPT1, RNF135, DIP2B, RNF34, ZBED1, DYRK1A, ABHD17B, ERGIC2, BRMS1L, ATAD5, FZD4, TRIP10, HHIPL1, WDR76, PPP3R2, FLCN, TLCD4, SH3RF1, CCNL1, F2, TBL1XR1, TMEM251, FNIP1, PRPF38A, RWDD3, DSTN, NOTCH2, UBE2L6, BRIX1, SERINC3, AP3S1, GPN2, CPSF2, STRAP, CUL4B, UBB, DOCK7, UBAC2, CRTAP, ERI1, HMBOX, KLF10,MAOA, MAT2A, LAD1, KIAA0586, DLD, SOX13, TMPRSS4, PCDHB11, ANKRD50, OSBP, SDAD1, HIVEP2, SHTN1, HIF1A, MFSD6, NCKAP5, FRMD5, DICER1, DCC, SPRY4, PCDHB15, C3ORF70, SLC30A1, STC2, GNAQ, CHRM2, TFPI, CPSF6, GAB1, IPH1, ZNF557, HOXA13, DENND1C, ANP32R, XRN1, CD200R1, GALNT13, KATNBL1, IAZF1, WNT3, FNBP1, TP53INP1, NEK1, and THAP9. The associated pathways with hsa-mir-4495 was shown in figure 3.61. Clathrin-mediated endocytosis, cargo recognition for clathrin-mediated endocytosis, and regulation of FZD by ubiquitination were the enriched pathways for the shared genes (Figure 3.62).

Figure 3.60: This Venn diagram compares the inputted gene sets (0: hsa-mir-4495 target genes; 1: control vs mCRC differential expression gene list; 2: CRC vs mCRC differential expression gene list) and displays the intersections between them.

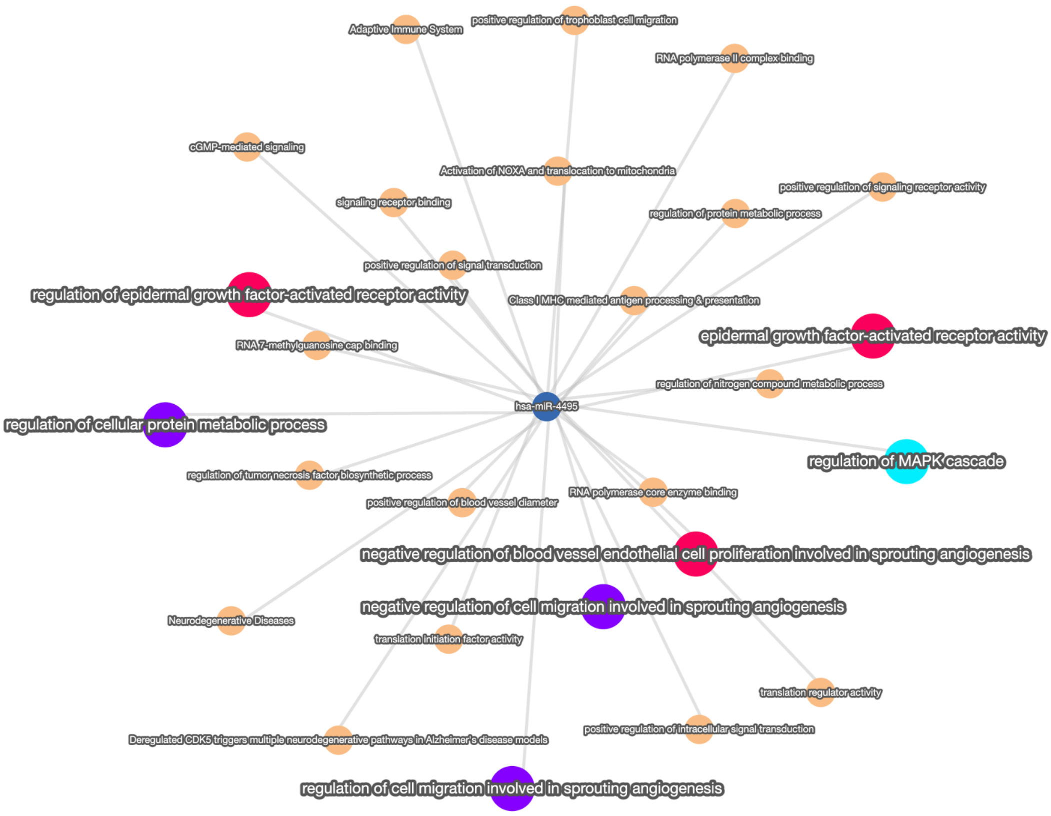

Figure 3.61: The network depiction of associated pathways with hsa-mir-4495. Purple nodes represent sprouting angiogenesis related pathways. Red nodes represent epidermal growth factor (EGF) activated angiogenesis-related pathways and the blue node represents the MAPK cascade.

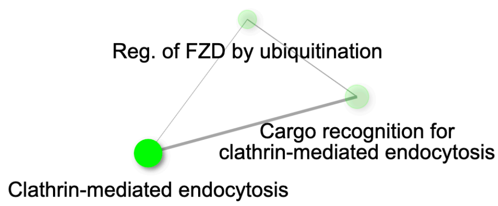

Figure 3.62: The network depiction of the enriched pathways for the shared genes.

hsa-let-7d (AGAGGUAGUAGGUUGCAUAGUU) was differentially expressed in mCRC samples in comparison with CRC samples. The shared genes among its target genes and the initial differentially expressed genes were uploaded into Set Comparison Appyter and the below venn diagram was obtained (Figure 3.63). The shared genes were MSFD6, PHLPP2, TLCD4-RWDD3, TP53INP1, MRAP2, CD200R1, TMPRSS4, RASL11B, CYP46A1, UBB, FZD4 TBC1D10B, DCC, STAT2, FNIP1, ACTRT3, GNAQ, SDAD1, SIGLEC9, SLC7A6, RIMKLA, CSRNP3, BRIX1, ORM1, CLDN1, TMEM251, SYT7, SNPH, DSTN, MVB12B, C3ORF70, RNF135, PEX7, DUS4L, GFPT1, SH3RF1, FBXW4, KRT33B, HMBOX1, HHIPL1, MAT2A, TLCD4, STXBP4, DNAIC6, HOXA13, CBLN3, RND3, TRIP10, NUP62CL, ATAD5, CYTIP, PRPF38A, KNCAB3, SOX13, MPC2, NFU1, SPRY4, KATNBL1, NOTCH2, SNAP23, KLF10, MRTFA, POLL, DICER1, WDR76, CHMP1B, ERGIC2, XRN1, ANP32E, GALNT13, ABHD17B, DYRK1A, ETNPPL, MAOA, TOR1A, DOCK7, INPP5B, ELL, CPSF6, STRAP, USP24, F2, PLA2G2F, CRTAP, ERI1, CNOT1, GPATCH3, RBM4, CPSF2, SLC2A1, SLC30A1, MAPT, MRAS, ESCO1, TRIM35, FRMD5, PCDHB15, CDCA7, FNBP1, PCDHB11, PKP1, CCNL1, IPH1, SHTN1, KIAA0586, THAP9, CFAP44, ZNF557, BRMS1L, GPN2, FLCN, and GCNT3. The associated pathways with has-let-7d were shown in figure 3.64. Fold enrichment dot plot of associated pathways for the shared genes between hsa-let-7d targets and mCRC differentially expressed genes shows that the common genes were enriched in epithelial to mesenchymal transition in colorectal cancer (Figure 3.65).

Figure 3.63: This Venn diagram compares the inputted gene sets (0: hsa-let-7d target genes; 1: control vs mCRC differential expression gene list; 2: CRC vs mCRC differential expression gene list) and displays the intersections between them.

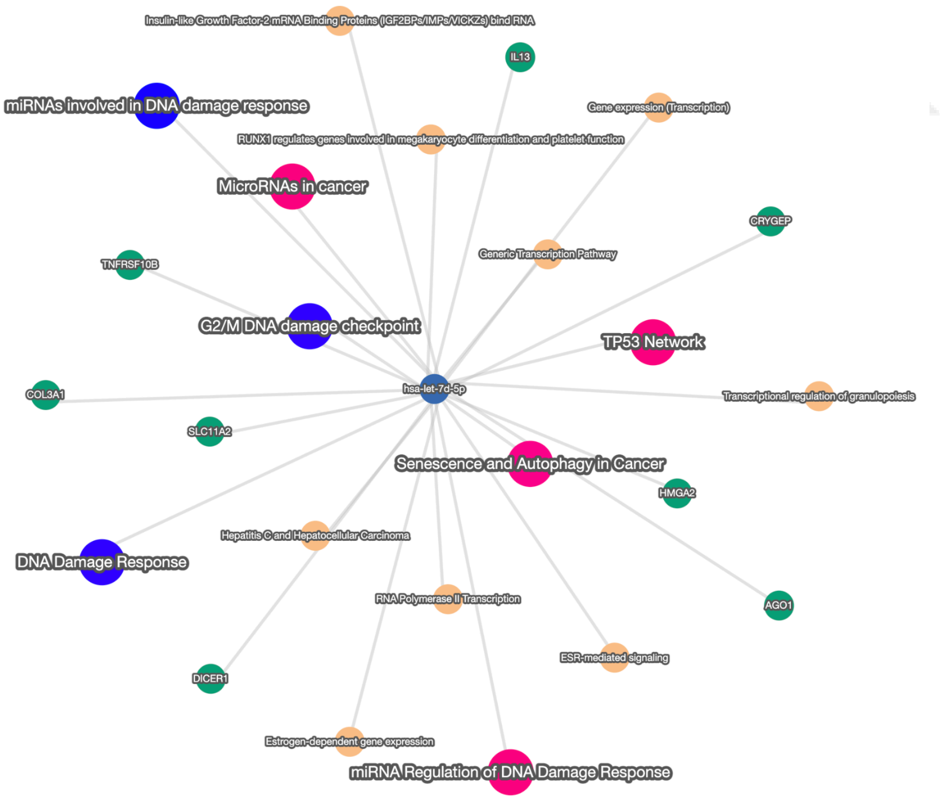

Figure 3.65: The network depiction of associated pathways with hsa-let-7d. Blue nodes represent DNA damage related pathways. Pink nodes represent cancer related pathways.

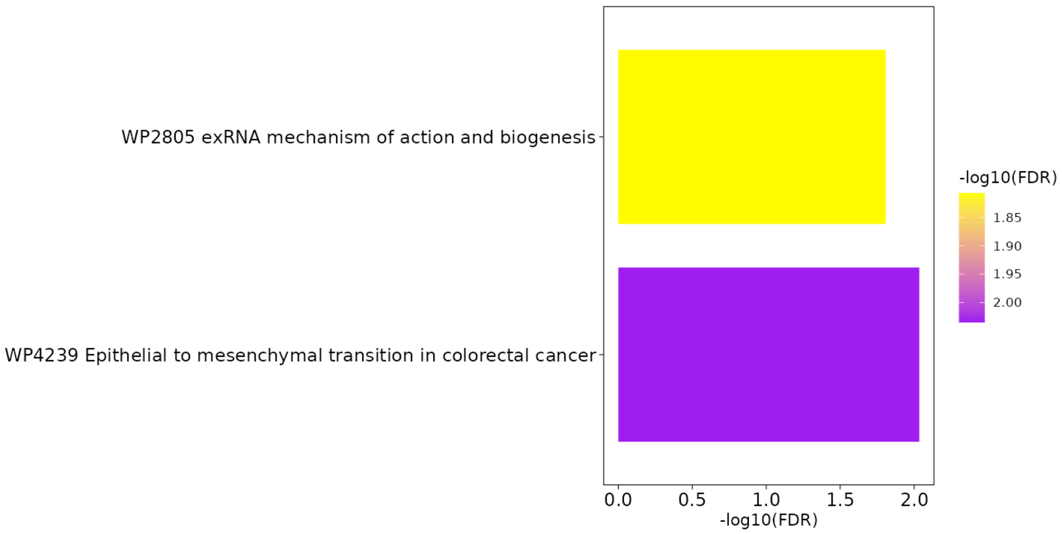

Figure 3.65: Fold enrichment dot plot of associated pathways for the shared genes between hsa-let-7d targets and mCRC differentially expressed genes .

4. DISCUSSION

Reprogramming of erythroblasts of colorectal cancer patients was investigated and healthy donors' erythroblasts were used as control group. Cells were transduced with Sendai viral vectors encode for the reprogramming factors Klf4, c-Myc, and a polycistronic vector that contains Klf4, Sox2, and Oct3/4. The day after transduction of exogenous TFs, cells were cultured on vitronectin-coated plates and two days later cells were fed with either homemade iPSC medium (table 2.4) or TeSR-E7/ReproTeSR medium. Depending on the donor, 6-10 days after the first colony-forming cells appeared, which were passaged and transferred onto vitronectin-coated plates. The reprogramming of cells of patient#2 (CRC#2-iPSCs) could not be reprogrammed with TeSR-E7 medium. CRC#1-iPSCs could be reprogrammed with both medium types even at the lower concentrations of Sendai vectors (MOI: 3:1.5:2). Varied reprogramming statuses show that the efficiency of the procedure could change donor to donor. After re-plating, single cells formed tightly packed colonies on vitronectin and these cells were positive for alkaline phosphatase (AP) activity, which is an early marker of reprogramming (Figure 3.5). One of the strongest indicators of functional iPSCs is the elavated expression of the endogenous pluripotency markers. Sox2 is the orchestrated the hierarchical network of pluripotency factors in ongoing reprogramming (Buganim et al., 2012). Partially reprogrammed cells have lower expression levels of endogenous pluripotency markers even if the exogeneous transgenes are expressed. All of iPSC line reprogrammed in this thesis study were highly expressed endogenous pluripotency genes in both protein and transcript levels (Figure 3.6-3.8). These data indicate that continuous expression of reprogramming TFs successfully induced pluripotency in EPCs.

The reprogramming process includes a erasing of epigenetic make-ups. In iPSCs, DNTM3L has an important role during the erasing process (Ooi et al., 2010).

DNMT3L is upregulated in ESCs to prevent hypomethylation of developmental genes and keep ESCs at undifferentiated state (Neri et al., 2013). Here, DNMT3a was found to be upregulated in iPSCs at levels comparable to their sometic origins. Successful reprogramming procedure needs a completed MET. E-cadherin (CDH1) is considered as a representative surface marker of MET. Epithelial transition allows to monitor the change of non-adherent cells' characteristics during reprogramming process and can be considered as an early indicator of reprogramming (LiL. et al., 2010). CDH1 increased 20-fold compared to parental cells. Increased expression 1 (REX1) is an another widely used pluripotency marker. Previous studies show that REX1-silenced pluripotent cells lose the self-renewal capacity and mesodermal differentiation potential (Son et al., 2013). The expression of undifferentiated embryonic stem cell factor 1 (UTF1) is directly regulated by Oct4 and Sox2. UTF1 plays an important role in chromatin re-organization. UTF-1 works as both transcription factor and epigenetic factor controlling H3K27me3 deposition on the promoters of bivalent genes in pluripotent cells (Bao et al., 2017). REX1 and UTF-1 were found to be highly expressed in all of iPSC lines in this study.

Complex molecules called heparan sulfate proteoglycans (HSPGs) are found in the cellular membrane and extracellular moeity. HSPGs are essential for cellular adhesion, migration, proliferation, and signaling transduction pathways. Syndecan-2 is one of the cell surface proteoglycans and it increases in CRC and promotes cell motility. Other two syndecan protein, syndecan-1 and syndecan-4, are decreased. Syndecan-1 and -4 have anticancer characterictics and decrease in CRC. Glypicans and perlecan expression levels are also altered in CRC, however, it remains unclear how syndecans contribute to tumor initiation (Vicente et al., 2018). Our bioinformatics results showed that Perlecan (HSPG2), which is a matrix HSPG, levels were decreased in mCRC donors in comparison with CRC donors. In general, all of our results demonstrated "proteoglycans in cancer" is one of the most enriched pathways in healhty intestinal organoids of CRC and mCRC patients. The differential expression gene lists were filtered with the key phrases "Colorectal cancer" and "Proteoglycans in cancer". Obtained gene list (Table 3.4A) was uploaded into GeneCodis and ShinyGo to retrieve enriched pathways specifically. The final result showed "Focal adhesion", "Wnt signaling pathway", and "PI3K-Akt signaling pathway" were enriched in the differentially expressed genes in CRC (Figure 3.28, 3.30). These pathways might be linked with CRC carcinogenesis. "Ras signaling pathway", "MAPK signaling pathway", and "Regulation of actin cytoskeleton" were enriched in the differentially expressed genes obtained from control vs mCRC comparison (Figure 3.31, 3.33). These pathways are directly or indirectly linked with metastasis process. "Wnt signaling pathway" was the only signaling pathway which enriched in the differentially expressed genes obtained from CRC vs mCRC comparison. This gene list contains 27 genes and only with these genes directly gave the cancer pathways such as colorectal cancer, breast cancer, hepatocellular carcinoma, and gastric cancer (Figure 3.35, 3.37). The pathway enrichment analysis was performed according to the identified markers in previous literature. In addition to these enriched pathways retrieved from KEGG database, carbon metabolism, glycolysis/gluconeogenesis, and metabolic pathways were also enriched in mCRC donors.

Metabolic reprogramming is one of the driving factors of cancer initiation. The metabolic reprogramming is carried on by mutations and epigenetic changes. Altered epigenetic make-up and oncogenic mutations might end up with increase in cellular stress factors such as accumulation of reactive oxygen species generation. Increasing cellular stress can cause damage in essential macromolecules including proteins, lipids, and DNA. Especially damaged DNA might cause genomic instability and promote tumor development. The nutrient absorption takes place in the small intestine, mainly. In addition, small intestine also has endocrine secretion thus certain immunological responses are orchestrated by small intestine. In recent years the interest in lipid metabolism has been risen as a critical factor CRC initiation, and our understanding of underlying mechanisms remains inadequate. The role of lipid metabolism in cell-cell and cell-tumor microenvironment (TME) communications. A detailed molecular understanding of the role of lipid metabolism might help us to find new biomarkers and new therapeutic approaches for CRC (Hanahan Weinberg, 2011).

As cancer cells need elevated levels of energy to promote rapid growth, cancer cells switch from oxidative phosphorylation to glycolysis and lactic acid fermentation, according to the theory of Otto Warburg (Warburg, 1956 ; Warburg et al., 1927). Recent studies showed that lipid metabolism is considered as another important initiator of malignant transformation as cancer cells have dysregulated lipid-associated pathways (Matsushita et al., 2021). Molendijk et al. studied on alterations in lipid metabolism, describing lipid metabolism as a crucial factor in carcinogenesis (Molendijk et al., 2020).

Our bioinformatics analysis showed that especially in CRC group has differentially expressed genes associated with lipid metasbolism. Further analysis were also done with the detailed gene list that compose lipid metabolism enrichment network. From three differential expression gene lists, genes involved in lipid metabolism were found (Table 3.5, control vs CRC, control vs mCRC, and CRC vs mCRC). In Table 3.5B, the common genes are shown, the gene list is sorted, and the log2(fold-change) values are given. The enrichment pathway analysis of the mentioned genes featured, and they were graded based on how many genes were present in the pathways they were linked to (Figure 3.39 for control vs CRC, Figure 3.42 for control vs mCRC, Figure 3.45 for CRC vs mCRC). Consequently, networks of control vs. CRC and control vs. mCRC (Figure 3.41 and Figure 3.44), and networks of CRC vs. mCRC were displayed (Figure 3.47). The primary structural components of both networks are, in general, lipid synthesis, and lipid metabolism. If two pathways share 20% or more genes, they are depicted as connected. Gene sets are enriched in darker nodes. Larger gene sets are displayed by bigger nodes. Thicker edges represent more shared genes. Fat digestion and absorption, glycerophospholipid metabolism, and ether lipid metabolism have the thicker edges as differentially expressed in specifically mCRC patients' healthy intestinal organoids (Figure 3.47).

The main pathways that Ras protein functions in are the phosphoinositide-3 kinase (PI3K) and mitogen-activated protein kinase (MAPK) pathways. Many of the known growth factors bind to receptor tyrosine kinases, which causes them to dimerize and autophosphorylate and initiates the downstream cascades. After the ligand binding, the following step includes PI3Ks. PI3Ks are classified in three distinct classes yet class IA has higher impact on the cancer initiation and development. Class IA regulatory subunit, p85, binds to the receptor tyrosine kinase (RTKs) phosphotyrosine residues within other adaptors. PIP2 is phosphorylated and turn into PIP3 (Nandan Yang, 2011). By directly interacting with p110 (PIK3CA), which is catalytical subunit, Ras can also physiologically activate the pathway (Shaw Cantley, 2006). PTEN functions a a tumor suppressor protein and can reverse the activation by dephosphorylating PIP3 back to PIP2 (Nandan Yang, 2011). PIP3 recruits pyruvate dehydrogenase kinase 1 (PDK1) and AKT kinases. AKT is phosphorylated by PDK1. As a result, AKT is activated and produces a number of downstream signals. The primary role of these signals is to aid cells proliferaten and avoid apoptosis. In our differential expression gene list of CRC donors showed the increase in PDK1 transcript. Under normal circumstances acetylation of AKT prevents binding of AKT and PDK1 and their localization, yet SIRT1 deacetylases AKT and increases binding of AKT-PDK1. SIRT1 and PDK1 expressions increased in healthy colon organoids of CRC patients. Our findings can be interpreted as SIRT1-PDK1 axis might be a potential mechanism that initiates PDK1-activated effector kinases activities. PDK1 is a crucial master kinase as it phosphorylates at least 23 downstream kinases various signal transduction pathways (Levina et al., 2022).

Ras mutations frequently occur with PIK3CA exon mutations (Baldus et al., 2010). It was proposed that when Ras is mutated, it loses its ability of binding wild-type P110. The functional binding of mutated Ras requires the altered version of PIK3CA, which presumably will encode for mutated and shortened form of P110. In CRC, PIK3CA mutations are reported that occur 15%–25% and may increase PI3K activity (Fearon, 2011). When the differential expression results of the mCRC group are examined, it is seen that the expression of PI3K interacting protein 1 (PIK3IP1) is significantly increased compared to the control group (Appendix 2). PIK3IP1 is found in the literature as a negative regulator of hepatic PI3K activity. Under physiological conditions, it allows functional binding of PI3Ks. As explained, the extensive role of the PI3K signaling pathway in CRC initiation, it should be considered that a protein function as PIK3AIP1 may play a role in the development of early-stage cancer. The fact that PIK3AIP1 expression was increased only in healthy organoids of metastatic CRC patients. The difference between the gene expression profile of CRC and mCRC donors might be important to assess the cancer or metastasis initiation susceptibility of donors with different stages of malignancy. Previous studies demonstrated that SIRT1 expression increases in colorectal cancer tissues (YuD.-F. et al., 2016).

Our bioinformatics results showed that Ras signaling pathway was enriched in healthy intestinal organoids of mCRC donors. This pathway is initially activated when a ligand interacts with a RTK. A ligand-bound RTK is dimerized and phosphorylated (Reuter et al., 2000). The growth factor receptor-bound protein 2 (GRB2) attaches to RTK while being bound by son of sevenless (SOS), and downstream complex of proteins is recruited. GRB2-bound SOS protein binds RAS (Courtney et al., 2010). After joining with RAS, SOS functions as a guanine nucleotide exchange factor. SOS pulls guanosine diphosphate (GDP) molecules away from RAS, allowing guanosine triphosphate (GTP) molecules to bind and activate it. An active GTP-Ras complex attracts A-RAF, B-RAF, and C-RAF proteins towards the cell surface, recruited RAF proteins are separated from their cytosolic partners and become activated; at the end they pair up to form heterodimers that can bind to and activate the KSR1 enzyme (Courtney et al., 2010). In a healthy cell, the aforementioned process is completely normal and is stopped by RAS-GTPase activating (GAP) proteins. These proteins, as their name implies, activate RAS-located GTPase enzymes, which hydrolyze GTP to GDP and so turn RAS off (Courtney et al., 2010). AGAP-1 gene was increased in healthy intestinal organoids of CRC donors as expected because of the non-malignant nature of the organoids (Appendix-2). However, the same gene was decreased in mCRC patients' healhty organoids when their RNA profile was compared with the CRC patients' profiles but not with the control donors. Additionally, other GAP proteins such as ARHGAP12, SRGAP1, and antisense RNA-2 and -3 of SRGAP3 were also decreased in the same list (Appendix-2). This differential expression of

AGAP-1 and other decreasing GAP proteins might indicate that the metastasis potential of patient can be detected even before the cancer initiation.

Tight junctions, adheren junctions, desmosomes, and gap junctions form the apical junctional complex (AJC). Monolayer polarized cells which attach to their neighbour cells compose the epithelium lining of gastrointestinal tract. Another function of Rho GTPases is to orchestrate both assembly and disassembly of AJC. The disassmbly of AJC and following cell-cell adhesion loss promote signal transduction that lead epithelial cell progression. AJC and actin cytoskeleton organization sustain apico-basal polarity in epithelial cells. A loss in cell-cell connection and polarity, increased proliferation rate, decreasing cell death, and acquired cell motility and increasing invasiveness are the distict chaaracteristics of metastasis. Tight junctions and adheren junctions are disassembled by the increasing levels of lipoproteinA (LPA) and lower calcium levels, which result in Rho activation and finally change in epithelial characteristic of cells and promotion of cell migration. Our mCRC healthy colon organoids have elavated LPA levels (Appendix-2). BRAF mutation activates a Rac1b (tumor-specific splice variant of Rac1 GTPase), it promotes survival of CRC cells. Our mCRC donors' healthy colon organoids have decreased levels of BRAF, but the levels of CDC42, Rac1, and RhoA were not changed. As explained above, GAP proteins hydrolyze RAS-bound GTP to GDP and inactivates RAS, NF1 functions as a negative regulator of RAS. Alterations in NF1 structure disallows its efficient binding so it cannot function as an inhibitor of Ras signaling. It was proposed that NF1 may contribute to the initiation of CRC. Our results also showed that our mCRC data showed increased expression of the NF1 gene compared to the control group. Although no further mutation analysis was performed, the increase in NF1 expression in healthy organoids of mCRC donors has led us to think that increasing levels of NF1 may be associated with metastasis. The decrasing levels of GAP proteins indicate that Ras signaling cannot be controlled as it controlled under physiological conditions in mCRC patients intestinal tissue even there is no detected malignancy. Increasing levels of NF1 might has a compensatory function for reduced GAP levels. In our study, the intestinal organoids serve as a patient-specific in vitro models and control group did not have differential changes in either GAP or NF1 gene levels.

Rho GTPases are essential participants in cancer cell proliferation and invasion (Vega Ridley, 2008). A member of the Rho family named RhoA has a crucial role sustaining cellular morphology, migration and invasion capacity of cancer cells (Ridley, 2013). RHOT1 (Ras homolog family member T1, known as mitochondrial Rho; MIRO-1), involves in mitochondrial transport (Fransson et al., 2003). In a 2015 study, it was discovered that pancreatic cancer lines had significantly higher transcript levels of RHOT1. According to their research, RHOT1 might control cell migration and proliferation by inhibiting the expression of SMAD4 in pancreatic cancer (LiQ. et al., 2015). Another study shows that microvesicles derived from CRC cells carry RHOT1 protein and the microvesicles stimulated endothelial cell proliferation. Their results indicate that microvesicles obtained from CRC cells may contribute to tumor growth and metastasis by promoting angiogenesis-related activities (HongB. S. et al., 2009). However, its function in CRC development and prognosis is still unclear. Our results demonstrated that RHOT1 expression was increased in both CRC and mCRC patients' healthy organoids when their profiles were compared with the control donors. There is no differential expression change between CRC and mCRC donors. This might indicate that RHOT1 might function in cancer initiation. The cell migration process is two distint types: mesenchymal migration and ameoboid migration. Mesenchymal migration is the result of EMT process and includes a partial loss of polarity and cells have fibroblastic phenotype. Ameoboid migration includes the complete loss of polarity and cells have round morpholgy. Cancer cells can switch between different motility formats depends on the Rho GTPase activity (Sanz-Moreno, 2008). For mesenchymal migration, Rho expression is needed to be reduced only at one side of cells as to provide partial loss of polarity at the front of cells. The loss of cell polarity results in stress fiber contractions and weakens cell-extracellular matrix interation that reduces the strength of focal complexes. Membrane extension and protrusion direct the migration. Increase in Rho GTPase expression leads the increase of invasiveness (Vishnubhotla, 2007). PAK1, Rho-associated p21-activated kinase 1, and PKN2 (protein kinase novel-2) were also upregulated in mCRC donors' healthy colon organoids. PAK1 has a important role in lamellipodia formation. Rho binding of PKN require the catalytic activation of PDK1 which might be the link between dysregulated PI3K-Akt pathway and Rho GTPase signaling during the initiation of CRC metastatis (Zhao Manser, 2005).

The tripartite-motif (TRIM) family is a single protein RING-finger E3 ubiquitin ligase class. Cancer initiation, progression, oncogenic or tumor suppressive functions are some of the processes which TRIM family involves. All TRIM members have RING domain, yet the other domains like SPRY or bromo domain varies among the members. PRY and SPRY domains are presented on the C-terminal of the proteins. This specific portion contains PRY ans SPRY domains frrequently responsible for the target recognition. Our CRC donors have elevated TRIM37 expression in their healthy intestinal organoids. TRIM37 is a class VIII TRIM protein and has meprin (MATH) domain. mCRC donors have increased TRIM5 and TRIM35 expression in their healthy intestinal organoids. TRIM35 is a member of class IV TRIM protein which has PRY, SPRY, and COS domain. TRIM5 is also a member of class IV TRIM protein but does not have PRY domain. Previous studies showed that TRIM37 has role in tumorigenesis through reprogramming of glucose metabolism. Also, it has an effect on chemetherapy and targetted therapt contolling. HCC (hepatocellular carcinome), RCC (renal cell carcinoma), and pancreatic carcinoma have differential TRIM37 expression. CRC and lung carcinoma have differential TRIM35 expression (Huang et al., 2022). Another study showed that TRIM37 was significantly upregulated in CRC tissue compared with the matched adjecent normal tissue (Hu Gan, 2017). Among our samples, healthy intestinal organoids from CRC patients have significant levels of TRIM37 expression. Although the difference between mCRC patients and control patients is not statistically significant, it is expressed much less than in CRC patients. In CRC cell lines, TRIM37 was both overexpressed and knocked down. Increased TRIM37 expression was found to promote CRC cell invasion and proliferation (Hu Gan, 2017). The studies either used CRC tissue and its paired healthy tissue or CRC cell lines. We think that testing the function of TRIM37 in cells that have not yet developed into malignant cells would be more accurate to reveal the TRIM37 function in cancer initiation. In terms of diagnostic/prognostic marker research, TRIM37 evaluation in prospective studies on its potential as an early carcinogenesis marker can be valuable. Our hypothesis that TRIM37 may have a role in carcinogenesis is supported by its low expression in healthy intestinal organoids of mCRC patients but high expression in healthy intestinal organoids in CRC patients. Tumor-suppressing properties of TRIM35 have previously been discovered in experiments with HCC cells (ChenZ. et al., 2015). In mCRC patient organoids that have healthy phenotype, TRIM35 expression is elevated. Since this expression increase is in organoids that have not yet developed cancer yet the donor is known to develop CRC, we have a speculative hypothesis that TRIM35 may have a temporary stopper impact on carcinogenesis. Patients with low TRIM5 and TRIM35 expressions showed poorer survival rates than those with high expression, according the analysis of RNA samples in the TCGA database. $TRIM5^{low}$ 30% and $TRIM35^{low}$ 53% are the 5-year survival rates, respectively (Figure 4.1-4.2). The 5-year survival rates for TRIM37 are $TRIM37^{high}$ 67% and $TRIM37^{low}$ 57% when the TCGA data is examined (Figure 4.3). Studies conducted in vitro demonstrate that TRIM37 affects EMT. In contrast to TRIM5 and TRIM35, TRIM37 expression levels have survival rates that are more comparable. We believe that TRIM5 and TRIM35 can be at least as conclusive as TRIM37 in this situation.

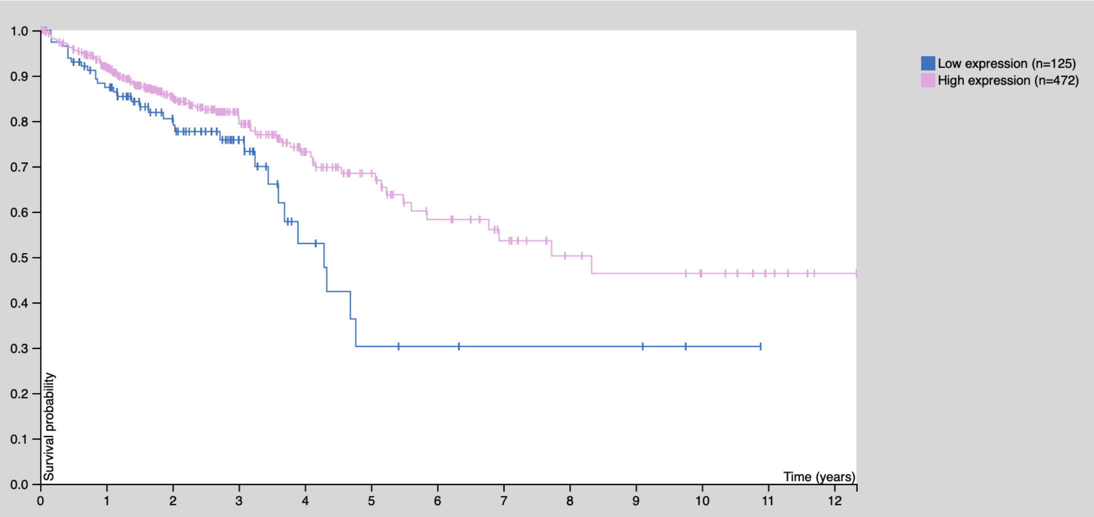

Figure 4.1: The survival plot of CRC patients according to the TRIM5 expression levels. The plot was retrieved from Human Protein Atlas on date 29.03.2023.

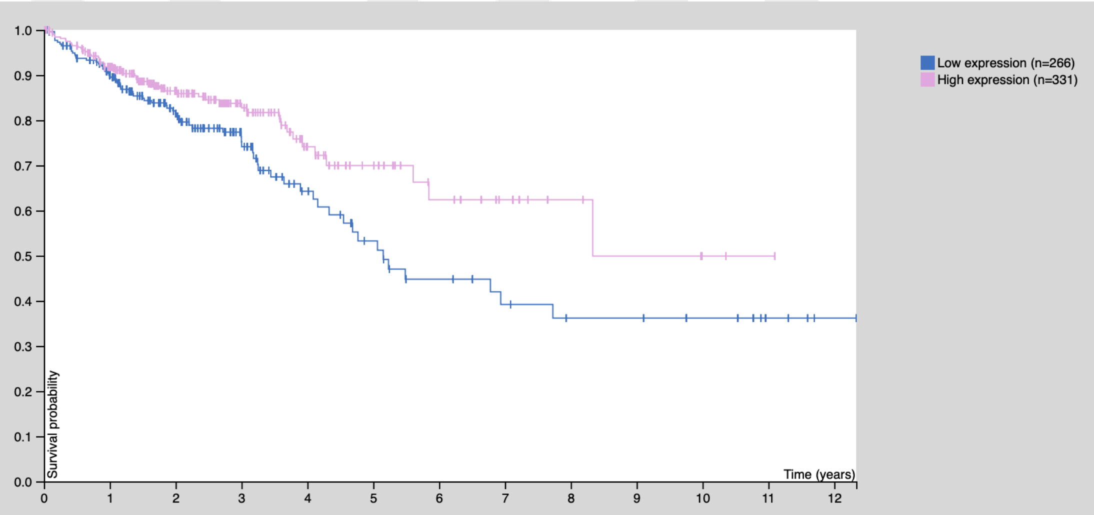

Figure 4.2: The survival plot of CRC patients according to the TRIM35 expression levels. The plot was retrieved from Human Protein Atlas on date 29.03.2023.

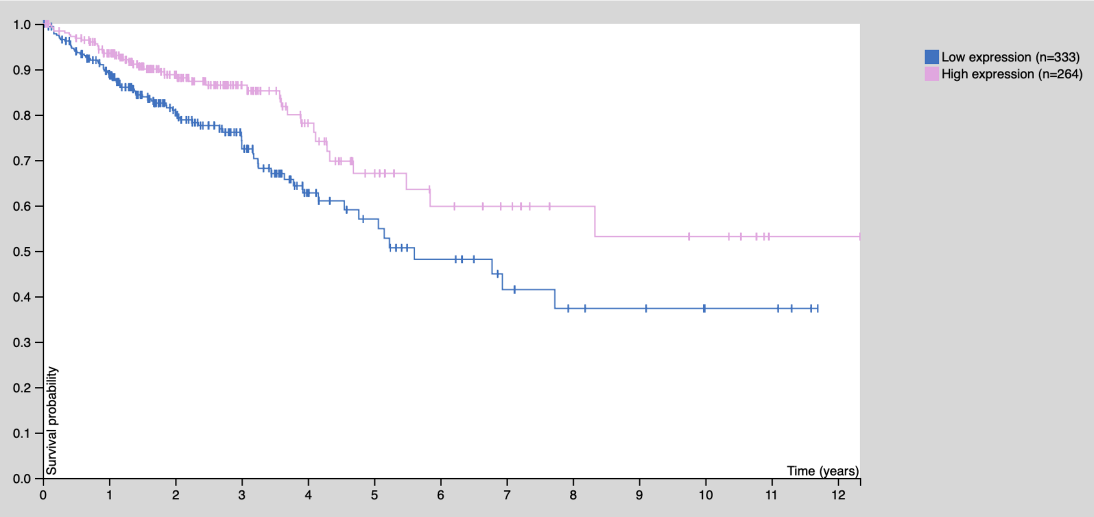

Figure 4.3: The survival plot of CRC patients according to the TRIM37 expression levels. The plot was retrieved from Human Protein Atlas on date 29.03.2023.

Hsa-mir-3157 targets were listed and shared genes with our differential expression analysis were obtained from Set Comparison Appyter, shared genes were listed in the results section. However, these shared genes are not associated with any GO biological processes and pathways. Overall, all targets were analyzed and their associated pathway is Wnt signaling pathway. The sama analysis was sone for hsa-mir-4495. Its targets mainly associated with the regulation of cell migration and angiogenesis. This miRNA was differentially expressed in the healthy intestinal organoids of mCRC donors compared with CRC donors. miR-4495 might has a reglatory role in CRC metastasis through HIF1A. Recently, there is no study focused on miR-4495 and colorectal cancer relation. Has-let-7d is another differentially expressed micro RNA in CRC vs mCRC comparison. Previous studies showed that let-7d has inhibitory effect on colorectal cancer cell proliferation. Reduced expression of let-7d was associated with poor outcome of CRC (Nair, 2012). In our mCRC differential expression gene list, let-7d expression was high. Let-7d also has a role in EMT process and formation of cancer initiating cells. Previous studies showed over-expression of let-7d causes cell differentiation and neural phenotypes *in vitro*. Another study showed that let-7d overexpressed fibroblasts have less mesenchymal-like but have more epithelial-like phenotype. As in this case let-7d partially changes cell morphology. In general, current literature suggests that let-7d functions as a switch between EMT and MET (Kolenda et al., 2014).

The pathway enrichment analysis of control and CRC healthy intestinal organoids showed 6 enriched pathways: NAD+ metbolism, focal adhesion, Wnt signaling pathway, TGF-ß signaling pathway, Hippo-Merlin signaling pathway, and glycogen synthesis. The same analysis for control and mCRC donors showed 7 enriched pathways: eicosanoid synthesis, Hippo-Merlin dysregulation, HIF1A regulation of glycogenesis, lipid metabolism, Ras signaling, EMT in colorectal cancer, and regulation of microtubule cytoskeleton. The last comparison was done for CRC and mCRC donors, only three pathways were enriched: amplification and expansion of oncogenic pathways, Wnt/ß-catenin signaling by small molecules, and regulation of microtubule cytoskeleton. VEGF receptor mediating signal transduction and PI3K/Akt/mTOR signaling pathway were also enriched for mCRC donors with lower scores.

VEGF receptor mediating signal transduction is induced by VEGF ligands. VEGFR1 (Flt1) and VEGFR2 (KDR) are VEGF receptors. The main VEGF mechanism promotes angiogenesis through endothelial cell proliferation is VEGF signaling through KDR. The VEGF/KDR signaling cascade has cumulative effects on tumor growth and invasion (Dong et al., 2012). When VEGF and KDR interact with each other, MAPK and PI3K/Akt, and other downstream signaling pathways are activated and the activation favors the survival of endothelial cells (Dong et al., 2012 ; Shibuya Claesson-Welsh, 2006). 3.3% of people with CRC have differential expression in KDR (AACR Project, 2017). In our findings, KDR is downregulated in both groups when CRC and mCRC are analyzed with control donors separately. However, Flt1 expression was decreased in mCRC donors in comparison with CRC donors. There are no statistically significant change in control vs mCRC results. This might be interpreted as Flt1 possibly had slightly higher expression in CRC donors but the difference was not statistically significant. The similar case is must likely be applicable for control vs mCRC comparison as mCRC donors had lower Flt1 expression than control donors but there is no statistically significant difference. Yet, the expression difference between CRC and mCRC donors is statistically significant. VEGF signaling is activated in CRC metastasis; bevacizumab, which is a monoclonal antibody targets VEGF, is currently used for metastatic CRC. If the patient-specific mechanism that mediated VEGF signaling in CRC can be detected before the metastasis proceeds, metastasis can be avoided thorugh the inhibition of dominant VEGFR that promotes malignancy. Another downstream VEGF signaling protein is NOS1 (neural nitric oxide synthase 1), which responsible for nitric oxide (NO) production after the Flt1 activation by VEGF-B. NO accumulation promotes angiogenesis and vascularization. In our differential expression list of CRC vs mCRC comparison, NOS1 expression was downregulated in parallel with Flt1 expression and there are no significant changes in other two gene lists (Appendix-2).

HIF1a is one of the master proteins that has role in angiogenesis, tumor growth, and EMT in several cancer types. Increasning levels of HIF-1 expression was associated with metastatic tumor aggressiveness in the liver, according to a prior study (Wada et al., 2020). Another study showed that HIF1a expression changed from primary to metastatic areas, and that a high level of HIF1a expression in the metastatic site was associated with a poor prognosis (Shimomura et al., 2013). To sum, HIF1a expression may play a crucial part in controlling tumor aggressiveness in colorectal liver metastasis (CRLM). Our findings showed that HIF1a, HK1, and BAP1 increased in healthy intestinal organoids of mCRC patients. HK1 is a one of the HIF1 downstream genes and BAP1 is one of the upstream genes. HIF1a is a crucial regulatory gene that activates glycolytic genes like HK1 and promotes metabolic adaptation in cancer cells. HIF1a expression is expressen in both primary CRC and matched metastatic tissues (Yin et al., 2020). HIF1a overexpression is associated with the poor prognosis of CRLM (Wada et al., 2020). In this study, mCRC patients have liver metastasis and their healthy colon organoids showed elevated levels of HIF1a. This differential expression change between mCRC organoids and CRC organoids might be an important indicator that upcoming metastasis of colorectal cancer. HIF1a also induces VEGF expression either directly or indirectly. Recent studies demonstrate that HIF1a and VEGF are overexpressed in both CRC tissues and their matched metastatic tissues (Uttarawichien et al., 2021). Our transcriptome analysis showed that both Flt1 and KDR were downregulated in mCRC healthy organoids. Increased HIF1a levels and decreased VEGFR levels might be seen as a controversy. However, nuclear translocation of HIF1a is important for VEGFR signaling cascade and the elevated expression does not an indicator of functional translocation of the HIF1a protein. As we examined, Flt1 and KDR expression levels of mCRC organoids were lower than the control organoids. There might be an unknown mechanism that possibly strings on the induction of Flt1 and KDR expression levels. If this is the case, HIF1a increase cannot be enough to trigger angiogenic cascades through VEGF signaling.

The most common reason for mortality in people with CRLM. The liver resection is not a permanent treatment for CRLM as majority of patients experience recurrence following liver surgery. Current understanding of CRC carcinogenesis has broaden with the characterization of genetic changes in this disease. Potential biomarkers were found in CRC and CRLM tissues by numerous proteomics investigations that have been reported. When we examined our transcriptome results, we found that 5 genes that have been identified as CRLM associated markers increased in healthy organoids of mCRC patients in comparison with healthy CRC organoids. These genes are FNDC1, JAG2, ADAMTS3, AP2A1, and HNRNPA2B1. FNDC1 is an extracellular matrix protein encoding gene and its identified as characteristics of CRLM (Naba et al., 2012). ADAMTS3 and JAG2 are associated with vascular invasion in CRLM tissues (Kirana et al., 2019). AP2A1 and HNRNPA2B1 are also significantly correlated with CRLM (YangW. et al., 2019). These 5 genes were identified as specific biomarkers in CRLM tissues. Our patient-specific intestinal organoids did not have malignant characteristics but their donors have CRC or mCRC. Our results showed all five genes were upregulated in intestinal organoids of mCRC. It can be interpreted as 5 genes can be earlier biomarkers that indicate further metastatic characteristics of a possible primary colorectal cancer. Moreover, C1RL gene is also identified as a CRLM associated protein, but our results showed that our mCRC healthy organoids have increasing expression of its anti-sense RNA C1RL-

AS1. Anti-sense RNAs are a class of non-coding RNAs, and they can function as transcriptional regulators. Anti-sense RNA can both increase and decrease the gene encoded by their sense strand. The function of C1RL-AS1 is unknown but it might have an important role in CRC metastasis

RNA-binding proteins (RBPs) involve in the maintaining cellular homeostasis as they regulate post-transcriptional gene expression (Mittal et al., 2009). RBPs have roles in transcriptional regulation of both tumor proteins and tumor-suppressor proteins in various cancer types (Pereira et al., 2017). Chang et al. obtained the raw RNA-Seq data of colorectal cancer patients from TCGA in 2021 and discovered 472 RBPs genes that were differentially expressed. Next, they carried out enrichment analysis on genes that had been up- and down-regulated. They discovered CELF4, LRRFIP2, ZNF385A, and PPARGC1A as the four down-regulated RBPs (Chang et al., 2021). Our enrichment analysis revealed that ZNF385A expression was downregulated in healthy organoids from patients with CRC and mCRC. We suggest that studies can be conducted in this area and that the decrease in ZNF385A expression shown in intestinal organoids, where cancer growth has not yet been identified, can be considered as an early marker.

Dysregulation of protein synthesis is a known background mechanism of the cancer development. More than one signaling pathways contribute the translation initiation process. In CRC, translation initiation is dysregulated and the dysregulated initiation leads translational reprogramming. The reprogramming ends up with the selective translation of mRNAs especially genes that are critical for the oncogenic processes. Alterations in Wnt, MAPK, and PI3K/Akt pathways were common in CRC formation and progression. To support varitey of oncogenic phenotypes, cells selectively translate certain mRNAs through shifting their translation process. The primary initiation mode is cap-dependent but it can be suppressed in response to physiological/pathophysiological stress factors. Under such conditions, cell can switch to cap-independent translation initiation mechanism. At this point, the translation initiation machinery promotes the increasing in cellular stress response genes (Minnee

Faller, 2021). Our bioinformatics results showed that only in mCRC donors display the alteration in translation initiation-related genes. When mCRC results compared with control donors, eukaryotic initiation factor 3 (eIF3) and eukaryotic initiation factor 5B (eIF5B) were differentially upregulated but when mCRC donor compared with CRC donors there is no statistically significant change in these two genes. This situation might be interpreted as these genes were probably show expression change in both CRC and mCRC patients healhty intestinal organoids. However, CRC donors do not have significant expression change in comparison with healthy donors. The change in cap-dependent translation and joining of 60S ribosomal subunit to 48S protein initiation compelex (PIC) might have a connection between the matastasis process. As our network results displayed that joining of 60S ribosomal subunit also has statistically significant.

5. CONCLUSION AND FUTURE ASPECT

The villi, which are tiny finger-like structures, and the crypts, which are invaginations of the epithelium around the villi, are the two connected structures that make up the small intestinal epithelium (Allaire et al., 2018 ; van der Flier Clevers, 2009). Every 4-5 days, the intestinal epithelium undergoes complete regeneration and the process is mediated by constant cell division and maturation in crypts.

RNA sequencing provides a broad differential mRNA profile. We sequenced three samples for eah group and performed dual comparison. The gene lists obtained from the analysis were given in Appendix 2. Reprogramming of metabolism, carcinogenesis related signal transduction pathways, proteoglycans in cancer, and Rho GTPases were interpreted in parallel with the bioinformatics analysis. For the better understanding of cancer initiation and underlying mechanisms that push metastasis, further investigations are crucial. Proteoglycan regulation, lipid metabolism, VEGF signaling, Rho GTPases, and protein initiation machinery are the most promising concepts to asses cancer initiation and susceptibility.

Proteoglycans are located in basement membrane and lamina propria in intestinal tract. They involve tissue regeneration and tissue repair mechanism. As intestinal tract undergoes constant tissue regeneration, the errors occur in proteoglycan-cell or proteoglycan-ECM interaction might lead cancer initiation. Syndecans and glypicans are the specific proteoglycans that help tissue maintenance of small intestine. Our bioinformatics results showed that Perlecan (HSPG2), which is a matrix HSPG, levels were decreased in mCRC donors in comparison with CRC donors. The further investigations of HSPG2 and revaling its molecular interaction might have an impact on the understanding of cancer initiation.

Lipid metabolism is important energy supplier for intestinal stem cells (ISCs) and its tightly regulated in intestinal tissue. Cell membrane and ligand biosynthesis require lipid and fatty acid supply. Morover, sphingolipid biosynthesis is crucial for ISCs maintanence and sphingolipids involve signal transduction pathways. As previously explained, distrupted sphingolipid metabolism is associated with intestinal diseases and CRC. Fatty acid oxidation (FAO) is another important process for the intestinal tissue regeneration. It is the process that break down fatty acids for energy and the reprogramming of FAO might be one of the cancer initiating metabolic alterations.

VEGF signaling is a well-known pathway that involve intestinal tissue regeneration. Intestinal epithelium turn over is maintained by proliferation and differentiation of ISCs and the VEGF signaling is one of the promoting mechanism. The dysregulation of VEGF signaling ends up with CRC development and VEGF signaling is a valuable pathway to examine for new biomarkers to assess cancer susceptibility of individuals. Flt1 and KDR expression were differentially changed in our CRC and mCRC donors' healthy intestinal organoids. Also, HIF1a levels were upregulated in mCRC organoids. However, the location of HIF1a is critical for the functioning of HIF1a. For the deeper understanding, protein localization of HIF1a and other molecular interaction between VEGFRs have to be examined.

Small GTP binding proteins involve in almost all cellular processes. Rho GTPases is one of the small GTP binding proteins and they have roles in cell migration regulation, cytoskeleton organization, and proliferation. Our bioinformatics results showed that several Rho GTPase related genes (Table 3.6) were differentially expressed in the intestinal organoids of CRC and mCRC donors even the organoids have no malignant phenotype. Several GAP genes, AGAP-1, ARHGAP12, SRGAP1, and antisense RNA-2 and -3 of SRGAP3, NF1, PI3K-involved genes, SIRT1, PDK1, PAK1, and PKN2 are involved in Rho GTPase cascade. The links between these genes and PI3K-Akt pathway/VEGF pathway are worth to examine for deeper understanding of molecular organization in *in vitro* healthy intestinal model of CRC/mCRC donors.

The protein translation initiation machinery is another crucial mechanism that has to be maintained for the healthy intestinal tissue regeneration. Dysregulation of protein translation initiation machinery is reported as a factor of CRC development. Our results showed that genes involved in cap-dependent initiation and 43S protein initiation complex formation were decreased. As we know, cells can shift their cap-dependent protein translation initiation mechanism to cap-independent mechasims towards their cellular needs. Cap-independent mechanism favors the upregulation of cellular stress response genes. Morover, eiF5B and eiF3L are genes involved in the joining of 60S ribosomal subunit to 48S protein initiation complex were increased. The differential expression changes in eukaryotic translation initiation complex proteins might be the beginnig of metabolic reprogramming of proteins which associates with CRC development.

We conducted a joint analysis of our results with two different published datasets. The first data set used (GSE32323) included gene expression profiling of cancer tissue biopsies accompanied by healthy colon biopsy of 17 CRC patients (Khamas et al., 2012). Of the CRC patients in this data set, 10 were non-metastatic, 7 were metastatic. In our own sample, our groups were grouped into non-metastatic and metastatic. When the DEG list of the data set was created, patients were grouped by metastatic status. According to the statuses of the DEG lists (GSE32323 without metastasis and GSE 32323 with metastases), crossings with our DEG Lists were examined as “Control vs CRC” or “Control vs mCRC”, “CRC vs m CRC”. (Figure 4.4). In our own sample, our groups were grouped into non-metastatic and metastatic. When the DEG list of the data set was created, patients were grouped by metastatic status. When the results were examined, when the healthy intestinal organoids of metastatic patients were compared with the metastasized patient samples, the results found to be more meaningful than in the non-metastatic comparative group. In particular, the Rho GTPase signal pathway was also found to be enriched when compared with patient samples in metastatic groups. In addition, protein translation initiation and ribosomal activity were also shown to be prominent in metastatic groups.

CRC vs mCRC comparison of metastatic patient samples contains a total of 232 genes in the intersection set (Figure 4.4).

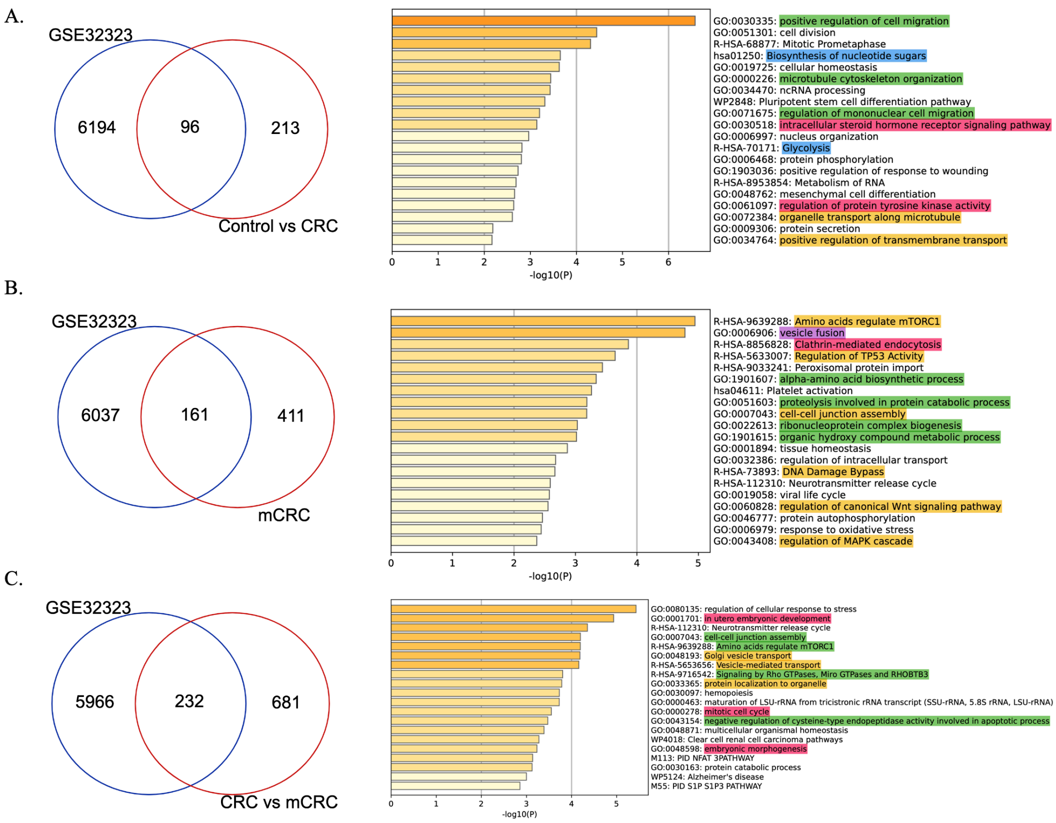

Figure 4.4: Results of intersection of DEG lists obtained from RNA-seq results of healthy intestinal organoids of non-metastatic (A) and (B-C) CRC patients with GSE32323 dataset. The results of pathway enrichment analyses of the obtained common genes are given in the right panel.

The analyses we did up to this stage were based on comparisons of studies at the mRNA level. Another published CRC study (GSE25071) was used to compare the results we obtained at RNA level also in the protein level (Danielsen et al., 2011). This data set included microarray data from a total of 31 CRC patients. Colon tissues used as controls in the data set are not accompanying healthy tissue biopsies, as opposed to the GSE32323 data set, but control biopsy samples taken from healthy individuals. With the GSE25071 data set, when we examined the correspondence of 232 genes at the protein level in CRC patients, which are the intersection of metastatic samples we obtained in the previous stage, we found that 69 genes were common (Figure

4.5).When the pathway enrichment analysis of the 69 gene was carried out with Metascape, the protein translation initiation, the Mitotic cell Cycle and the VEGFA-VEGF2 signal pathways were enriched. Change in cellular metabolism, protein translation machinery and Rho GTPase signal pathway are the three most prominent concepts in this regard.

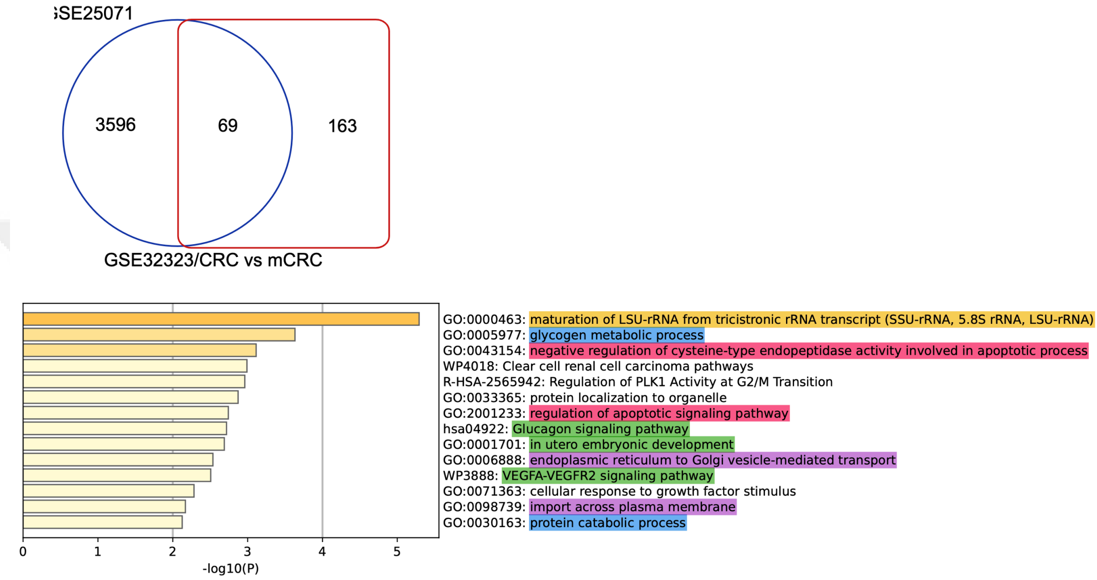

Figure 4.5: A list of common genes with the GSE25071 microarray data set of 232 genes, which is the intersection of our CRC vs. mCRC DEG list with GSE32323 dataset.

ÖZET

Metastazlı ve Metastazsız Kolorektal Kanser Hastalarının İndüklenmiş Pluripotent Kök Hücrelerinden Sağlıklı Organoidlerinin Geliştirilmesi ve Transkriptom Analizi

Kanser günümüzde ölüm oranı ve görülme sıklığı yüksek multifaktöriyel bir hastalıktır. Bir gastrointestinal kanser türü olan kolorektal kanser (KRK) her yıl dünya genelinde yaklaşık 700.000 insanın ölümüne sebep olmaktadır. KRK oluşumuna neden olan mekanizmalar şu an için kısmi olarak genetik faktörlerle açıklanmaya çalışılsa da net bir kanser başlangıç mekanizması ortaya konulmamıştır. Yaş ve çevresel faktörler KRK oluşumunda ön plandadır fakat kolon hücrelerinin bu gibi faktörlerden neye göre etkilendiği hala bilinmemektedir. Erken teşhis, diğer kanser türlerinde de olduğu gibi, KRK için de hayati önem taşır. Güncel olarak kullanılan en güvenilir KRK tanı yöntemi distal kolon ve rektum içi kolonoskopi sırasında alınan şüpheli doku biyopsilerinin patolojik incelemesidir. Ancak KRK hastalarının hissedilir belirti vermesi genellikle daha ileri evrelerde olduğu için henüz şikâyeti olmayan bireylere bu kadar invaziv bir yöntemin erken tanı için uygulanması pratik değildir. Bu sebeple, KRK gelişiminin erken tanısının konulabilmesi için yeni metotların geliştirilmesi oldukça önemlidir. İndüklenmiş pluripotent kök hücreler (iPKH), somatik hücrelere temel pluripotensi transkripsiyon faktörlerinin (Oct4, Sox2, Klf4, c-Myc) aktarılmasıyla oluşturulmaktadır. Embriyonik kök hücre evresine yeniden programlanan iPKH'lerin en temel özelliği üç germ yaprağına ait hücre tiplerine farklılaşabilme kapasiteleridir. Güncel olarak kanser çalışmalarında kullanılan hücre modellerinin kanserin son evrelerini simüle ediyor olması *in vitro* çalışmaların kanser başlangıcı ve gelişimi üzerine yoğunlaşabilmesinin önünü kesmektedir. Özelikle erken tanı ve kişiye uygun tedavinin belirlenmesi konusunda iPKH'ler umut vaat etmektedir. Bu tez çalışmasında KRK hastalarının periferik kanlarından izole edilen eritroid progenitör hücreler Sendai virüs sistemiyle yeniden programlayarak kolon organoidlerine farklılaştırıldı. KRK hastalarına ait sağlıklı kolon organoidlerinin geliştirilmesinin ardından RNA sekanslama yöntemi ile transkriptom analizleri tamamlandı. KRK gelişen bireylerde kanser oluşumunda yatkınlığa sebep olabilecek transkriptom seviyesinde örüntülerin olup olmadığı bu şekilde değerlendirildi. Bu tez çalışmasının başarıyla tamamlanmasının ardından KRK'in bireylerde gelişmesinden önce bu hastaların sağlıklı kolon organoidlerinde zaten kanser ile ilişkilendirilmiş yolakların sağlıklı-kanser öyküsü olmayan donörlere kıyasla farklı bir profilde ifade edildiği görüldü. Ek olarak metastazsız ve metastazlı hastaların sağlıklı kolon organoidlerinde de epitel-mezenkimal trasizyon ile ilişkili gen kümelerinin diferansiyel olarak ifade edildiği görüldü.

Anahtar sözcükler: Kolorektal kanser, indüklenmiş pluripotent kök hücre (iPKH), kolon organoid, RNA-seq

SUMMARY

Generation Of Patient Specific iPSC-Derived Healthy Organoids from Primary Colorectal Cancer Patients With/Without Metastasis and Transcriptome Analysis

Cancer is a multifactorial disease with high mortality and incidence rate. Colorectal cancer (CRC) is a type of gastrointestinal cancer and causes about 700,000 deaths worldwide every year. Although CRC propagation mechanisms are partially explained by genetic factors, a clear cancer initiation mechanism has not been revealed. Age and environmental factors are particularly prominent in non-hereditary (sporadic) CRC formation, but it is still unknown how and why certain colon cells are affected by such factors. Early diagnosis is vital for CRC, as in other types of cancer. The most reliable diagnostic method is the pathological examination of suspicious tissue biopsies taken during colonoscopy in the distal colon and rectum. However, since the perceptible symptoms of CRC patients are usually at more advanced stages, it is not practical to apply such an invasive method for early diagnosis to individuals who do not yet have any complaints. For this reason, it is very important to develop new methods for the early diagnosis of sporadic CRC development. Induced pluripotent stem cells (iPSCs) are formed by transferring certain pluripotent transcription factors (Oct4, Sox2, Klf4, c-Myc) into somatic cells. The most basic feature of iPSCs, which are reprogrammed to the embryonic stem cell stage, is their ability to differentiate into cell types of three germ layers. The fact that the cell models currently used in cancer studies simulate the final stages of cancer limits in vitro studies from being able to study cancer initiation and development. In particular, iPSCs show promise for early diagnosis and determination of appropriate treatment. In this thesis study, we reprogrammed erythroid progenitor cells from peripheral blood of CRC patients into iPSCs by using the Sendai viral system. After that, we differentiated iPSCs into colon organoids. Following the development of healthy colon organoids of CRC patients, transcriptome analysis was done by RNA sequencing. Whether there were transcriptomic patterns that may cause susceptibility to cancer formation in individuals who develop CRC. In this way, it was assessed to see if there were any trends at the transcriptome level in people who had CRC that would indicate a susceptibility to cancer. After this thesis was successfully completed, it was discovered that the pathways already linked to cancer were expressed differently in healthy colon organoids from CRC patients in comparison with the donors without a history of cancer. Also, it was shown that the expression of gene clusters linked to the epithelial-mesenchymal transition shifted between healthy colon organoids from patients with and without metastases.

Key Words: Colorectal cancer, induced pluripotent stem cells (iPSC), colon organoid, RNA-seq

REFERENCES

AACR PROJECT. (2017). AACR Project GENIE: Powering Precision Medicine through an International Consortium. *Cancer discovery*, *7*:818-831.

ALLAIRE JM, CROWLEY SM, LAW HT, CHANG S-Y, KO H-J, VALLANCE BA. (2018). The Intestinal Epithelium: Central Coordinator of Mucosal Immunity. *Trends in immunology*, ***39***(9): 677-696.

BALDUS SE, SCHAEFER K-L, ENGERS R, HARTLEB D, STOECKLEIN NH, GABBERT HE. (2010). Prevalence and heterogeneity of KRAS, BRAF, and PIK3CA mutations in primary colorectal adenocarcinomas and their corresponding metastases. *Clinical cancer research : an official journal of the American Association for Cancer Research*, ***16***(3), 790-799.

BANITO A, RASHID ST, ACOSTA JC, LI S, PEREIRA CF, GETI I, PINHO S, SILVA JC, AZUARA V, WALSH M. (2009). Senescence impairs successful reprogramming to pluripotent stem cells. *Genes & development*, ***23***(18): 2134-2139.

BAO Q, MORSHEDI A, WANG F, BHARGY S, PERVUSHIN K, YU WP, DRÖGE P. (2017). Utf1 contributes to intergenerational epigenetic inheritance of pluripotency. *Scientific Reports*, ***7***(1): 1-11.

BARKER N, VAN ES JH, KUIPERS J, KUJALA P, VAN DEN BORN M, COZIJNSEN M, HAEGEBARTH A, KORVING J, BEGTHEL H, PETERS PJ. (2007). Identification of stem cells in small intestine and colon by marker gene Lgr5. *Nature*, ***449***(7165): 1003-1007.

BARTFELD S, BAYRAM T, VAN DE WETERING M, HUCH M, BEGTHEL H, KUJALA P, VRIES R, PETERS PJ, CLEVERS H. (2015). In vitro expansion of human gastric epithelial stem cells and their responses to bacterial infection. *Gastroenterology*, ***148***(1): 126-136.e6.

BUGANIM Y, FADDAH DA, CHENG AW, ITSKOVICH E, MARKOULAKI S, GANZ K, KLEMM SL, VAN OUDENAARDEN A, JAENISCH R. (2012). Single-cell expression analyses during cellular reprogramming reveal an early stochastic and a late hierarchic phase. *Cell*, ***150***(6): 1209-1222.

CHANG K, YUAN C, LIU X. (2021). A New RBPs-Related Signature Predicts the Prognosis of Colon Adenocarcinoma Patients. *Frontiers in oncology*, ***11*:** 627504.

CHEN AE, GINTY DD, FAN C-M. (2005). Protein kinase A signalling via CREB controls myogenesis induced by Wnt proteins. *Nature*, ***433***(7023): 317-322.

CHEN Z, LU X, WANG Z, JIN G, WANG Q, CHEN D, CHEN T, LI J, FAN J, CONG W, GAO Q, HE X. (2015). Co-expression of PKM2 and TRIM35 predicts survival and recurrence in hepatocellular carcinoma. *Oncotarget*, ***6***(4): 2538-2548.

CHEUNG AYL, HORVATH LM, GRAFODATSKAYA D, PASCERI P, WEKSBERG R, HOTTA A, CARREL L, ELLIS J. (2011). Isolation of MECP2-null Rett Syndrome patient hiPS cells and isogenic controls through X-chromosome inactivation. *Human molecular genetics*, ***20***(11): 2103-2115.

CLEVERS H. (2016). Modeling Development and Disease with Organoids. *Cell*, ***165***(7): 1586-1597.

COHEN DE, MELTON D. (2011). Turning straw into gold: directing cell fate for regenerative medicine. *Nature Reviews Genetics*, ***12***(4): 243-252.

COURTNEY KD, CORCORAN RB, ENGELMAN JA. (2010). The PI3K pathway as drug target in human cancer. *Journal of clinical oncology : official journal of the American Society of Clinical Oncology*, ***28***(6): 1075-1083.

CRESPO M, VILAR E, TSAI SY, CHANG K, AMIN S, SRINIVASAN T, ZHANG T, PIPALIA NH, CHEN HJ, WITHERSPOON M, GORDILLO M, XIANG JZ, MAXFIELD FR, LIPKIN S, EVANS T, CHEN S. (2017). Colonic organoids derived from human induced pluripotent stem cells for modeling colorectal cancer and drug testing. *Nature Medicine*, ***23***(7): 878-884.

DANIELSEN SA, CEKAITE L, ÅGESEN TH, SVEEN A, NESBAKKEN A, THIIS-EVENSEN E, SKOTHEIM RI, LIND GE, LOTHE RA. (2011). Phospholipase C Isozymes Are Deregulated in Colorectal Cancer – Insights Gained from Gene Set Enrichment Analysis of the Transcriptome. *PLOS ONE*, ***6***(9): 24419.

DI CLAUDIO F, MUGLIA CI, SMALDINI PL, ORSINI DELGADO ML, TREJO FM, GRIGERA JR, DOCENA GH. (2017). Use of a collagen membrane to enhance the survival of primary intestinal epithelial cells. *Journal of cellular physiology*, ***232***(9): 2489-2496.

DONG G, GUO X, FU X, WAN S, ZHOU F, MYERS RE, BAO G, BURKART A, YANG

H, XING J. (2012). Potentially functional genetic variants in KDR gene as prognostic markers in patients with resected colorectal cancer. *Cancer science*, ***103***(3): 561-568.

FEARON ER. (2011). Molecular genetics of colorectal cancer. *Annual review of pathology*, ***6***: 479-507.

FRANSSON A, RUUSALA A, ASPENSTRÖM P. (2003). Atypical Rho GTPases have roles in mitochondrial homeostasis and apoptosis. *The Journal of biological chemistry*, ***278***(8): 6495-6502.

GRAND RJ, WATKINS JB, TORTI FM. (1976). Development of the human gastrointestinal tract: a review. *Gastroenterology*, ***70***(5): 790-810.

GREGO-BESSA J, DÍEZ J, POMPA JL DE LA. (2004). Notch and epithelial-mesenchyme transition in development and tumor progression: another turn of the screw. *Cell cycle*, ***3***(6): 716-719.

HANAHAN D, WEINBERG RA. (2011). Hallmarks of cancer: the next generation. *cell*, ***144***(5): 646-674.

HEISENBERG C-P, BELLAÏCHE Y. (2013). Forces in tissue morphogenesis and patterning. *Cell*, ***153***(5): 948-962.

HIGUCHI A, LING Q-D, KUMAR SS, MUNUSAMY MA, ALARFAJ AA, CHANG Y, KAO S-H, LIN K-C, WANG H-C, UMEZAWA A. (2015). Generation of pluripotent stem cells without the use of genetic material. *Laboratory Investigation*, ***95***(1): 26-42.

HONG BS, CHO J-H, KIM H, CHOI E-J, RHO S, KIM J, KIM JH, CHOI D-S, KIM Y-K, HWANG D, GHO YS. (2009). Colorectal cancer cell-derived microvesicles are enriched in cell cycle-related mRNAs that promote proliferation of endothelial cells. *BMC Genomics*, ***10***(1): 556.

HONG H, TAKAHASHI K, ICHISAKA T, AOI T, KANAGAWA O, NAKAGAWA M, OKITA K, YAMANAKA S. (2009). Suppression of induced pluripotent stem cell generation by the p53–p21 pathway. *Nature*, ***460***(7259): 1132-1135.

HU CE, GAN J. (2017). TRIM37 promotes epithelial-mesenchymal transition in colorectal cancer. *Molecular Medicine Reports*, ***15***(3), 1057-1062.

HUANG N, SUN X, LI P, LIU X, ZHANG X, CHEN Q, XIN H. (2022). TRIM family contribute to tumorigenesis, cancer development, and drug resistance. *Experimental*

Hematology and Oncology, ***11***(1), 1-22.

IWAO T, TOYOTA M, MIYAGAWA Y, OKITA H, KIYOKAWA N, AKUTSU H, UMEZAWA A, NAGATA K, MATSUNAGA T. (2014). Differentiation of human induced pluripotent stem cells into functional enterocyte-like cells using a simple method. *Drug Metabolism and Pharmacokinetics*, ***29***(1): 44-51.

JESS T, RUNGOE C, PEYRIN–BIROULET L. (2012). Risk of colorectal cancer in patients with ulcerative colitis: a meta-analysis of population-based cohort studies. *Clinical gastroenterology and hepatology*, ***10***(6): 639-645.

JIAO S, PETERS U, BERNDT S, BRENNER H, BUTTERBACH K, CAAN BJ, CARLSON CS, CHAN AT, CHANG-CLAUDE J, CHANOCK S. (2014). Estimating the heritability of colorectal cancer. *Human molecular genetics*, ***23***(14): 3898-3905.

KAUFFMAN AL, GYURDIEVA A V., MABUS JR, FERGUSON C, YAN Z, HORNBY PJ. (2013). Alternative functional in vitro models of human intestinal epithelia. *Frontiers in Pharmacology*, ***4***: 1-18.

KAWAMURA T, SUZUKI J, WANG Y V, MENENDEZ S, MORERA LB, RAYA A, WAHL GM, BELMONTE JCI. (2009). Linking the p53 tumour suppressor pathway to somatic cell reprogramming. *Nature*, ***460***(7259): 1140-1144.

KELLEHER F, FENNELLY D, RAFFERTY M. (2006). Common critical pathways in embryogenesis and cancer. *Acta Oncologica*, ***45***(4): 375-388.

KELLER R. (2012). Developmental biology. Physical biology returns to morphogenesis. *Science (New York, NY)*, ***338***(6104): 201-203.

KELM JM, FUSSENEGGER M. (2004). Microscale tissue engineering using gravity-enforced cell assembly. *Trends in biotechnology*, ***22***(4): 195-202.

KHAMAS A, ISHIKAWA T, SHIMOKAWA K, MOGUSHI K, IIDA S, ISHIGURO M, MIZUSHIMA H, TANAKA H, UETAKE H, SUGIHARA K. (2012). Screening for Epigenetically Masked Genes in Colorectal Cancer Using 5-Aza-2’-deoxycytidine, Microarray and Gene Expression Profile. *Cancer Genomics - Proteomics*, ***9***(2): 67 LP - 75.

KIEL MJ, HE S, ASHKENAZI R, GENTRY SN, TETA M, KUSHNER JA, JACKSON TL, MORRISON SJ. (2007). Haematopoietic stem cells do not asymmetrically segregate chromosomes or retain BrdU. *Nature*, ***449***(7159): 238-242.

KIM D, KIM C-H, MOON J-I, CHUNG Y-G, CHANG M-Y, HAN B-S, KO S, YANG E, CHA KY, LANZA R, KIM K-S. (2009). Generation of Human Induced Pluripotent Stem Cells by Direct Delivery of Reprogramming Proteins. *Cell Stem Cell*, ***4***(6): 472-476.

KIRANA C, PENG L, MILLER R, KEATING JP, GLENN C, SHI H, JORDAN TW, MADDERN GJ, STUBBS RS. (2019). Combination of laser microdissection, 2D-DIGE and MALDI-TOF MS to identify protein biomarkers to predict colorectal cancer spread. *Clinical Proteomics*, ***16***(1): 3.

KOLENDA T, PRZYBYLA W, TERESIAK A, MACKIEWICZ A, LAMPERSKA KM. (2014). The mystery of let-7d - A small RNA with great power. *Wspolczesna Onkologia*, ***18***(5): 293-301.

KONDO S, MIZUNO S, HASHITA T, IWAO T, MATSUNAGA T. (2020). Establishment of a novel culture method for maintaining intestinal stem cells derived from human induced pluripotent stem cells. *Biology Open*, ***9***(1).

LASCHKE MW, MENGER MD. (2017). Spheroids as vascularization units: From angiogenesis research to tissue engineering applications. *Biotechnology advances*, ***35***(6): 782-791.

LEVINA A, FLEMING KD, BURKE JE, LEONARD TA. (2022). Activation of the essential kinase PDK1 by phosphoinositide-driven trans-autophosphorylation. *Nature Communications*, ***13***(1): 1874.

LEWIS J. (1998). Notch signalling and the control of cell fate choices in vertebrates. *Seminars in cell & developmental biology*, ***9***(6): 583-589.

LI L, WANG S, JEZIERSKI A, MOALIM-NOUR L, MOHIB K, PARKS RJ, RETTA SF, WANG L. (2010). A unique interplay between Rap1 and E-cadherin in the endocytic pathway regulates self-renewal of human embryonic stem cells. *Stem cells (Dayton, Ohio)*, *28*(2): 247-257.

LI Q, YAO L, WEI Y, GENG S, HE C, JIANG H. (2015). Role of RHOT1 on migration and proliferation of pancreatic cancer. *American journal of cancer research*, ***5***(4): 1460-1470.

MAHAJAN T, GANGULY S, PAGRUT N. (2018). Embryogenesis : a comprehensive review Embryogenesis : A comprehensive review, (February).

MARIÓN RM, STRATI K, LI H, MURGA M, BLANCO R, ORTEGA S, FERNANDEZ-CAPETILLO O, SERRANO M, BLASCO MA. (2009). A p53-mediated DNA damage response limits reprogramming to ensure iPS cell genomic integrity. *Nature*, ***460***(7259): 1149-1153.

MATSUSHITA Y, NAKAGAWA H, KOIKE K. (2021). Lipid metabolism in oncology: why it matters, how to research, and how to treat. *Cancers*, ***13***(3): 474.

MAURY Y, GAUTHIER M, PESCHANSKI M, MARTINAT C. (2012). Human pluripotent stem cells for disease modelling and drug screening. *Bioessays*, ***34***(1): 61-71.

MCCAULEY HA, WELLS JM. (2017). Pluripotent stem cell-derived organoids: using principles of developmental biology to grow human tissues in a dish. *Development (Cambridge, England)*, ***144***(6): 958-962.

MEDEMA JP. (2013). Cancer stem cells: the challenges ahead. *Nature cell biology*, ***15***(4): 338-344.

MEKHOUBAD S, BOCK C, DE BOER AS, KISKINIS E, MEISSNER A, EGGAN K. (2012). Erosion of dosage compensation impacts human iPSC disease modeling. *Cell stem cell*, ***10***(5): 595-609.

MIKKELSEN TS, HANNA J, ZHANG X, KU M, WERNIG M, SCHORDERET P, BERNSTEIN BE, JAENISCH R, LANDER ES, MEISSNER A. (2008). Dissecting direct reprogramming through integrative genomic analysis. *Nature*, ***454***(7200): 49-55.

MINNEE E, FALLER WJ. (2021). Translation initiation and its relevance in colorectal cancer. *FEBS Journal*, ***288***(23): 6635-6651.

MITTAL N, ROY N, BABU MM, JANGA SC. (2009). Dissecting the expression dynamics of RNA-binding proteins in posttranscriptional regulatory networks. *Proceedings of the National Academy of Sciences of the United States of America*, ***106***(48): 20300-20305.

MOLENDIJK J, ROBINSON H, DJURIC Z, HILL MM. (2020). Lipid mechanisms in hallmarks of cancer. *Molecular omics*, ***16***(1): 6-18.

MUELLER-KLIESER W. (1997). Three-dimensional cell cultures: from molecular mechanisms to clinical applications. *American Journal of Physiology-Cell Physiology*, ***273***(4): C1109-C1123.

MUZNY DM, BAINBRIDGE MN, CHANG K, DINH HH, DRUMMOND JA (2012). Comprehensive molecular characterization of human colon and rectal cancer. *Nature*, ***487***(7407): 330-337.

NABA A, CLAUSER KR, HOERSCH S, LIU H, CARR SA, HYNES RO. (2012). The matrisome: in silico definition and in vivo characterization by proteomics of normal and tumor extracellular matrices. *Molecular & cellular proteomics : MCP*, ***11***(4): M111.014647.

NANDAN MO, YANG VW. (2011). An Update on the Biology of RAS/RAF Mutations in Colorectal Cancer. *Current colorectal cancer reports*, *7*(2): 113-120.

NASSAR D, BLANPAIN C. (2016). Cancer Stem Cells: Basic Concepts and Therapeutic Implications. *Annual review of pathology*, ***11***: 47-76.

NEGORO R, TAKAYAMA K, KAWAI K, HARADA K, SAKURAI F, HIRATA K, MIZUGUCHI H. (2018). Efficient Generation of Small Intestinal Epithelial-like Cells from Human iPSCs for Drug Absorption and Metabolism Studies. *Stem Cell Reports*, ***11***(6): 1539-1550.

NERI F, KREPELOVA A, INCARNATO D, MALDOTTI M, PARLATO C, GALVAGNI F, MATARESE F, STUNNENBERG HG, OLIVIERO S. (2013). Dnmt3L antagonizes DNA methylation at bivalent promoters and favors DNA methylation at gene bodies in ESCs. *Cell*, ***155***(1): 121.

OCHOA-BERNAL MA, FAZLEABAS AT. (2020). Physiologic Events of Embryo Implantation and Decidualization in Human and Non-Human Primates. *International Journal of Molecular Sciences*.

OGAKI S, MOROOKA M, OTERA K, KUME S. (2015). A cost-effective system for differentiation of intestinal epithelium from human induced pluripotent stem cells. *Scientific Reports*, ***5***: 1-11.

OOI SKT, WOLF D, HARTUNG O, AGARWAL S, DALEY GQ, GOFF SP, BESTOR TH. (2010). Dynamic instability of genomic methylation patterns in pluripotent stem cells. *Epigenetics and Chromatin*, ***3***(1): 1-10.

OSEFO N, ITO T, JENSEN RT. (2009). Gastric acid hypersecretory states: recent insights and advances. *Current gastroenterology reports*, ***11***(6): 433-441.

PAPAPETROU E. (2016). Patient-derived induced pluripotent stem cells in cancer research and precision oncology. *Nature Medicine*, 1392-1401.

PARK I-H, ZHAO R, WEST JA, YABUUCHI A, HUO H, INCE TA, LEROU PH, LENSCH MW, DALEY GQ. (2008). Reprogramming of human somatic cells to pluripotency with defined factors. *nature*, ***451***(7175): 141-146.

PEREIRA B, BILLAUD M, ALMEIDA R. (2017). RNA-Binding Proteins in Cancer: Old Players and New Actors. *Trends in cancer*, ***3***(7): 506-528.

POMP O, DREESEN O, LEONG DFM, MELLER-POMP O, TAN TT, ZHOU F, COLMAN A. (2011). Unexpected X chromosome skewing during culture and reprogramming of human somatic cells can be alleviated by exogenous telomerase. *Cell stem cell*, ***9***(2): 156-165.

PRADOS FJ, DEBROCK S, LEMMEN JG, AGERHOLM I. (2012). The cleavage stage embryo. *Human reproduction (Oxford, England)*, *27 Suppl* ***1*****:** 50-71.

REUTER CW, MORGAN MA, BERGMANN L. (2000). Targeting the Ras signaling pathway: a rational, mechanism-based treatment for hematologic malignancies? *Blood*, ***96***(5): 1655-1669.

RIDLEY AJ. (2013). RhoA, RhoB and RhoC have different roles in cancer cell migration. *Journal of microscopy*, ***251***(3): 242-249.

ROXBURGH CSD, RICHARDS CH, MOUG SJ, FOULIS AK, MCMILLAN DC, HORGAN PG. (2012). Determinants of short- and long-term outcome in patients undergoing simultaneous resection of colorectal cancer and synchronous colorectal liver metastases. *International journal of colorectal disease*, ***27***(3): 363-369.

SAKALEM ME, DE SIBIO MT, DA COSTA FA DA S, DE OLIVEIRA M. (2021). Historical evolution of spheroids and organoids, and possibilities of use in life sciences and medicine. *Biotechnology Journal*, ***16***(5).

SARKAR L, SHARPE PT. (1999). Expression of Wnt signalling pathway genes during tooth development. *Mechanisms of development*, ***85***(1-2): 197-200.

SCHOEN RE, RAZZAK A, KELLY JY, BERNDT SI, FIRL K, RILEY TL, PINSKY PF. (2015). Incidence and mortality of colorectal cancer in individuals with a family history of colorectal cancer. *Gastroenterology*, ***149***(6): 1438-1445.

SEKI T, FUKUDA K. (2015). Methods of induced pluripotent stem cells for clinical application. *World journal of stem cells*, ***7***(1): 116.

SHAW RJ, CANTLEY LC. (2006). Ras, PI(3)K and mTOR signalling controls tumour cell growth. *Nature*, ***441***(7092): 424-430.

SHAWBER C, NOFZIGER D, HSIEH JJ, LINDSELL C, BÖGLER O, HAYWARD D, WEINMASTER G. (1996). Notch signaling inhibits muscle cell differentiation through a CBF1-independent pathway. *Development (Cambridge, England)*, ***122***(12): 3765-3773.

SHERWOOD RI, MAEHR R, MAZZONI EO, MELTON DA. (2011). Wnt signaling specifies and patterns intestinal endoderm. *Mechanisms of development*, ***128***(7-10): 387-400.

SHIBUYA M, CLAESSON-WELSH L. (2006). Signal transduction by VEGF receptors in regulation of angiogenesis and lymphangiogenesis. *Experimental cell research*, ***312***(5): 549-560.

SHIMOGORI T, BANUCHI V, NG HY, STRAUSS JB, GROVE EA. (2004). Embryonic signaling centers expressing BMP, WNT and FGF proteins interact to pattern the cerebral cortex. *Development (Cambridge, England)*, ***131***(22): 5639-5647.

SHIMOMURA M, HINOI T, KURODA S, ADACHI T, KAWAGUCHI Y, SASADA T, TAKAKURA Y, EGI H, OKAJIMA M, TASHIRO H, NISHIZAKA T, OHDAN H. (2013). Overexpression of Hypoxia Inducible Factor-1 Alpha is an Independent Risk Factor for Recurrence After Curative Resection of Colorectal Liver Metastases. *Annals of Surgical Oncology*, ***20***(3): 527-536.

SIEGEL RL, MILLER KD, GODING SAUER A, FEDEWA SA, BUTTERLY LF, ANDERSON JC, CERCEK A, SMITH RA, JEMAL A. (2020). Colorectal cancer statistics, 2020. *CA: a cancer journal for clinicians*, ***70***(3): 145-164.

SIEGEL RL, MILLER KD, JEMAL A. (2017). Cancer Statistics, 2017. *CA Cancer J Clin*, ***67***(1): 7-30.

SON M-Y, CHOI H, HAN Y-M, CHO YS. (2013). Unveiling the critical role of REX1 in the regulation of human stem cell pluripotency. *Stem cells (Dayton, Ohio)*, ***31***(11): 2374-2387.

SPENCE JR, MAYHEW CN, RANKIN SA, KUHAR MF, VALLANCE JE, TOLLE K, HOSKINS EE, KALINICHENKO V V., WELLS SI, ZORN AM, SHROYER NF, WELLS JM. (2011a). Directed differentiation of human pluripotent stem cells into intestinal tissue in vitro. *Nature*, ***470***(7332): 105-110.

SPENCE JR, MAYHEW CN, RANKIN SA, KUHAR MF, VALLANCE JE, TOLLE K, HOSKINS EE, KALINICHENKO V V., WELLS SI, ZORN AM, SHROYER NF, WELLS JM. (2011b). Directed differentiation of human pluripotent stem cells into intestinal tissue in vitro. *Nature*, ***470***(7332): 105-110.

SRIDHARAN R, GONZALES-COPE M, CHRONIS C, BONORA G, MCKEE R, HUANG C, PATEL S, LOPEZ D, MISHRA N, PELLEGRINI M. (2013). Proteomic and genomic approaches reveal critical functions of H3K9 methylation and heterochromatin protein-1γ in reprogramming to pluripotency. *Nature cell biology*, ***15***(7): 872-882.

STERNECKERT JL, REINHARDT P, SCHÖLER HR. (2014). Investigating human disease using stem cell models. *Nature Reviews Genetics*, ***15***(9): 625-639.

STOIKA RS, PANCHUK* RR, STOIKA BR. (2004). Parallels and Antagonisms of Embryogenesis and Carcinogenesis. *Russian Journal of Developmental Biology*, ***35***(2): 57-62.

SUN H, CHOW ECY, LIU S, DU Y, PANG KS. (2008). The Caco-2 cell monolayer: usefulness and limitations. *Expert opinion on drug metabolism & toxicology*, ***4***(4): 395-411.

SYNGAL S, BRAND RE, CHURCH JM, GIARDIELLO FM, HAMPEL HL, BURT RW. (2015). ACG clinical guideline: genetic testing and management of hereditary gastrointestinal cancer syndromes. *The American journal of gastroenterology*, ***110***(2): 223.

TAKAHASHI K, YAMANAKA S. (2006). Induction of pluripotent stem cells from mouse embryonic and adult fibroblast cultures by defined factors. *cell*, ***126***(4): 663-676.

TAKASATO M, ER PX, CHIU HS, MAIER B, BAILLIE GJ, FERGUSON C, PARTON RG, WOLVETANG EJ, ROOST MS, CHUVA DE SOUSA LOPES SM, LITTLE MH. (2015). Kidney organoids from human iPS cells contain multiple lineages and model human nephrogenesis. *Nature*, ***526***(7574): 564-568.

TAKAYAMA K, MORISAKI Y, KUNO S, NAGAMOTO Y, HARADA K, FURUKAWA N, OHTAKA M, NISHIMURA K, IMAGAWA K, SAKURAI F, TACHIBANA M, SUMAZAKI R, NOGUCHI E, NAKANISHI M, HIRATA K, KAWABATA K, MIZUGUCHI H. (2014). Prediction of interindividual differences in hepatic functions and drug sensitivity by using human iPS-derived hepatocytes. *Proceedings of the National Academy of Sciences of the United States of America*, ***111***(47): 16772-16777.

TAYLOR MJ, TANNA S, SAHOTA T. (2010). In vivo study of a polymeric glucose-sensitive insulin delivery system using a rat model. *Journal of pharmaceutical sciences*, ***99***(10): 4215-4227.

TCHIEU J, KUOY E, CHIN MH, TRINH H, PATTERSON M, SHERMAN SP, AIMIUWU O, LINDGREN A, HAKIMIAN S, ZACK JA. (2010). Female human iPSCs retain an inactive X chromosome. *Cell stem cell*, *7*(3): 329-342.

TETSU O, MCCORMICK F. (1999). Beta-catenin regulates expression of cyclin D1 in colon carcinoma cells. *Nature*, ***398***(6726): 422-426.

UTTARAWICHIEN T, KAMNERDNOND C, INWISAI T, SUWANNALERT P, SIBMOOH N, PAYUHAKRIT W. (2021). Quercetin Inhibits Colorectal Cancer Cells Induced-Angiogenesis in Both Colorectal Cancer Cell and Endothelial Cell through Downregulation of VEGF-A/VEGFR2. *Scientia Pharmaceutica*.

VAN DER FLIER LG, CLEVERS H. (2009). Stem cells, self-renewal, and differentiation in the intestinal epithelium. *Annual review of physiology*, ***71***: 241-260.

VEGA FM, RIDLEY AJ. (2008). Rho GTPases in cancer cell biology. *FEBS letters*, ***582***(14): 2093-2101

VENOOK AP, NIEDZWIECKI D, INNOCENTI F, FRUTH B, GREENE C, O'NEIL BH, SHAW JE, ATKINS JN, HORVATH LE, POLITE BN. (2016). Impact of primary (1°) tumor location on overall survival (OS) and progression-free survival (PFS) in patients (pts) with metastatic colorectal cancer (mCRC): Analysis of CALGB/SWOG 80405 (Alliance). American Society of Clinical Oncology.

VICENTE CM, DA SILVA DA, SARTORIO PV, SILVA TD, SAAD SS, NADER HB, FORONES NM, TOMA L. (2018). Heparan Sulfate Proteoglycans in Human Colorectal Cancer. *Analytical cellular pathology (Amsterdam)*, ***2018***: 389595.

WADA Y, MORINE Y, IMURA S, IKEMOTO T, SAITO Y, TAKASU C, YAMADA S, SHIMADA M. (2020). HIF-1α expression in liver metastasis but not primary colorectal cancer is associated with prognosis of patients with colorectal liver metastasis. *World Journal of Surgical Oncology*, ***18***(1): 241.

WARBURG O. (1956). On the origin of cancer cells. *Science*, *123*(3191), 309-314.

WARBURG O, WIND F, NEGELEIN E. (1927). The metabolism of tumors in the body. *The Journal of general physiology*, ***8***(6): 519.

XU W, HE Y, WANG Y, LI X, YOUNG J, IOANNIDIS JPA, DUNLOP MG, THEODORATOU E. (2020). Risk factors and risk prediction models for colorectal cancer metastasis and recurrence: an umbrella review of systematic reviews and meta-analyses of observational studies. *BMC Medicine*, ***18***(1): 172.

YANG W, SHI J, ZHOU Y, LIU T, LI J, HONG F, ZHANG K, LIU N. (2019). Co-expression Network Analysis Identified Key Proteins in Association With Hepatic Metastatic Colorectal Cancer. *PROTEOMICS – Clinical Applications*, ***13***(6): 1900017.

YANG Y. (2003). Wnts and wing: Wnt signaling in vertebrate limb development and musculoskeletal morphogenesis. *Birth defects research. Part C, Embryo today : reviews*, ***69***(4): 305-317.

YE L, MUENCH MO, FUSAKI N, BEYER AI, WANG J, QI Z, YU J, KAN YW. (2013). Blood Cell-Derived Induced Pluripotent Stem Cells Free of Reprogramming Factors Generated by Sendai Viral Vectors. *STEM CELLS Translational Medicine*, ***2***(8), 558-566.

YILMAZER-AKTUNA A, TAHERI H, CAN A. (2017). Efficient transduction of melanoma cells with Sendai viral vectors. *Turk Hijyen ve Deneysel Biyoloji Dergisi*, ***74***(2): 113-120.

YIN L, LI J, MA D, LI D, SUN Y. (2020). Angiogenesis in primary colorectal cancer and matched metastatic tissues: Biological and clinical implications for anti-angiogenic therapies. *Oncol Lett*, ***19***(5): 3558-3566.

YU D-F, JIANG S-J, PAN Z-P, CHENG W-D, ZHANG W-J, YAO X-K, LI Y-C, LUN Y-Z. (2016). Expression and clinical significance of Sirt1 in colorectal cancer. *Oncology letters*, ***11***(2): 1167-1172.

YU J. (2007). Induced pluripotent stem cell lines derived from human somatic cells. *Science*, ***318***(5858): 1917-20.

YUI S, NAKAMURA T, SATO T, NEMOTO Y, MIZUTANI T, ZHENG X, ICHINOSE S, NAGAISHI T, OKAMOTO R, TSUCHIYA K, CLEVERS H, WATANABE M. (2012). Functional engraftment of colon epithelium expanded in vitro from a single adult Lgr5 + stem cell. *Nature Medicine*, ***18***(4): 618-623.

ZAKRZEWSKI W. (2019). Stem Cells: Past, Present and Future. *Stem Cell Research and Therapy*, ***10***(68): 329-332.

ZHAO ZS, MANSER E. (2005). PAK and other Rho-associated kinases – effectors with surprisingly diverse mechanisms of regulation. *Biochemical Journal*, ***386***: 201.

APPENDIX-1

Lokman Hekim Üniversitesi
Girişimsel Olmayan Klinik Araştırmalar
Etik Kurulu

Toplantı sayısı	Karar Sayısı	Toplantı tarihi
2021/19	1	23 Aralık 2021

Lokman Hekim Üniversitesi girişimsel olmayan klinik araştırmalar etik kurulu Başkan Prof.Dr.Feyyaz ONUR'un daveti üzerine 23 Aralık 2021 tarihinde aşağıdaki gündemle toplandı. Toplantıda Lokman Hekim Üniversitesi girişimsel olmayan etik kurul çalışma esasları hakkındaki yönergenin 5-1 maddesi gereğince etik kuruldaki görevli üyelerin çoğunluğunun toplantıda bulunduğu tespit edildi.

KARARLAR

Karar No. 2021/157: Prof. Dr. K.Can AKÇALI'nın sorumlu araştırmacısı olduğu **"Kolon Adenokarsinom Hatalarının İndüklenmiş Pluripotent Hücrelerinin (İPKH) Oluşturulması"** başlıklı (Kod No.**2021150)**girişimsel olmayan klinik araştırma **ETİK OLARAK UYGUN BULUNMUŞTUR.**

ETİK KURUL ÜYESİ	İMZA
Prof. Dr. Feyyaz ONUR, Eczacılık Fakültesi *Başkan*	[redacted]
Doç. Dr. Fatih BAKIR, Tıp Fakültesi *Başkan Yardımcısı*	
Prof. Dr. Belma TURAN, Tıp Fakültesi *Üye*	
Prof. Dr. Engin TUTKUN, BOZOK Üniversitesi Tıp Fakültesi *Üye*	
Dr. Öğr. Üyesi Safiye GÖÇER, Tıp Fakültesi *Üye*	
Dr. Öğr. Üyesi Hatice KARABULUT, Sağlık Bilimleri Fakültesi *Üye*	
Dr. Öğr. Elif Tuba AKÇİN Diş Hekimliği Fakültesi *Üye*	
Dr. Öğr. Üyesi Aybike ŞAHLANAN Diş Hekimliği Fakültesi *Üye*	
Dr. Öğr. Üyesi Hasan Erkan KILINÇ Sağlık Bilimleri Fakültesi *Üye*	
Dr. Öğr. Üyesi Ezgi EROĞLU, Eczacılık Fakültesi *Üye*	
Av. İlker IŞIKCI, Hukuk Müşavirliği *Üye*	

Lokman Hekim Üniversitesi Sayfa 1/1

APPENDIX-2

	Total Gene Number	p-value cut off
Control vs CRC	309	0.05
Control vs mCRC	572	0.05
CRC vs mCRC	913	0.05

Control vs CRC

Gene ID	log2(FC)
A1BG-AS1	0,3901
ABCA12	0,8589
ABCB4	0,9060
ABHD13	0,9033
ACSM6	-0,6185
ACTG1P4	-0,8328
ACTR10	1,0228
ADAMTS9-AS1	-1,6099
ADGRF5	1,0106
ADGRV1	-1,0213
ADI1	1,1710
AGAP1	1,1964
AGL	1,0813
AKAP7	-0,8569
ALG5	0,9526
AMY2B	-2,7954
ANO6	1,1732
AOC1	1,2903
APCDD1L	0,9653
ATG2B	1,2864
ATP10A	0,8450
BARHL2	1,1101
BBOX1	1,3213

BDNF-AS	-0,9728
BLOC1S6	1,2903
BMS1	-1,0074
C10orf105	-1,1112
C2CD6	-1,0513
C2orf88	1,7500
C8orf34	-2,2198
CAAP1	0,9081
CALCR	1,2580
CCAR1	0,9867
CCDC138	-1,4694
CCDC144NL	-1,0500
CDK5RAP2	-0,9678
CELSR1	1,0122
CENPF	-0,8277
CFAP221	-1,1811
CHRNA7	0,9947
CKAP5	-1,3077
CLASP2	-1,2307
COL3A1	0,8565
COPG2	-1,1924
CPSF7	-1,1359
CPZ	-1,1725
CSF1R	-1,2087
CYP2U1	-1,5991
CYP7B1	1,2366
DDX18	0,8788
DDX50	1,0090
DENND10P1	1,0607
DENND4C	0,7544
DISP2	-1,1929
DLEC1	1,0956
DLG1-AS1	0,9650
DLG5	-0,8912
DMBT1	0,8575
DMRTC2	-0,9419
DMXL2	0,9931
DOP1B	-0,7073
DPH7	-1,0145
DPYSL3	2,5934

DSCAM	-0,7620
DUOXA2	-1,4136
DUS4L	-0,6997
ECEL1	-1,0986
EPRS1	1,0500
EXOC8	0,9541
FAM181A-AS1	0,9151
FAM86B3P	-0,6231
FANCM	0,9361
FGF23	-1,3770
FGFBP3	2,3130
FGFR1	1,1310
FGFR1OP	0,7249
FIBIN	1,2324
FRRS1L	0,8682
FSCN3	0,9222
FUT9	0,8851
GABRA5	1,2467
GAREM1	-1,2736
GFER	-0,9607
GGA1	-1,0594
GLP2R	-1,1225
GMFG	-0,9700
GNPNAT1	-1,0899
GPD2	1,0137
GPR137B	-1,1309
GRN	-1,5845
GVINP1	0,9905
HDGFL3	-0,8140
HDHD2	-0,7659
HEATR1	-1,1938
HEPACAM2	1,0828
HIPK2	-0,9329
HK1	1,1947
HKDC1	1,1025
HLA-DMA	1,4423
HMGA2-AS1	-1,0732
HOXA-AS3	0,6690
HOXB8	-0,7262
HSD3B1	-1,5710

HYDIN	-0,9145
HYKK	-1,0945
INSIG1	-0,9872
INSIG2	1,0770
INTS6	0,9743
IQUB	0,8350
ITGA2	1,1795
ITGA5	-1,3353
ITGAV	0,9110
JAKMIP2-AS1	0,9249
JPH2	-0,9392
KCNA6	-0,9046
KCNH8	0,9071
KDM3A	0,8726
KDR	-1,7629
KHDRBS1	-0,6436
KIFBP	0,8685
KLF12	-0,9288
KLF7	1,0413
KNSTRN	-0,7788
KPNA6	-1,7375
KRBA1	0,9282
LECT2	1,1625
LEKR1	1,0378
LETM2	-1,3427
LHPP	1,0732
LILRA4	1,1746
LIMS1	-1,4323
LINC00470	1,7110
LINC00934	1,2089
LINC01093	0,7793
LINC01128	-1,0680
LINC01339	0,8888
LINC01583	1,6524
LINC01640	0,9359
LINC01668	0,9626
LINC01719	-1,1920
LINC01917	0,9585
LINC02010	-1,5754
LINC02029	1,4025

LINC02050	2,5371
LINC02197	0,8759
LINC02443	1,2680
LOC100128340	-1,0160
LOC100130357	-1,0729
LOC100132078	-0,9072
LOC100506497	-0,9125
LOC101927884	1,2656
LOC101929460	-0,8936
LOC101929538	-1,2306
LOC102724604	0,7690
LOC107985939	0,7887
LOC389641	-0,9592
LOC401478	0,8780
LOC728554	-1,0757
LRRC2-AS1	-1,1369
LRRC39	1,1012
LRRC55	-1,2953
LYSMD2	0,9774
M6PR	-1,8940
MACC1-AS1	0,9016
MACROH2A1	-1,2525
MAP7	-1,1813
MAPK8	-1,4414
MAPRE2	0,9298
MAST4	1,2371
MCM4	0,8321
MDN1	-0,8380
MED12L	-1,7628
MEF2C-AS1	1,3053
MGAT4C	2,8074
MICOS13	0,9691
MIR455	0,9870
MRGPRE	1,1160
MRS2P2	-0,9018
MUC2	-0,8297
MYO6	-2,0832
MYO9A	0,7731
MYPN	1,1394
MYT1L-AS1	1,1606

N4BP2L2-IT2	0,9861
NANOS1	-0,7709
NAV2-AS4	0,8566
NAV2-AS5	0,9086
NBR1	-0,8634
NDUFA5	1,7931
NECAP1	-1,0817
NIPAL2	0,8998
NT5E	-1,0393
NUB1	1,0416
NUDT12	0,9513
NUDT9P1	1,7324
OLA1	-0,6541
OR7E37P	1,0873
PAUPAR	0,7569
PAWR	0,6920
PAX2	-0,8097
PBDC1	0,8385
PCAT19	1,0693
PCBD2	-1,8889
PCDHB1	-1,0745
PDK1	0,9069
PDXDC2P-NPIPB14P	0,9276
PENK	1,0599
PGM3	-1,0364
PHACTR4	-0,7600
PI4KAP2	-0,9253
PKP4	-0,7553
PLAG1	1,0309
PLPP1	0,9477
POC5	0,8645
POLR3A	-1,1447
POLR3G	-1,2730
PPCS	0,9767
PPOX	-1,4479
PPP1R14C	-0,8802
PPP4R1L	0,9684
PPP4R3B	0,9612
PRC1	-0,6121
PRKACB	0,9980

PRPF39	1,0341
PRPF8	-0,8641
PSMC2	1,0764
PTH1R	-1,6593
PYROXD1	1,3199
PZP	0,6890
QRFPR	1,6492
RANBP2	-1,5929
RASSF9	2,3203
RCHY1	-1,1030
RDH10	1,3417
RELN	1,0188
RHOT1	1,3458
RNPC3	-1,7051
RTN4	0,8832
SAXO2	1,1894
SDS	0,9011
SEMA3F	-0,8785
SEMA4G	-1,0201
SERTM1	0,7745
SFI1	-1,0566
SGMS2	-1,7312
SIRT1	1,0495
SKA2	0,7872
SLC10A6	-0,9744
SLC1A2	-1,3031
SLC28A1	-0,8419
SLC39A5	-1,0802
SMC2	2,0465
SOGA3	-1,0135
SPATA31A3	1,0342
SPX	1,0209
STK10	0,9451
STK36	-0,8799
SUSD6	0,8682
TAB3	1,2782
TAPBPL	-1,1735
TARBP1	-0,9594
TCEANC2	-1,0585
TCFL5	0,8602

TEKT1	-1,1039
TERT	0,9418
TESPA1	1,1799
TET1	1,3052
THBS1	1,4760
THOC5	-0,8761
THYN1	0,9595
TNFRSF13C	0,7566
TNIP3	1,0079
TOX2	-0,6954
TRAF3IP1	-1,6629
TRAIP	-1,1879
TRIM37	1,0280
TRMT13	0,9019
TRPC7-AS2	-0,9525
TRPM7	0,5647
TSPAN12	-1,0898
TSPOAP1	0,9212
TTLL4	-1,0674
TWNK	-0,8744
UCN	-2,1623
USP21	-1,5841
USP39	-0,8456
VNN3	-0,8842
VPS26A	1,4937
VSIG2	0,9184
WASL	0,9914
WDFY3-AS2	1,3407
WLS	-0,5790
WNT2	-0,9261
WNT7B	-1,0562
WWC1	-1,0860
ZBTB20-AS1	-0,8404
ZC3H12A	0,9055
ZKSCAN2	1,1768
ZNF148	-0,9313
ZNF233	-1,3766
ZNF234	-0,7942
ZNF26	-1,2000
ZNF385A	-1,1283

ZNF454	-0,9310
ZNF480	-1,4704
ZNF597	1,2863
ZNF707	0,9124
ZNF789	1,5956
ZNF888	0,8364

Control vs mCRC

GeneID	log2(FC)
ABHD17B	1,1236
ABHD18	2,6881
ACSBG2	-1,1537
ACSM6	1,2131
ACTG1P4	-1,9269
ACTRT3	1,6418
ADAMTS7P1	-0,9119
ADAMTS9-AS1	-1,5088
ADAP2	1,4247
ADAT2	1,1832
ADK	1,3755
AFG3L2	-1,1970
AHSA2P	1,5244
ALDH1A2	1,5109
ALDH3B2	1,8061
ALKBH1	1,9039
AMY2B	-2,9594
ANKRD28	1,0412
ANKRD50	1,3139
ANP32E	-1,5366
ANPEP	-0,9083
AP3S1	1,4847
APBA3	1,4321
APOH	-1,0498
AQP4-AS1	1,6303
ARMC9	1,9110
ATAD2B	-1,0984
ATAD5	1,4282
ATF7	2,1163
ATP13A2	-1,8741
ATP2C2-AS1	1,4831
ATP4A	1,4507

ATP5MC2	-1,0101
ATP6V0E2	1,6408
ATP6V1B1	-0,8992
ATP6V1C1	-1,0888
ATP6V1E2	1,5314
ATR	-0,7814
BAP1	0,8847
BLOC1S5-TXNDC5	-1,7178
BOK-AS1	1,9676
BRIX1	1,5071
BRMS1L	0,8496
C10orf105	-1,6036
C14orf180	2,0540
C2orf42	1,3989
C2orf74	1,6512
C2orf88	2,3767
C3orf70	1,2545
C4BPA	1,7058
C4BPB	1,8032
C9orf147	1,7722
CA12	1,0050
CALML5	0,8774
CASC11	1,8646
CBLN3	1,0595
CBX7	0,9900
CCDC173	1,4230
CCDC178	0,9660
CCDC18-AS1	-2,2595
CCDC180	2,2343
CCDC192	-1,2987
CCL18	1,7681
CCL4L2	1,6010
CCL8	1,7603
CCNL1	-1,1582
CCT6B	1,0604
CD200R1	-0,7930
CD47	1,9865
CDC37	1,4232
CDCA7	1,4082
CDH3	-1,3250

CELA2A	1,4352
CEP250	-0,8527
CFAP221	-2,7818
CFAP44	1,4495
CFAP74	1,3682
CHDH	2,1770
CHL1-AS1	-1,7708
CHMP1B	2,0678
CHRM2	-1,3965
CHRNA2	1,4983
CLASRP	1,9993
CLDN1	1,8956
CLEC18B	1,5693
CNGA1	1,7482
CNGA4	1,0147
CNOT1	-0,8389
CNOT6L	1,5317
COL15A1	1,5204
COL25A1	1,4911
COPS7A	1,5427
CPSF2	1,8615
CPSF6	2,7434
CRISP3	2,1182
CROCCP3	1,6140
CRTAP	1,0259
CSF1R	-1,8243
CSRNP3	1,5970
CTU2	1,1896
CUL4B	2,2675
CYB5R2	1,2582
CYB5R4	1,3793
CYP2R1	0,8681
CYP46A1	1,5071
CYTIP	1,2123
DBNL	0,8676
DCAF17	-1,8202
DCC	-0,8796
DDC	-1,6116
DDC-AS1	1,9411
DDX25	-0,9586

DDX55	1,3560
DEAF1	1,3201
DENND1C	1,4279
DHCR7	2,6618
DICER1	2,6369
DIO2	-0,8287
DIP2B	2,4540
DLD	-0,9034
DMAC2	2,1527
DMTF1	1,5189
DNAJB5	2,1074
DNAJC6	1,0042
DOCK7	1,2229
DR1	1,2781
DSTN	1,3959
DUS4L	0,7903
DUSP19	-1,3979
DYRK1A	1,6427
E2F4	1,3882
ECH1	1,5673
EDC4	1,3352
EGFR-AS1	1,4944
EIF3L	1,1706
EIF5B	1,7418
ELL	1,2952
ELOA	-0,9230
EMCN	2,1666
ENTPD1-AS1	1,2689
ENTPD6	1,4493
EPN1	1,7436
ERGIC2	1,5909
ERI1	1,3080
ERI3-IT1	-1,2968
ERLIN2	1,1419
ESCO1	1,4672
ETNPPL	1,6759
EZR	0,9982
F2	1,2911
FAF1	-1,4478
FBXO34	1,9651

FBXW4	2,0114
FER1L4	1,9117
FGF1	1,3547
FGFBP3	1,5620
FGFR1	1,8950
FKSG29	2,6147
FLCN	-1,0138
FLJ42102	2,7616
FNBP1	1,1212
FNDC1	1,0990
FNIP1	1,1087
FOXN1	1,7806
FRMD5	1,3313
FST	1,0709
FUCA2	1,2000
FZD4	0,8898
GAB1	1,9759
GAL3ST4	1,1089
GALNT13	1,6215
GAREM1	-1,5218
GCNT3	1,1192
GDE1	1,9239
GDPD4	1,5936
GDPD5	1,6832
GFPT1	-1,0975
GLP2R	-1,7199
GLS2	1,3513
GNA14-AS1	2,7339
GNAL	0,7708
GNAQ	1,5794
GNG12-AS1	1,4891
GOLGA6L6	-2,1503
GPATCH3	1,5931
GPN2	1,0912
GRIN2B	1,8197
GRN	-2,0711
HAPLN2	1,4481
HAS2-AS1	1,3872
HEATR1	-1,8897
HEATR5A	-1,2284

HERC1	1,0441
HHIPL1	1,3070
HIF1A	1,4472
HIVEP2	0,9930
HMBOX1	1,3800
HMGA2-AS1	-1,5316
HOXA13	-1,8519
HOXB9	1,1006
HSD3B1	-2,3214
HYKK	-1,6856
HYLS1	-0,9354
IGFLR1	1,5442
IGSF11-AS1	1,1996
IGSF9	2,2993
IK	1,4539
IL17F	1,2681
IL17RC	1,6758
IL6R-AS1	1,6674
INHBE	-0,9139
INPP5B	1,4366
ITGA5	-1,8349
ITGAL	2,1850
JAZF1	0,7599
JPH1	1,2736
KALRN	2,0711
KANK4	1,0470
KATNBL1	-1,8247
KCNAB3	1,8010
KCNN2	-1,2986
KDELR3	1,4569
KDM7A	1,2899
KDR	-1,6720
KEL	1,1185
KIAA0586	-0,9406
KIAA2012-AS1	1,7422
KLF10	1,1450
KLHL13	1,3762
KPNA6	-1,7365
KRT33A	0,8890
KRT33B	1,2227

KRT8P41	-1,3460
LAD1	1,9018
LCORL	-0,9184
LDLRAP1	0,7495
LECT2	2,3856
LGALS4	1,8335
LGALS7	1,5540
LGI2	-1,7296
LGR5	1,7494
LILRB4	1,4745
LIN7B	1,5646
LINC00673	1,8623
LINC01143	-1,0027
LINC01181	-1,1650
LINC01333	1,6813
LINC01376	1,7691
LINC01416	1,3603
LINC01523	-2,0666
LINC01592	-0,9401
LINC01920	2,2620
LINC01975	1,3548
LINC01992	-1,3263
LINC02082	1,5471
LINC02283	1,5767
LINC02324	1,1845
LINC02348	1,3330
LINC02585	0,9591
LINC02586	1,5504
LINC02691	1,4287
LMNB1-DT	-1,1092
LOC100128340	-1,7036
LOC100131257	3,1912
LOC100132078	-1,6928
LOC100506142	2,0077
LOC100506585	1,2784
LOC101593348	1,4536
LOC101927377	-1,5349
LOC101927854	2,0517
LOC101927914	-0,8941
LOC101928834	2,0220

LOC101929089	-0,9835
LOC101929099	2,3854
LOC101929188	1,4403
LOC101929622	1,1737
LOC102725021	-0,8553
LOC105370068	1,7069
LOC105372440	2,0616
LOC105373064	1,5401
LOC107984974	1,6711
LOC646626	1,3698
LPA	1,0856
LRIG2-DT	0,9745
LRRC34	1,7158
LRRC37A4P	1,8911
LRRC49	1,0535
LTF	1,5881
M6PR	-2,4204
MACC1-AS1	2,4462
MAOA	2,3126
MAPK8	-2,0159
MAPT	1,3434
MAST1	1,0154
MAT2A	1,0377
MED22	1,2517
MFSD6	1,7958
MINK1	0,8114
MIR3157	1,4238
MIR548I2	1,4362
MKRN2	1,8653
MMP25-AS1	1,8229
MORN3	1,6447
MPC2	0,8715
MPV17	1,3074
MRAP2	1,3249
MRAS	0,8371
MROH2A	1,9392
MRPL2	-1,1473
MRPL42	2,0955
MRTFA	1,3486
MUC12	-1,0240

MVB12B	1,2557
MYLK3	-0,9715
MYO6	-2,2586
NAMPT	1,6617
NANOG	1,8602
NCKAP5	1,9074
NCKAP5-AS1	-2,5031
NDUFV1	1,7513
NEBL-AS1	1,4516
NEK1	-0,9547
NELL2	1,5414
NENF	-2,1261
NET1	1,8407
NF1	1,3965
NFU1	-1,0296
NIPAL3	2,0887
NKPD1	1,2464
NKX6-1	2,0974
NOG	1,4194
NOTCH2	3,0175
NUP62CL	1,3649
NYAP1	0,9876
OR10G3	1,6608
OR1I1	-1,9437
OR7E37P	1,1020
ORM1	1,3435
ORM2	1,2800
OSBP	1,3386
OSBPL11	1,4399
OSBPL9	1,7227
OSTCP1	1,1913
OTOG	1,4650
OTUD5	0,9592
PAK1	2,1006
PAN2	1,6411
PATE4	-1,1778
PCAT19	1,8905
PCBD1	0,9563
PCBD2	-1,9362
PCDHB11	1,4781

PCDHB13	1,2261
PCDHB14	1,3741
PCDHB15	1,5572
PCDHB16	1,6660
PCDHB18P	1,6808
PCDHB19P	1,5623
PCDHB7	2,1873
PCDHB9	1,4291
PCM1	1,0485
PCMT1	1,5737
PDCD6IP	1,3360
PDCL2	-1,2078
PDGFRL	1,4454
PEF1	-1,8653
PEX7	1,4935
PGLYRP4	1,5120
PHACTR2-AS1	1,4425
PHLPP2	1,9081
PI4KAP2	-2,3738
PIGX	1,7750
PIK3IP1	1,3294
PIP4P2	0,9546
PKN2	2,1110
PKNOX2-AS1	-0,9634
PKP1	2,0708
PLA2G2A	1,6649
PLA2G2F	2,3211
PLA2G5	1,8267
PLAAT1	1,7536
PMS2P7	1,9537
PNLIPRP3	2,1223
PNPLA1	1,6299
POLL	2,1554
POLR2F	2,2342
POLR3B	-1,1599
POU1F1	1,0334
PPCS	2,2428
PPOX	-1,6908
PPP3R2	1,0926
PRKACB	1,8258

PRMT5	-1,5799
PROCA1	0,9412
PRPF38A	1,6983
PRR15	1,5085
PRR26	-0,8502
PRRT3	1,6207
PRSS48	1,2415
PSMG3-AS1	1,7794
PSTPIP1	0,7698
PTGES	1,1596
PTPRA	1,7483
RAB3B	2,4401
RASL11B	2,1002
RASSF1-AS1	1,4049
RBM41	1,3338
RCAN3	1,7413
REM2	-1,7094
RFC4	1,3031
RGCC	1,1782
RGSL1	1,4554
RHOT1	2,3420
RIMKLA	2,0111
RIMS4	-1,7357
RND3	1,9979
RNF115	1,9800
RNF123	1,5553
RNF13	1,9676
RNF135	1,4516
RNF212B	1,8445
RNF34	1,7378
RNPC3	-2,1847
RPS13	1,6382
RRAS2	0,8319
RUFY3	1,6075
RUNDC3B	1,1124
RUNX3	2,1193
RWDD3	1,5261
SAMD12-AS1	2,2436
SCARA3	-1,0830
SDAD1	0,8997

SEC22C	2,0202
SERINC3	1,8693
SERPINA7	1,5995
SETD4	1,4965
SH2D3A	1,4028
SH3RF1	1,6299
SH3TC2	1,1773
SHANK1	1,4146
SHANK2-AS1	1,3509
SHANK2-AS3	1,6441
SHTN1	-0,8666
SIGLEC9	-1,7436
SLAMF9	2,1131
SLC14A2	1,4283
SLC15A5	0,7601
SLC16A12	1,8800
SLC17A1	1,5848
SLC22A12	1,1835
SLC22A17	1,3445
SLC25A11	1,4687
SLC25A48	2,1082
SLC27A2	1,6825
SLC28A1	-1,3121
SLC2A1	0,8692
SLC30A1	1,1422
SLC7A13	1,6774
SLC7A14-AS1	3,0450
SLC7A2	1,1404
SLC7A6	1,2220
SLC8B1	-2,5398
SLC9A3-AS1	2,1991
SLFN13	1,6561
SMC2	1,6575
SNAP23	0,7577
SNPH	2,2776
SNW1	1,8040
SOCS3	0,9041
SORCS1	-1,1204
SOX13	1,7484
SPRY4	1,5277

SPRY4-IT1	1,6287
SQOR	1,6106
SSPO	1,7728
ST8SIA3	-1,4036
STAT2	1,8067
STAT4	2,0075
STC2	1,3591
STMN4	1,9660
STRAP	1,6300
STX6	1,6271
STXBP4	0,7758
SURF4	1,2486
SURF6	1,3234
SVEP1	1,6122
SYNGR4	2,4060
SYT7	1,0262
SYTL3	1,8911
TAF4B	1,8839
TBC1D10B	1,1279
TBC1D3P5	0,9169
TBC1D9	1,5258
TBL1XR1	2,3133
TCF4-AS1	1,5473
TERC	1,8964
TERT	2,7552
TEX48	1,1862
TFPI	0,8140
THAP9	2,2152
THRB-AS1	1,9442
TIGD6	1,6618
TIMM10	1,3047
TIMM10B	1,4156
TIMM17A	1,5317
TIRAP	-1,8160
TLCD4	1,4694
TLCD4-RWDD3	1,2908
TMEM119	1,3381
TMEM147-AS1	1,6003
TMEM175	1,1013
TMEM218	-0,8152

TMEM25	1,8016
TMEM251	2,3523
TMPRSS4	1,6870
TNNT2	1,7349
TNRC18P1	1,9491
TOR1A	1,5795
TP53INP1	1,2543
TPTE2P3	0,9370
TRAF3IP1	-2,2331
TRAIP	-1,5849
TRAPPC3L	1,2459
TRIM35	1,3525
TRIP10	1,7127
TRMT13	1,6595
TRMT6	-0,8851
TRMT61B	1,9172
TRPM6	1,7656
TSHR	-0,9882
TTC1	1,4993
TTC36	2,5838
TTF2	1,1690
TXNDC12	2,1277
UBAC2	2,3665
UBB	1,5283
UBE2L6	1,1053
UBL7-AS1	-1,5562
UBR7	1,9910
UBXN8	-1,6151
UCN	-2,1330
UFD1	-1,3253
UGDH-AS1	1,1194
USF3	0,9101
USP21	-1,8171
USP24	1,5270
USP8	2,1766
UTP3	2,3303
VAMP8	1,3905
VPS8	1,3487
VRK2	1,6428
WDR76	1,0009

WNT3	1,4253
XLOC_008559	1,7022
XRN1	1,2992
XRRA1	1,6211
ZBED1	1,7042
ZFAND6	1,2325
ZMYM1	1,6458
ZNF121	-1,1672
ZNF205-AS1	1,3990
ZNF385A	-2,2308
ZNF442	-1,1648
ZNF454	-1,7851
ZNF480	-1,7553
ZNF557	-1,5299
ZNF563	-1,2049
ZNF597	1,7758
ZNF610	-1,0016
ZNF833P	1,6766
ZNF862	1,7503
ZSCAN18	-1,1872

CRC vs mCRC

GeneID	Log2FC
A2M	-0,7216
AATBC	1,6722
ABCB6	1,3564
ABHD17B	1,2762
ACAD8	-1,2081
ACIN1	1,3215
ACO1	-1,3940
ACOT7	1,4500
ACSM6	1,8494
ACTRT3	1,5244
ACVR2B	-0,8815
ADAMTS3	1,3292
ADAP2	1,4842
ADGRE2	1,4801
ADGRG2	1,1777
ADGRV1	1,1278
ADI1	-1,3267
AGAP1	-2,5168

AKAP7	0,9750
ALDH1A2	1,6863
ALDH1L2	-0,8183
ALG1	0,9909
AMDHD2	-1,5040
ANK1	1,7027
ANK2	1,0759
ANKFN1	1,4142
ANKRD50	1,3623
ANKRD53	-1,1680
ANO6	-1,8059
ANP32E	-1,0990
AP2A1	-1,2764
AP3S1	1,0404
APBB2	0,9883
APCDD1L	-1,2554
APOBEC3C	-1,2895
APOBEC3F	-1,2360
APOH	-1,0716
AQP4-AS1	1,6929
ARCN1	-2,5437
AREG	1,5106
ARHGAP12	-0,8871
ARHGEF5	1,2674
ARMC2-AS1	1,2496
ARRB1	0,8686
ARSJ	-0,9326
ATAD5	1,1997
ATG2B	-1,8617
ATG4B	-1,3302
ATP2C2-AS1	1,8106
ATP4A	1,3823
ATP6V1B1	-1,1273
ATP6V1E1	1,3127
ATP6V1E2	1,5474
ATR	-0,8294
AXIN1	0,9288
B4GALT1-AS1	1,1844
BAIAP3	2,2066
BAP1	1,0553

BBOX1	-1,5634
BCAN	-1,1071
BCAP29	1,3850
BHLHE41	-1,1812
BIVM	-1,1227
BOK-AS1	1,7622
BOLA1	0,9887
BPESC1	0,8614
BRAF	-1,0496
BRIX1	1,4498
BRMS1L	1,4091
BTBD10	1,2670
BTBD7	0,9493
C11orf87	-1,3876
C12orf40	-0,7557
C14orf180	1,8660
C19orf48	1,6244
C1orf167-AS1	-1,3116
C1QTNF1-AS1	-0,9881
C1RL-AS1	0,9903
C2CD6	1,4313
C2orf27B	-1,0493
C2orf42	1,5260
C3orf70	1,1570
C7orf50	1,6444
C8orf34	1,5412
C9orf135	1,3502
CA12	1,0241
CABP1	0,9188
CALCR	-1,4731
CALML5	1,0971
CAMK4	-1,0575
CAPN2	1,7084
CARHSP1	-0,9328
CASP9	1,0223
CBLN3	0,8817
CCDC138	1,8536
CCDC14	-0,8281
CCDC159	1,0201
CCDC173	1,6471

CCDC178	1,1022
CCDC18-AS1	-2,1462
CCDC180	1,6998
CCDC28A-AS1	1,0840
CCDC28B	-1,1505
CCDC85A	-1,2970
CCL18	1,6999
CCL4L2	1,7879
CCN6	-0,9431
CCNA1	-0,8815
CCNDBP1	-0,9425
CCNL1	-0,9932
CD14	-1,2748
CD200R1	-0,9584
CD27	1,1714
CD300A	1,1897
CD47	2,1645
CD6	-1,1480
CDC37	1,7760
CDCA7	1,4074
CDH19	-1,2335
CDH4	-1,3354
CDK5RAP2	2,1274
CELSR3	-1,3171
CEP250	-0,7784
CFAP36	-0,9446
CFAP44	1,5230
CFAP74	1,4050
CFTR	-1,5363
CGREF1	-1,1145
CHMP1B	2,1541
CHRM2	-1,0656
CHRNA7	-1,7567
CHRNE	0,8837
CKAP5	1,5827
CLASP1	-1,0807
CLASRP	1,5092
CLDN1	1,9871
CLEC14A	1,6212
CNGA1	1,6053

CNGA4	1,0543
CNMD	2,0083
CNN3	0,8848
CNOT1	-0,8860
COCH	-1,8555
COL3A1	-1,8579
COL6A3	-1,4113
COPG2	2,2764
COPS7A	1,4817
CPA3	2,2926
CPA6	-1,2976
CPSF2	2,7298
CPSF6	3,0693
CPXM2	1,1425
CROCCP3	1,6987
CRTAP	1,2921
CRY1	-1,1985
CSNK1A1	1,5123
CSRNP3	1,2420
CT75	-0,9605
CTU2	1,3989
CTXN3	-0,9868
CUL4B	1,3872
CXXC4	-1,6798
CYB5R2	1,5586
CYB5R4	1,5789
CYP46A1	1,7625
CYTIP	1,2463
D2HGDH	-1,0657
DCAF6	-0,8089
DCC	-0,7599
DCDC2B	-1,2731
DDC-AS1	1,6970
DDN	-1,4198
DDX18	-0,9501
DDX47	-1,2259
DDX5	0,9118
DEAF1	1,4283
DEDD2	1,7259
DEFB119	-0,8753

DENND1C	1,5624
DGKG	0,8974
DGLUCY	-0,8458
DHCR7	1,9290
DICER1	2,4643
DIP2B	2,0865
DIS3L2	-1,5002
DLD	-0,9141
DLG1-AS1	-1,3768
DLG5	1,5678
DMBT1	-1,0811
DMBX1	-0,8120
DMRTC2	1,5885
DMTF1	1,5988
DMXL2	-1,2708
DNAH11	-1,4074
DNAJB6	-0,8671
DNAJC6	1,2951
DNASE1L2	-0,9491
DOCK7	1,3278
DOCK8-AS1	1,3164
DOP1B	1,4629
DPP4	0,7142
DPYSL3	-3,1079
DSTN	1,4297
DTNB	-1,3260
DTX2P1-UPK3BP1-PMS2P11	1,2037
DUOXA2	2,2709
DUS4L	1,5347
DUS4L-BCAP29	1,1297
DYRK1A	1,3122
E2F4	1,3924
E4F1	-1,0209
ECH1	1,3309
EFCAB14	-0,8400
EGFR-AS1	1,3771
EIF2AK4	-1,0623
EIF2B3	-1,5952
EIF3I	-0,9523
EIF3L	1,2582

ELL	1,1117
ELOA	-0,9434
ENTPD7	-1,6533
EPN2-AS1	-1,3847
EPS8	-1,0817
ERGIC2	1,6529
ERI1	1,3869
ERI2	1,4257
ERLIN2	1,3844
ERMN	1,2588
ESCO1	1,8110
ESYT3	0,7699
ETNPPL	1,2936
EXOC7	-0,8090
EYS	0,9514
F2	1,3250
FADS6	-1,1670
FAM118A	-0,9508
FAM160A1	0,8328
FAM185A	0,9035
FAM229B	-0,8715
FAM76A	0,8628
FAM86B3P	1,1459
FAM90A27P	0,9518
FANCD2OS	-0,8385
FAXC	-1,2090
FBXO11	-1,1151
FBXO16	-0,9989
FBXO34	1,4607
FBXW4	1,2797
FBXW7	1,1256
FCER2	1,1004
FDXR	-1,4931
FGF1	1,4044
FGFBP3	-2,1363
FGFR1OP	-1,0158
FIBIN	-1,4355
FIGNL2	-1,2614
FIZ1	1,3034
FLCN	-1,1235

FLJ39095	-0,8531
FLJ42102	2,0253
FLNC-AS1	-0,8593
FLT1	-1,2394
FMNL3	0,9780
FNBP1	0,9980
FNDC1	1,0594
FNDC3B	1,0104
FNIP1	1,1780
FREM2	1,2521
FRMD5	1,9941
FUT8	1,2147
FUT9	-1,1527
FZD4	1,0627
GAB1	1,2629
GAB3	-1,6040
GADD45GIP1	-1,2654
GADL1	1,3278
GALNT13	2,1109
GATA4	1,2354
GCC1	0,7170
GCNT3	0,8559
GCSAML-AS1	-1,1787
GDF5-AS1	-0,7997
GFER	1,5406
GFPT1	-0,9153
GFRA1	1,7255
GGA1	1,6820
GIMAP8	1,5332
GLS2	1,5797
GLYAT	1,2357
GLYR1	1,4170
GNA13	-0,9060
GNA14-AS1	2,1090
GNAQ	1,7918
GNG12-AS1	1,4479
GNL1	2,0691
GOLGA6L6	-1,9538
GOLIM4	-0,9101
GON4L	-1,0118

GPATCH3	1,2348
GPN2	0,9964
GPR15	-0,8208
GPR34	0,8528
GPR61	-1,1548
GREM1	-1,6680
GREM2	-1,0314
GRIN3A	1,1345
GTPBP3	0,8847
GTSE1	-1,2048
GYG1	2,4853
GYG2	1,4378
GZMH	1,0021
HAPLN2	1,8382
HAS2-AS1	1,3830
HDDC2	0,9422
HDDC3	1,2584
HEBP2	1,4813
HHIPL1	1,6709
HIF1A	1,5358
HIF1A-AS2	1,7185
HIVEP2	1,5182
HMBOX1	1,2826
HMOX2	1,2105
HNRNPA2B1	0,1637
HOGA1	-1,0856
HOXA13	-1,8107
HOXA5	-1,2128
HOXB9	1,2622
HPF1	-1,0941
HS3ST1	-1,5422
HSD3BP4	1,5134
HSPB6	1,7788
HSPG2	-1,1888
HVCN1	-1,1639
HYOU1	1,0528
IGBP1	-1,5553
IGFLR1	1,7223
IGSF11-AS1	1,3533
IGSF9B	-1,1137

IL17F	1,0961
IL32	1,3092
IL6R-AS1	1,7677
ILF3	1,4382
ING5	-1,2063
INPP5B	1,2435
INSIG2	-1,0655
INTS6	-1,3259
IQCC	-1,0421
IRX5	-1,1837
ITGB6	1,1549
JAG2	1,1700
JAZF1	0,9805
JMJD8	-1,3894
JPH1	1,5115
KANK4	1,4244
KATNBL1	-1,5398
KCMF1	0,9266
KCNAB1	1,1142
KCNAB3	2,1297
KCNB1	0,7888
KCNG3	0,9356
KCNN2	-1,0616
KCNQ1OT1	1,0023
KDM7A	1,4319
KEL	1,3743
KIAA0586	-1,0976
KIAA0930	1,2238
KIAA2012-AS1	1,4767
KLF10	1,6322
KLHL13	1,5673
KLHL23	-0,8472
KMT2D	-1,7908
KMT5B	0,8564
KNSTRN	0,7980
KRT33A	0,8543
KRT33B	1,2246
KRT7	-1,2014
KRT80	-1,0239
KRT8P41	-1,2638

KRTAP4-2	-1,4975
KRTCAP2	-1,1902
L3MBTL3	1,3726
LAD1	1,9425
LAMP5	-1,5084
LCOR	1,0031
LDB1	1,0883
LDLRAP1	0,8198
LENG8-AS1	-1,2494
LEPROT	1,0850
LGALS7	1,3324
LGR5	1,3243
LHPP	-1,3080
LIAS	1,1421
LIMS1	1,2859
LIN7B	1,4282
LINC00470	-2,2036
LINC00474	1,2440
LINC00520	0,7501
LINC00592	-1,2544
LINC00673	2,0721
LINC00970	1,2213
LINC00987	1,2881
LINC01022	0,8969
LINC01093	-1,2714
LINC01143	-1,2022
LINC01524	1,8238
LINC01583	-1,9274
LINC01592	-1,2133
LINC01625	1,3497
LINC01650	1,5372
LINC01686	-1,3740
LINC01920	1,4096
LINC01993	0,9604
LINC02003	-1,3166
LINC02029	-1,6622
LINC02050	-1,8066
LINC02082	1,5030
LINC02197	-0,9742
LINC02324	1,1795

LINC02348	1,8033
LINC02366	1,4763
LINC02443	-1,8383
LINC02500	1,5839
LINC02585	1,0830
LINC02691	1,5340
LIPE	0,9366
LMBRD1	-0,9423
LMNB1-DT	-0,1275
LNCPRESS2	1,2756
LOC100130027	1,3737
LOC100131257	2,5369
LOC100131496	-1,1552
LOC100133286	1,6616
LOC100505938	1,2585
LOC100506098	1,5698
LOC100506142	2,1263
LOC100506585	1,5453
LOC100506606	1,7040
LOC101593348	1,3555
LOC101926935	-1,4353
LOC101927138	1,5938
LOC101927157	1,2096
LOC101927377	-1,3453
LOC101927450	2,3868
LOC101927854	1,7246
LOC101927908	-1,3793
LOC101927914	-1,2116
LOC101928251	1,5019
LOC101928429	1,2685
LOC101928595	1,2045
LOC101928834	1,8015
LOC101928847	-0,9874
LOC101928882	-1,5212
LOC101929099	2,2879
LOC101929188	1,5307
LOC101929622	1,4921
LOC101929950	0,9053
LOC102724604	-1,1579
LOC102725021	-1,1104

LOC104968399	1,2925
LOC105372440	1,6381
LOC105373064	1,6684
LOC107984974	1,3898
LOC107985939	-1,0250
LOC145783	-1,4735
LOC284412	-1,0763
LOC284898	-0,9863
LOC286059	1,3951
LOC339803	1,2311
LOC440084	1,2533
LOC643406	1,7301
LOC645177	-0,8899
LOC729930	0,7008
LRFN1	1,4762
LRRC2-AS1	1,5252
LRRC39	-2,0538
LRRC49	1,1741
LSM10	-0,8701
LYPLA2	-0,9664
MAJIN	1,0399
MALAT1	-1,5348
MAMDC2	1,2647
MAN2B2	-1,0169
MAOA	1,4829
MAPKAPK3	1,1364
MAPRE1	-0,8180
MAPRE2	-1,3763
MAPT	1,4747
MARF1	-0,9092
MARS1	1,4393
MARVELD2	-1,7108
MAST1	1,0382
MAT2A	1,1962
MCF2	-1,2651
MCM4	-2,7372
MCM8	1,4407
MDFI	1,3365
MDN1	1,3008
MEAK7	1,3224

MECR	1,0929
MED12L	1,2720
MED25	-1,0450
MEF2C-AS1	-2,4268
MEIKIN	1,0767
MEX3A	-0,6848
MFSD6	1,6961
MGAM	-1,6176
MGAT4C	-1,9206
MICAL3	-0,8534
MICALL1	1,3284
MICOS13	-1,4971
MINK1	0,8586
MIR3157	1,3617
MIR3187	-1,1671
MIR3945HG	-0,8870
MIR4307HG	-1,0231
MIR4455	-0,9951
MIR4495	-1,3217
MIR4527	1,4982
MIR4746	1,0955
MIR548AI	-1,3600
MIR548I2	1,7783
MIRLET7D	1,5035
MMP25-AS1	1,8280
MOB2	-1,1565
MON2	-1,0601
MORN3	1,3063
MPC2	0,9806
MPHOSPH9	-1,2281
MPPE1	-0,9940
MRAP2	1,2165
MRAS	0,9631
MRPS33	-0,9604
MRTFA	1,2547
MTA1	-1,0476
MTERF2	-0,9802
MTHFR	-0,7930
MVB12B	0,8778
MYL1	-0,8700

N4BP2L2-IT2	-1,4863
NBPF26	-0,9113
NBR1	1,1351
NCAM1	-1,5107
NCKAP5	1,4272
NCOA6	0,9685
NDUFS7	-1,3937
NEAT1	0,8916
NEK1	-1,0376
NELL2	1,0493
NEPRO	-1,1606
NEURL4	-0,9068
NEUROG1	1,4793
NF1	1,1325
NFAM1	-1,1942
NFU1	-0,8786
NHSL1	1,1824
NIFK	-1,0907
NISCH	1,9877
NKPD1	1,1692
NLRP11	-1,0918
NLRP7	-1,2325
NOC2L	-1,1377
NOS1	-0,8916
NOTCH1	-1,7489
NOTCH2	1,5835
NRDC	1,2587
NTSR2	-1,3625
NUDT9P1	-3,4013
NUP210L	-1,3101
NUP214	-1,2000
NUP62CL	1,5200
NYAP1	1,0563
OR10G3	1,5965
OR10G6	1,0573
OR4D9	1,5549
OR5AU1	1,4404
OR6V1	-1,2153
ORM1	1,3096
OSBP	1,4414

OSBPL9	1,4835
OTUD5	0,8889
OVCH1	1,3991
OVOS2	-1,0653
PAGR1	1,4209
PAN2	1,1869
PARP14	-1,0303
PARP15	-1,1798
PAUPAR	-1,6489
PAWR	-1,4323
PBDC1	-0,8944
PCBD1	1,2249
PCDH7	1,3571
PCDHAC2	0,8142
PCDHB11	1,2126
PCDHB14	1,1557
PCDHB15	1,5006
PCDHB18P	1,4229
PCDHB19P	1,5368
PCDHB7	1,6630
PCM1	0,9533
PDGFRL	1,3579
PDXK	1,7525
PECAM1	0,8281
PEX7	1,7765
PFKFB1	-1,0142
PGP	0,7620
PHACTR4	1,9693
PHC3	0,9782
PHF12	1,7776
PHKA1	-1,7095
PHLPP2	1,6775
PHTF2	-0,8986
PIGF	1,6588
PIGX	1,2087
PITRM1	1,3701
PKD1P6-NPIPP1	0,9693
PKNOX2-AS1	-1,0335
PKP1	1,5385
PKP4	0,9592

PLA2G15	1,6016
PLA2G2A	1,8837
PLA2G2F	2,1958
PLA2G5	1,8249
PLA2R1	1,1217
PLAGL1	0,9338
PLCD1	0,6971
PLEKHM1P1	0,9549
PLPPR2	0,8668
PLXNB1	-1,1793
PML	-1,4943
PMS2P7	1,8299
PNLIPRP3	1,9169
POLL	1,3807
POLR3A	1,8051
POU1F1	1,2351
PPFIA1	0,7642
PPFIA2-AS1	1,2688
PPM1F	0,6945
PPP1R12A	-1,1396
PPP1R12B	-1,0529
PPP1R37	1,3879
PPP1R3D	-1,0654
PPP2R2A	-0,9171
PPP3CB	-1,0403
PPP3R2	1,1875
PPP4R1L	-1,1245
PRB1	1,2637
PRC1	1,0471
PREB	-0,9263
PRKCSH	1,0682
PRMT8	-1,6536
PROCA1	1,0932
PRPF38A	1,1053
PRPF38B	1,0168
PRPF8	0,7909
PRR26	-0,7795
PRR29	-1,1232
PRR30	-0,9925
PRRC2C	1,6071

PRRT3	1,4619
PRSS48	1,1096
PTBP1	-1,0688
PTP4A2	1,3676
PTPRA	1,5653
PYROXD1	-1,8552
PZP	-1,0858
RAB35	1,0518
RAB3C	1,0917
RAB7A	1,1188
RABL3	-1,0950
RAI1	1,1235
RANBP2	1,9402
RAP1GDS1	-1,8707
RASL11B	1,7108
RASSF1-AS1	1,5291
RASSF9	-2,1800
RBM41	1,4939
RBM42	1,3505
RCAN3	1,6963
RCHY1	2,1008
RDH10	-2,7965
RELL1	1,2429
RFC4	1,3546
RGS22	0,7767
RGSL1	1,3010
RIC1	1,0682
RIC3	-0,9904
RIMKLA	1,1593
RIT2	2,0108
RLF	1,3382
RND3	1,3738
RNF115	1,4410
RNF135	1,5153
RNF141	1,2501
RNF157	1,1779
RNF34	1,6885
ROR1-AS1	1,0313
RORA-AS2	1,1180
RORC	1,2097

RRN3	0,8942
RTN3	-0,8444
RUNX1	0,7756
RWDD3	1,6314
SAMD11	-1,5942
SART3	1,5623
SATB1	-2,7296
SAXO2	-1,7032
SC5D	1,6849
SCN8A	1,4824
SCNN1A	1,3489
SCUBE2	-1,4984
SDAD1	1,1805
SDHAF1	1,5606
SEC14L2	1,5927
SELENOKP3	-0,9850
SELPLG	1,5051
SEMA4F	0,9901
SEPTIN7P2	-0,9318
SERINC3	1,3188
SESN1	0,9334
SESTD1	-0,9146
SETD2	1,0185
SETD4	1,6095
SF3B5	0,9287
SH3RF1	1,8533
SHANK1	1,5031
SHANK2-AS1	1,7374
SHANK2-AS3	2,0686
SHTN1	-0,7565
SIGLEC7	-1,4872
SIGLEC9	-1,9826
SKA2	-1,3369
SLC10A1	-1,4508
SLC12A9	1,0372
SLC14A2	1,1765
SLC16A12	1,8614
SLC17A1	1,5108
SLC22A12	1,1787
SLC22A17	1,5536

SLC23A3	-1,5128
SLC24A1	-1,1908
SLC24A3	1,9738
SLC26A8	0,8576
SLC2A1	1,0850
SLC30A1	0,8974
SLC38A8	-1,2949
SLC41A2	-0,8857
SLC43A3	-0,6928
SLC6A9	0,9257
SLC7A2	1,1593
SLC7A6	1,4905
SLCO2B1	0,9944
SMIM18	0,8459
SNAP23	0,8692
SNPH	1,7615
SOCS3	1,1016
SON	-1,1602
SORBS1	1,5310
SOWAHD	1,0049
SOX13	2,2853
SP3	0,8622
SP7	1,4531
SPATA2L	1,6146
SPINK8	-0,8224
SPRY4	1,5625
SPRY4-IT1	1,6888
SPX	-2,4058
SQOR	1,5208
SRGAP1	-1,1940
SRGAP3-AS2	-1,0506
SRGAP3-AS3	-0,9817
SRP54	0,8852
SRP68	-0,7880
STARD4-AS1	-1,0077
STAT2	1,5627
STC2	1,0725
STK10	-0,8140
STMN4	1,9113
STRAP	1,3313

STX18	-1,3132
STXBP4	0,8669
SUCLG2-AS1	1,0458
SUSD6	-1,2018
SYCP2	-1,0474
SYN2	1,5859
SYNPR	1,4866
SYT7	1,2597
TACC3	-1,4923
TAF8	1,6920
TAPBPL	1,8657
TBC1D10B	1,0469
TBC1D3P5	0,8890
TBC1D9	1,4844
TBL1XR1	2,4143
TBXAS1	0,9990
TCF4-AS1	1,8552
TCFL5	-1,2943
TCL6	1,1152
TEKT1	2,5095
TERC	1,4346
TESPA1	-1,7638
TF	1,1002
TFPI	1,2055
THAP9	1,5317
THRB-AS1	1,9597
THUMPD2	1,2630
TIMM10	1,1878
TIMM17A	1,7141
TIMM22	0,9252
TKFC	1,2051
TKT	1,4410
TLCD4	1,7507
TLCD4-RWDD3	1,4389
TLR2	-1,2675
TM9SF2	1,4298
TMEM119	1,7810
TMEM147-AS1	1,5457
TMEM212-AS1	0,9840
TMEM251	1,6835

TMEM262	1,2876
TMEM272	-1,1116
TMIE	1,7711
TMPRSS4	0,1738
TMX1	-0,9047
TNFRSF1A	1,3551
TNKS	-1,1354
TNN	1,5018
TNNT2	1,8126
TNRC18P1	1,5945
TOR1A	1,1905
TOX2	1,5059
TP53BP1	0,8018
TP53I11	-1,2848
TP53INP1	1,3470
TPBG	0,9134
TPTE2P3	1,1055
TRAPPC3L	1,0097
TRAPPC6A	0,9515
TRIM35	1,3701
TRIM37	-1,2358
TRIM5	1,3729
TRIP10	1,9460
TRMU	-1,5483
TTC38	-1,4229
TTF2	1,1544
TXLNA	-1,1291
TXNDC12	1,5577
UBAC2	1,7769
UBAP1	-1,0276
UBB	1,4551
UBE2L6	0,9189
UBQLN4	1,3313
UBR3	-1,1177
UBR4	-0,9768
UBR7	1,3428
UBXN6	-1,2264
UGDH-AS1	1,3290
UGT8	0,8392
UPK3A	-1,0829

USP15	-1,1145
USP24	1,4404
USP39	1,9799
USP54	-1,5103
UTP3	2,2406
VAX2	-1,0312
VIM	-0,9524
VPS26B	-1,6900
VPS33B	1,0286
VPS8	1,3583
VSIG2	-0,9640
WAC	1,1289
WARS1	-0,8331
WDFY3-AS2	-2,0703
WDR12	-1,1436
WDR34	-0,9972
WDR37	0,9830
WDR76	0,9356
WLS	1,2595
WNT2	1,7582
WNT3	1,6857
WRAP73	-1,3625
XRN1	1,2924
YARS1	0,8750
YBX2	1,5391
YWHAEP1	-0,7197
ZBED1	2,4332
ZC3H10	1,1381
ZC3H7A	-1,2261
ZDHHC12	-1,2559
ZFAND6	1,2462
ZFP14	-1,1588
ZIM3	-0,8969
ZKSCAN4	-0,6278
ZMYM1	1,6854
ZMYM3	-0,9014
ZNF205-AS1	1,8144
ZNF233	1,3895
ZNF234	1,1816
ZNF252P	-1,6663

ZNF333	1,0714
ZNF407	1,5791
ZNF41	1,3346
ZNF491	-1,0556
ZNF497	0,6395
ZNF517	1,2845
ZNF529	-0,9979
ZNF557	-1,0231
ZNF746	-1,1215
ZNF75D	-1,1582
ZNF789	-1,1794
ZNF791	-0,7661
ZNF833P	1,4214
ZPLD2P	-0,8478
ZWILCH	-1,9182